Master Thesis, Department of Geosciences

Reservoir Quality of Lower-Middle Jurassic sandstones within the Johan Castberg Field in the SW Barents Sea

The role of sediment composition, facies distribution and post depositional processes

Abdul Jabbar

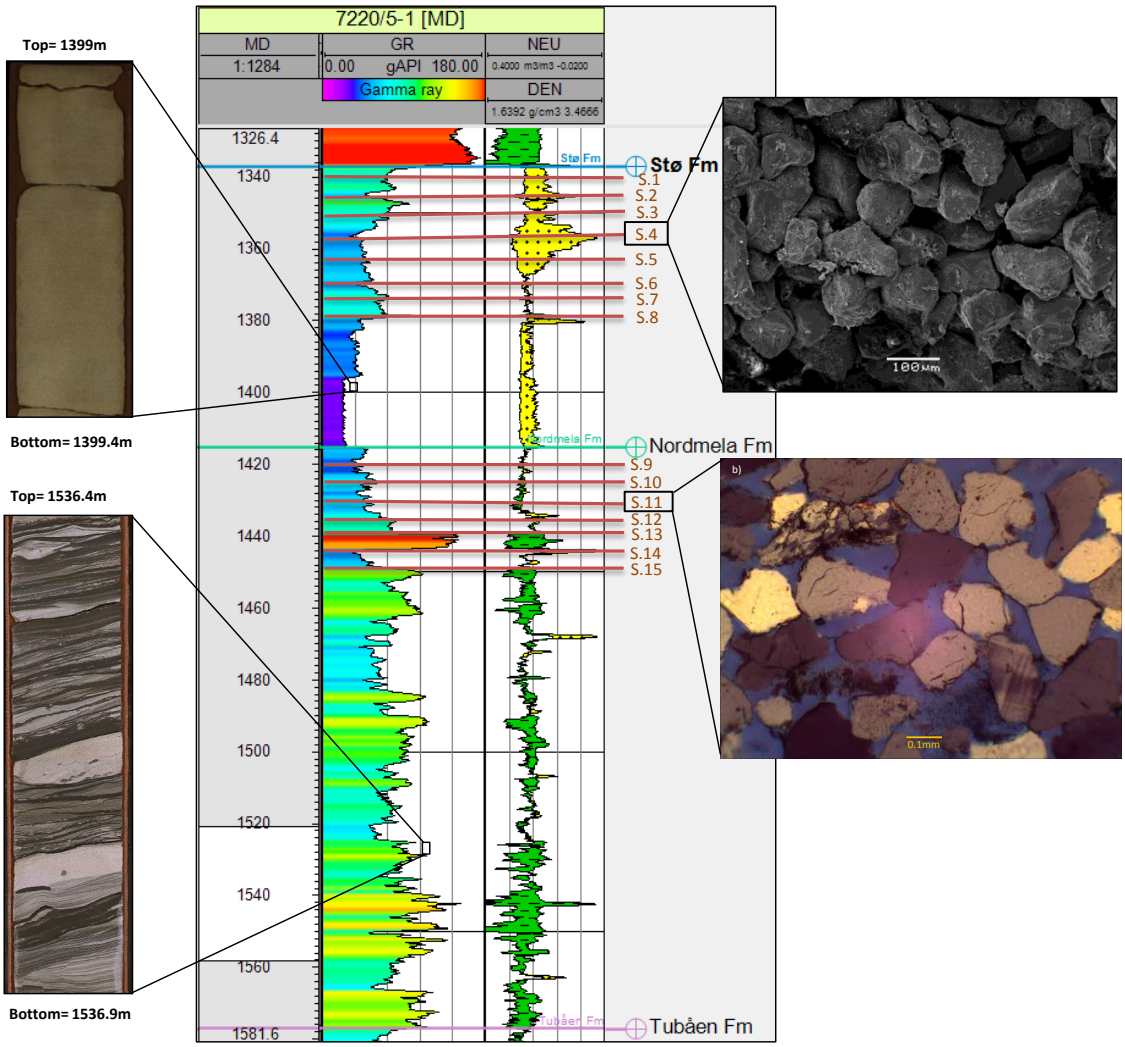

UNIVERSITY OF OSLO

FACULTY OF MATHEMATICS AND NATURAL SCIENCES

Reservoir Quality of Lower-Middle Jurassic sandstones within the Johan Castberg Field in the SW Barents Sea

The role of sediment composition, facies distribution and post depositional processes

Abdul Jabbar

Master Thesis in Geosciences

Discipline: PEGG

Department of Geosciences

Faculty of Mathematics and Natural Sciences

University of Oslo

01.06.2015

ACKNOWLEDGMENT

First and foremost, I am thankful to Almighty Allah whose blessings and gratitude enabled and helped me to complete this study. Special praises to Holy Prophet Muhammad (SAWW), who is the best role model for all human beings**.**

I would like to express my deep gratitude to my supervisor Associate Professor Jens Jahren for his tremendous contribution and support throughout this research work. I am able to finish this work under his dynamic supervision, auspicious and considerate guidance, encouragement and altruistic attitude.

I also extend my special thanks to Phd Students Irfan baig and Oluwakemi for their esteemed guidance, suggestions and discussions throughout my thesis work. I also thank to Berit Løken Berg for always being supportive and helpful in my SEM studies. Special thanks to Ahmed Salman and Arif butt for their suggestions and making improvement in my work.

I express my heartfelt gratefulness to Shahzaib Haider, Dr. Tausif Ahmad and Perzin Nizari for their support and inspiration during my stay in Oslo. Your friendship makes my life a wonderful experience. I also appreciate the efforts and collaborative attitude of Asad Khan, Saadullah Nisar, Syed Moiz and Shajahat Ahmed during this project.

At the end, I would like to express my heartiest gratitude to my family for their endless love and affection; I owe a lot to them. I am incomplete without their love and support.

Abdul Jabbar
01.06.2015

This thesis is dedicated to my parents.

For their endless Love, Support and Encouragement

ABSTRACT

The Johan Castberg Field is located on the western margin of Loppa High in the south-western Barents Sea and comprises a reservoir in Lower-Middle Jurassic sandstones of Stø and Nordmela formations containing both oil and gas. Cored intervals, 15 samples (well 7220/5-1) and wells log data (7219/8-1, 7219/9-1, 7220/8-1 and 7220/7-1) have been used for petrophysical and petrographical study of sandstone reservoirs. Reservoir properties are preserved significantly due to uplifting and erosion of the entire region. Sandstone diagenesis is a function of burial rate, mineralogical composition and texture, climate, and hydrodynamic and geothermal gradients.

X-ray diffraction (XRD), Optical Microscopy, Scanning Electron Microscopy (SEM) and Core Analysis have been performed to investigate the depositional environment, clay mineralogy, role of sediments composition, facies distribution, and provenance of the reservoir sandstones. Petrographical study has been carried out to find the diagenetic clay and microquartz coatings, quartz cementation and its distribution in the sandstone reservoirs.

The estimation of porosity and Intergranular Volume (IGV) values reflecting mechanical compaction of sandstone reservoirs were the main objectives during this research work. Quartz cementation has very limited effect on the porosity loss. In addition to mechanical compaction, the authigenic kaolinite and depositional matrix filling the pore space caused some porosity reduction.

Lower-Middle Jurassic sandstones are moderate to well sorted, fine to medium grained and are mineralogical mature. Sandstones are deposited in prograding coastal regime whereas shale interval indicates regional transgressive pulses during deposition. The porosity and IGV values of sandstones range 6-26% and 25-34% respectively. The porosity is still well preserved and reservoir quality of Lower-Middle Jurassic sandstones in well 7220/5-1 is very good.

Keywords: IGV, authigenic clays and porosity, facies distribution, quartz cementation, SEM, XRD

TABLE OF CONTENTS

TABLE OF FIGURES

CHAPTER 1

CHAPTER 2

CHAPTER 3

CHAPTER 4

CHAPTER 5

CHAPTER 6

CHAPTER 7

LIST OF TABLES

LIST OF APPENDICES

CHAPTER 1

INTRODUCTION

- BACKGROUND AND MOTIVATION
- STUDY AREA
- RESEARCH OBJECTIVES

This research work is a part of field developing project in collaboration between University of Oslo and Tullow Oil Norge AS. Main objective of this research work is to increase the understanding of reservoir quality within the Johan Castberg Field located in south-western Barents Sea.

1.1 Background and Motivation

The Norwegian continental shelf consists of three main provinces; North Sea, Mid-Norwegian continental margin and Western Barents Sea. The greater Barents Sea encompasses the shelf area between Svalbard and Norway. It is surrounded by Norwegian Sea in the southwest, the Islands of Franz Josef Land and Novaya Zemlya in the northeast and east, Norway in the south and the Islands of Svalbard in the northwest (Figure 1.1). Norwegian margin consists of a continental shelf and slope that vary significantly in width and morphology (Faleide et al., 2010a).

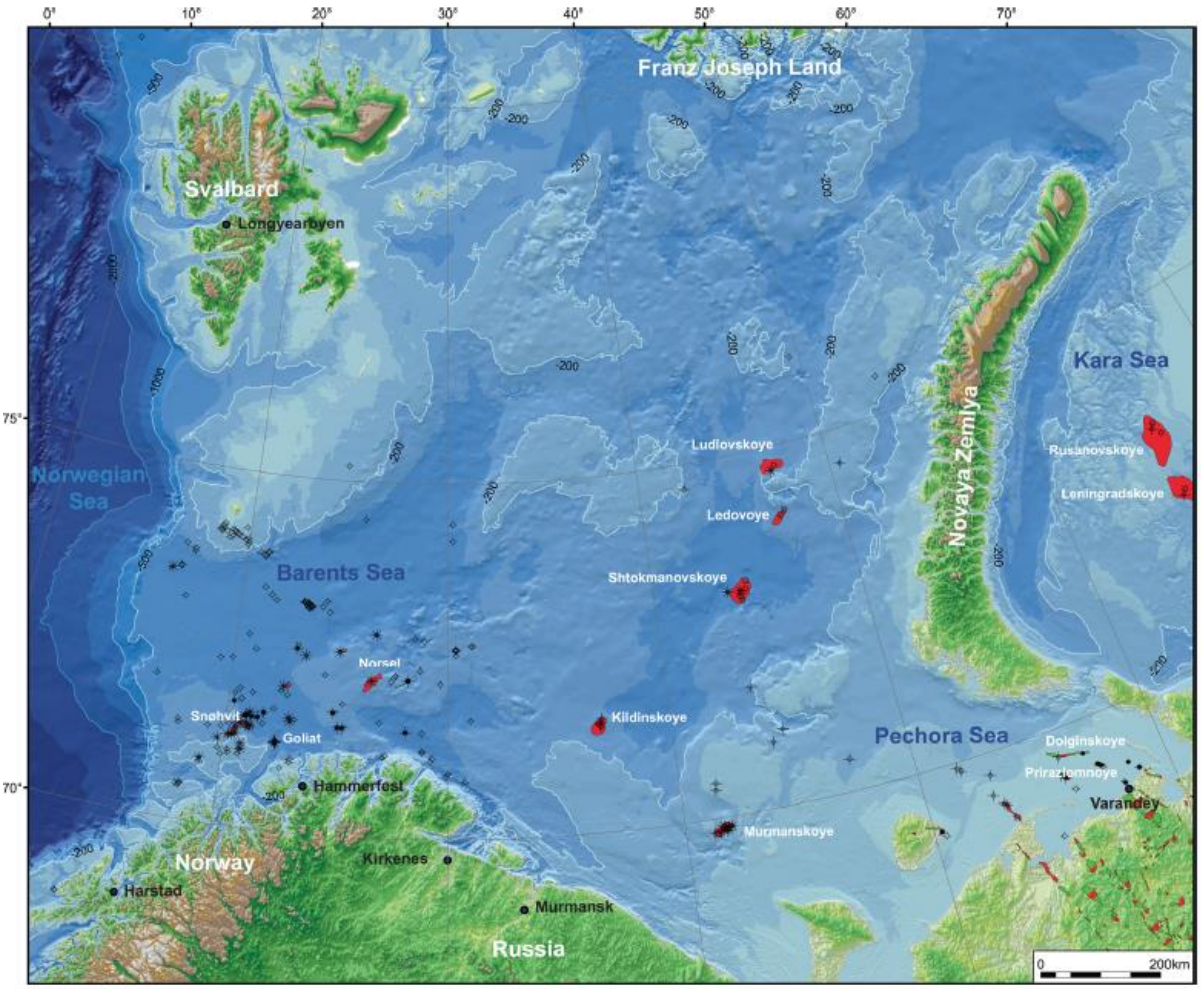

Figure 1.1: Regional setting (bathymetry/topography) of the Barents Sea and the adjacent areas (Henriksen et al., 2011b).

Barents Sea is one and a half times greater than the Norwegian portion of the North Sea and covers almost 230 000 km^2 of the Norwegian continental shelf (Doré, 1995). Barents Sea became an area of high interest after the first exploration in 1980. Especially in the recent years, Skrugard (April 2011), Havis (January 2012) and Drivis (May 2014) discoveries in the SW Barents Sea proved break-through in the exploration history. Until now approximately 21 development and 117 exploration wells have been drilled in the Barents Sea. However most of the discoveries lie in the south-western Barents Sea (www.npd.no). In the area, several different petroleum plays have proven hydrocarbon accumulation due to proper hydrocarbon generation, migration and trapping mechanism (Faleide et al., 2010b). The greater Barents shelf comprises a variety of petroleum source rocks ranging in age from Silurian to Cretaceous. Correlation of trapped oil to single source rock is difficult due to presence of multi-source rocks in the area (Henriksen et al., 2011b).

Barents Sea is characterized by thick sequence of sedimentary rocks in the basins ranging in age from Late Palaeozoic to Quaternary (Barrère et al., 2007). Barents Sea is considered to have some of the deepest sedimentary basins in the world. Deep Cretaceous (Harstad, Tromsø and Bjørnøya) Basins have been separated by Trom-Finnmark Fault Complex, Ringvassøy-Loppa Fault Complex, Bjørnøyrenna Fault Complex and Leirdjupet Fault Complex (Faleide et al., 1993b). The better understanding of regional geological and tectonic setting of the greater Barents Sea has increased significantly due to presence of hydrocarbon resources in the past few decades.

1.2 Study Area

The Johan Castberg Field is located in blocks 7219/9 and 7220/4, 5, 7, 8, approximately 100 km north of the Snøhvit Field in the Barents Sea (Figure 1.2). It is situated at water depth of about 360-390 meters and has capability to produce 400-600 million barrels of oil. The reservoir comprised of Lower-Middle Jurassic Sandstones (www.statoil.com).

The Johan Castberg Field is located in PL 532 that contains three main discoveries; Skrugard, Havis and Drivis. Statoil is the main operator with 50% shares whereas Eni Norge and Petoro have 30% and 20% shares respectively. Seven exploration wells have been drilled and most of them contain both oil and gas (www.npd.no).

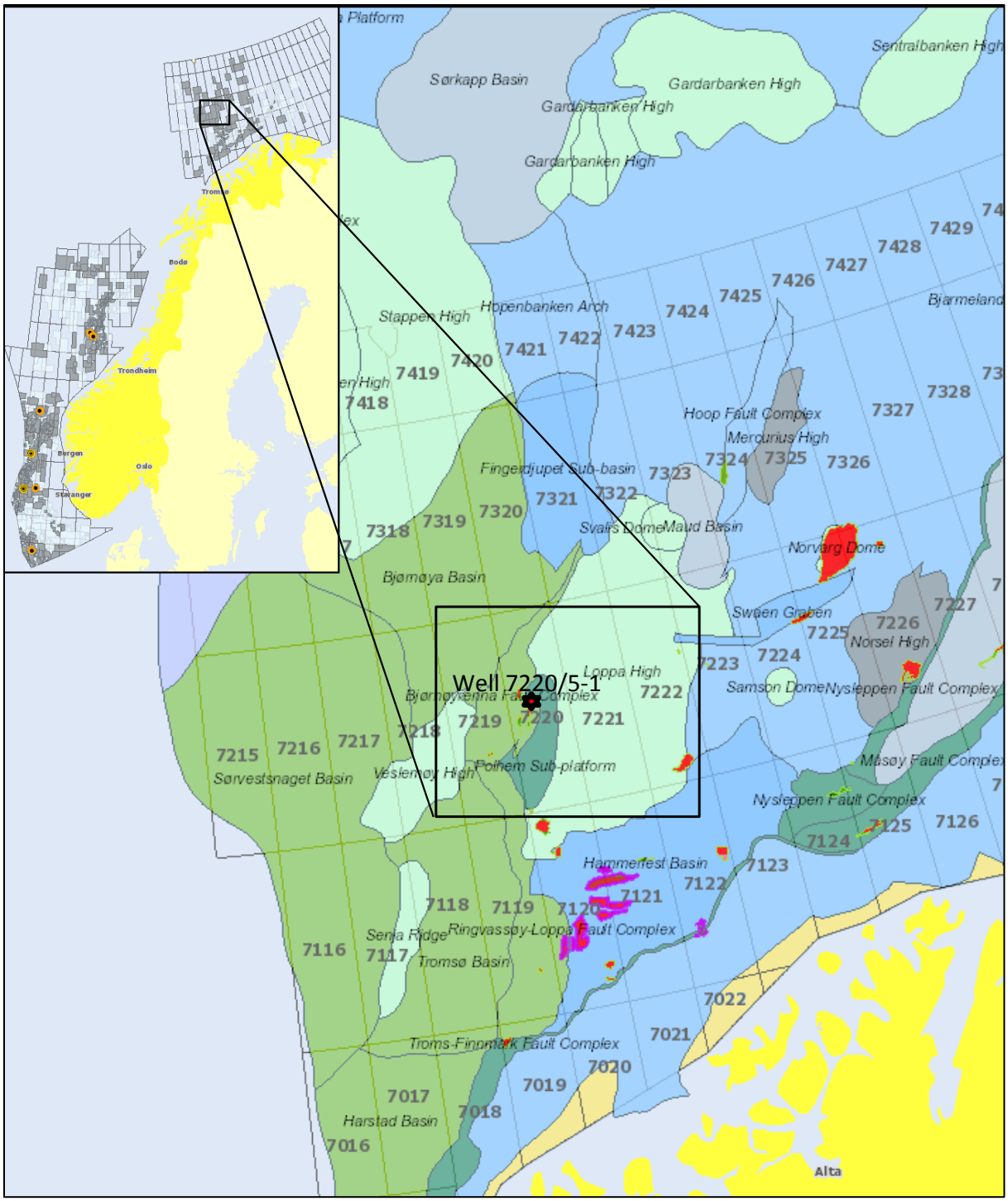

Figure 1.2: Map showing location of Study area and well 7220/5-1. Inset map shows the hydrocarbon exploration blocks on the Norwegian Continental Shelf (Source NPD).

1.3 Research Objectives

The main objective of this research work is to explore the reservoir quality of Jurassic sandstones in the Johan Castberg Field based on the samples from the well 7220/5-1 and well log data of four surrounding wells (7219/8-1, 7219/9-1, 7220/8-1 and 7220/7-1).

In more details, objectives of this study are to investigate

- Post depositional processes, clay mineralogy, facies distribution and role of sediments composition in the area.
- Controlling factors of the reservoir properties based on the grain size, sorting, mineralogical composition, cementation and amount of matrix.
- Depositional environment, climate, transport processes, and provenance of the reservoir sandstone based on X-ray diffraction, core logging, optical microscopy and scanning electron microscopy (SEM).
- Textural and mineralogical maturity of Lower-Middle Jurassic sandstones.
- Eventual diagenetic clay and micro quartz coating and their distribution in sandstones which effects on the reservoir quality.

CHAPTER 2

GEOLOGICAL FRAMEWORK

- GEOLOGICAL EVOLUTION
- TECTONIC SETTING AND STRUCTURAL ELEMENTS
- STRATIGRAPHY
- DEPOSITIONAL ENVIRONMENT
- PETROLEUM SYSTEM

2.1 Introduction

This chapter deals with the geological evolution, regional tectonic setting, structural elements and the stratigraphic setting of south-western Barents Sea. Furthermore, Depositional environment and petroleum system present in the Bjørnøya Basin and western limb of Loppa High have also been discussed.

2.2 Geological Evolution

The geological evolution of the Barents Sea started in Early Palaeozoic time due to opening of an ocean called Iapetus (Berglund et al., 1986). Sub-Basins in the south-western Barents Sea were formed by several regional tectonic phases in the North Atlantic-Arctic region. Barents Sea has been subjected to main four tectonic phases of evolution (Ziegler, 1978) (Figure 2.1).

- Caledonian Orogeny Phase
- Svalbardian-Ellesmerian Phase
- Hercynian-Varsican Phase
- Kimmerian Phase

2.2.1 Caledonian Orogeny Phase: Caledonides basement were consolidated in Late Silurian to Early Devonian due to collision of North America-Greenland and the Fennoscandian-Russian plates. Erosion of the uplifted consolidated sediments resulted in a deposition of old red sandstone in the western Norway and Svalbard (Faleide et al., 1984). Stappen and Loppa highs indicate very old basement terrains that were incorporated and closely connected by the end of the Caledonian orogeny (Gernigon et al., 2014).

2.2.2 Svalbardian-Ellesmerian Phase: Caledonides contractional regime evolved to a strong left-lateral shear regime in the Late Devonian (Faleide et al., 1984). This phase led to the extensive faulting and basaltic volcanism in the Novaya Zemlya (Bondarev et al., 1973) . Thin-skin folding above the base of Ordovician evaporites and large scale faulting in the northern Ellesmere Island was triggered during the Ellesmerian phase (Lawver et al., 2002).

2.2.3 Hercynian-Versican Phase: Hercynian-Versican phase occurred from Late Devonian to early Permian. Extensional regime dominated this area during Late-Devonian to Early Carboniferous and resulted in normal faults which are aligned to the Caledonian structures (Faleide et al., 1984).

2.2.4 Kimmerian Phase: Several small rifting episodes occurred during Kimmerian phase of extensional tectonic. Regional tectonic subsidence was initiated due to development of rift basin during Late-Middle Jurassic which led to the deposition of organic rick source rock in the south-western Barents Sea (Faleide et al., 1984). Old Caledonian and the Late Carboniferous highs remained undisturbed during Middle and Late-Kimmerian phase (van Hulten, 2008).

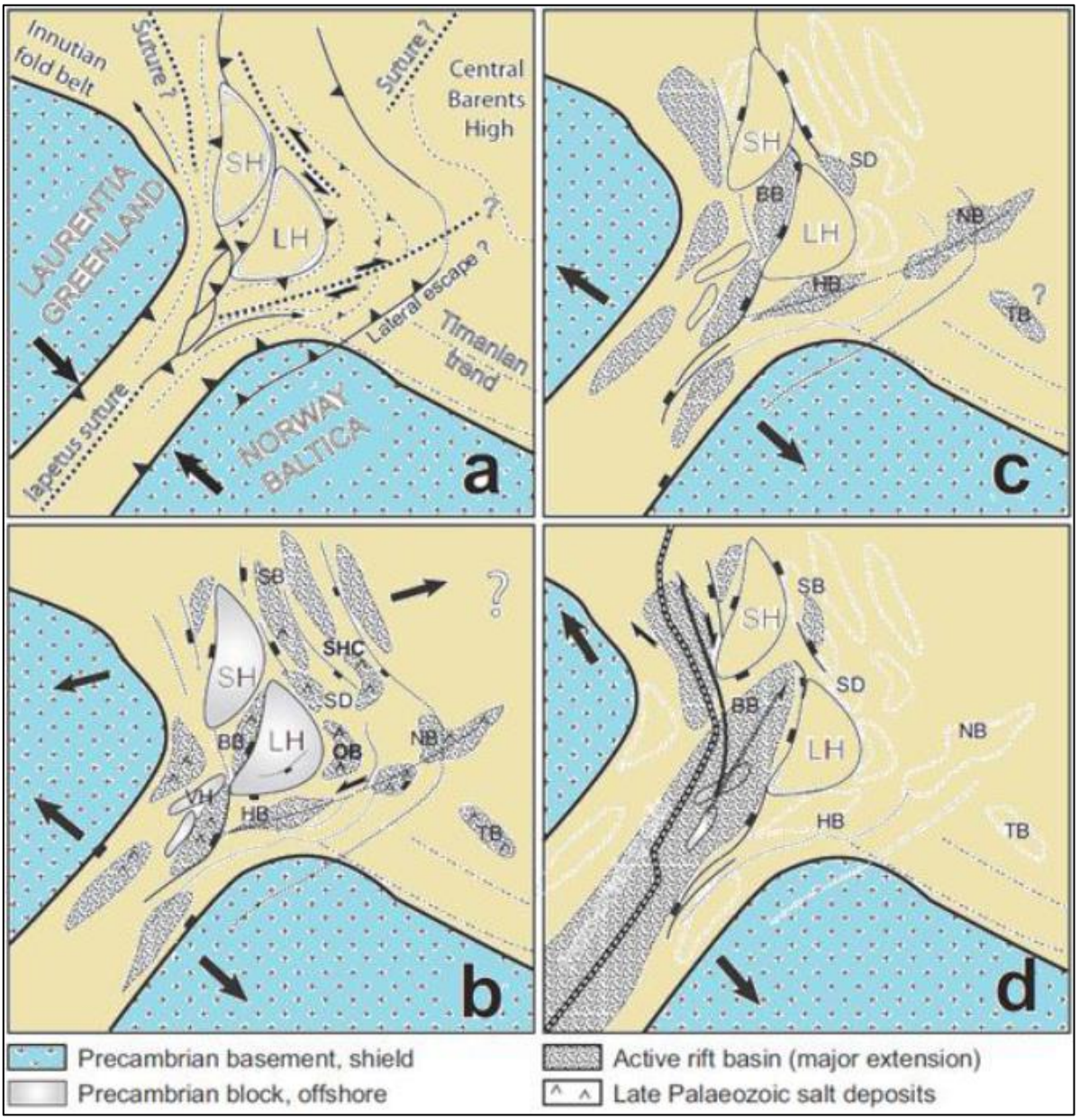

Figure 2.1: Sketches of the geodynamic evolution of the south-western Barents Sea (Gernigon et al., 2014). (a) Caledonian orogeny. (b) Reactivation of main inherited features. (c) Graben formation and salt tectonics during Hercynian-Versican extensional phase. (d) Thinning of crust in Late Mesozoic and final breakup between Baltica and Laurentia in Early Cenozoic. Abbreviations: BB: Bjørnøya Basin; BP: Bjarmeland Platform; HB: Hammerfest Basin; LH: Loppa High; NB: Nordkapp Basin; OB: Ottar Basin (south); SB: Sørkapp Basin; SD: Svalis Dome; SH: Stappen High; VH: Vestlemøy High; TB: Tiddlybanken Basin; SHC: Paleozoic Scott Hansen Complex.

Closure of Iapetus Ocean was diachronous that resulted in sinistral transpressional shear regime in the western margin of Baltica. The orientation of major faults was NE-SW to WNW-ESE in Late Devonian-Early Carboniferous time period (Rønnevik and Jacobsen., 1984) due to sinistral transpressional shear regime. One of these fault zones characterizes the present western limb of Loppa High and has N-S orientation. Loppa High and Hammerfest Basin tilted toward east during Late Carboniferous-Early Permian time due to reactivation of block-faulting in underlying older rocks (Berglund et al., 1986). Deposition of evaporites took place due to development of carbonate shelf in Late Permian whereas dark clays were deposited due to regional transgression in Late Jurassic (Gabrielsen, 1984).

During Triassic time the Pechora Basin was filled with clastic sediments from the Sverdrup Basin whereas tectonic activity was discrete in the Bjørnøya Basin. According to Faleide et al. (1984) igneous activities started in the Sverdrup Basin in Jurassic and terminated in Cretaceous with dolerite intrusions. The regional basin province subsided as compared to the Svalbard Platform and subsidence rate was faster in west relative to the eastern part of Loppa High Fault Complex. Loppa High inverted in between two subsiding basins during Cretaceous (Hammerfest and Bjørnøya).

In the Cenozoic Era deep Cretaceous and Tertiary basins (Harstad, Sørvestsnaget, Tromsø and Bjørnøya basins) were separated by intra-basinal highs (Senja Ridge, Veslemøy and Stappen highs) in the south-western Barents Sea. Sediments were eroded from Loppa High and deposited in the Tromsø Basin during Palaeocene. Erosion occurred due to combined effect of ice sheet movement and sea level fall during Late Cenozoic (Faleide et al., 1993a).

2.3 Tectonic Setting and Structural Elements

Barents Sea was a large epicontinental sea in the north-western corner of Eurasian Continental Shelf during the Triassic. It was surrounded by the North American continent to the west, Baltic continent to the south and an open seaway to the northwest (Glørstad-Clark et al., 2010).

Structural geological history of the south-western Barents Sea is influenced strongly by halokinesis during Mesozoic and Cenozoic. Horst and graben geometries were formed due to regional extensional tectonic events in the Late Palaeozoic (Glørstad-Clark et al., 2011). Three rift phases dominate the geological history of the western Barents Sea, Late Devonian – Carboniferous, Middle Jurassic-Early Cretaceous, and Early Tertiary where each rifting phase

involved numerous tectonic pulses. Crustal extension during Late Palaeozoic is generally distinguished by westward migration of the mid oceanic ridge (Faleide et al., 2010b).

In some areas thickness of relatively undeformed sedimentary cover with excellent horizontal extent exceeds 15 km in the Barents Sea. There are three main geological provinces in the Barents Sea based on sedimentary fill, tectonic style and crustal structure (1) The Lofoten Basin; (2) The south-western Barents Sea Basin province; and (3) Mesozoic Basin (Faleide et al., 1993b).

Main structural elements of south-western Barents Sea are Ringvassøy-Loppa Fault complex, Senja Fracture Zone, Troms-Finnmark Fault Complex, Leirdjupet Fault Complex, Bjørnøyrenna Fault Complex, Senja Ridge, Stappen High, Veslemøy High, Polheim Subplatform, Harstad Basin, Sørvestnaget Basin, Hammerfest Basin, Bjørnøya Basin, and Tromsø Basin (Figure 2.2).
Western Barents Sea can be separated into three following distinct regions (Faleide et al., 1993b).

1) The Svalbard Platform.
2) Basin between the Norwegian coast and the Svalbard Platform distinguished mainly by structural highs and sub-basins.
3) The western continental margin, which is further subdivided into three main segments:
    a) A southern sheared margin.
    b) A central rifted complex.
    c) The northern later rifted margin.

Description of main structural elements in the south-western Barents Sea is as below:

2.3.1 Bjørnøya Basin

The Bjørnøya Basin is a wide (100-150 km) and deep (approx. 10 km) sag basin (Gernigon et al., 2014)which trends NE-SW and is surrounded by Loppa High in the southeast and Stappen High in the northwest. It has been divided by the Leirdjupet Fault Complex into two parts; deeper part in the west and shallow part in the east. Bjørnøya Basin consists of enormously thick Cretaceous succession formed due to the major Mesozoic subsidence event (Gabrielsen et al., 1990). Thick Cretaceous succession thins towards the northern part of Stappen High and finally disappear due to erosion resulting from a significant Tertiary uplift (Gernigon et al., 2014).

In Early Cretaceous, major depocentres were developed within the Bjørnøya, Tromsø and Harstad basins due to rapid subsidence occurred in the south-western Barents Sea (Breivik et al., 1998). Rate of sedimentation was significant and most probably the Late Jurassic-Middle Cretaceous period marks a "sag" phase of the Bjørnøya Basin (Gernigon et al., 2014).

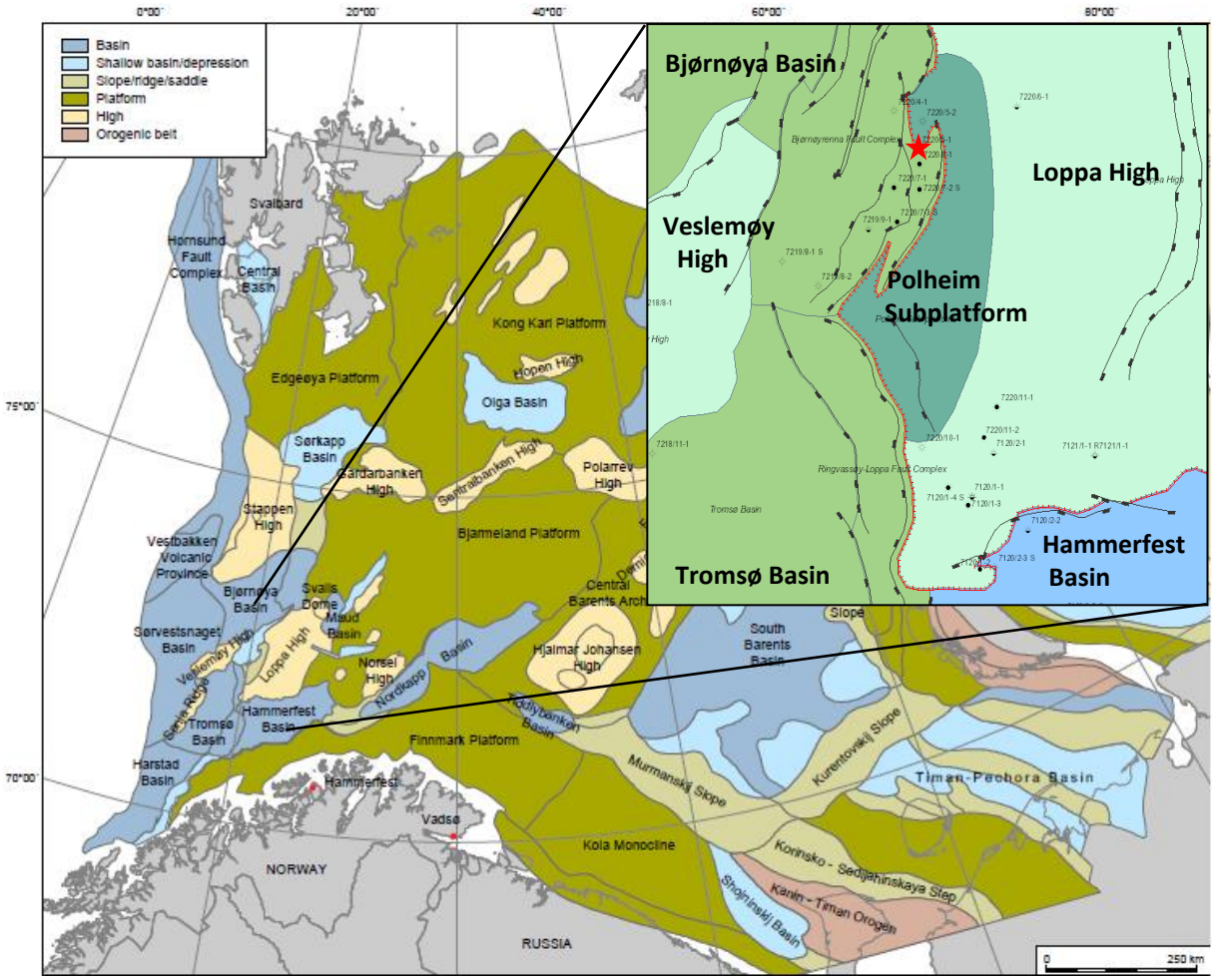

Figure 2.2: Structural geological elements in the Barents Sea, inset map shows the structural elements of south-western Barents Sea. Modified from (Henriksen et al., 2011a).

2.3.2 Loppa High

Loppa High is one of the most important basement high and structural elements in the south-western Barents Sea. It is situated in the north of Hammerfest Basin and southeast of Bjørnøya Basin. Asterias and Ringvassøy-Loppa fault complexes mark the southern and western limits of the Loppa High respectively. The Svalis Dome (major salt structure) with its related Maud Basin (rim syncline) marks the northeastern limit of Loppa High (Gabrielsen et al., 1990).

Polheim Subplatform is incorporated within Loppa High (Gabrielsen et al., 1990) and the formation of faulted blocks and traps such as Havis and Skrugard prospects on Polheim Subplatform developed during Triassic, Jurassic and Cretaceous periods (Gernigon et al., 2014). Barents Sea was separated into to two sub-basins (northern and southern) due to uplifting of Loppa High. However, it was quite stable platform during Early-Middle Jurassic (Ramberg, 2008). Loppa High and surrounding areas have a complex geological history due to several tectonic phases of uplift/subsidence and subsequent tilting and erosion (Larssen, 2005).

2.3.3 Polheim Subplatform

Polheim Subplatform is located to the west of Loppa High and is described as a part of the Loppa High by Gabrielsen et al. (1984). Polheim Subplatform was positive and tectonically active structural element of Loppa High during Late Paleozoic (Gabrielsen et al., 1990). Major substantial oil and gas discoveries (Skrugard and Havis) of the south-western Barents Sea are situated on the Polheim Subplatform (Fanavoll et al., 2014).

2.3.4 Tromsø Basin

The Tromsø Basin is surrounded by the Ringvassøy-Loppa Fault Complex to the east and Senja Ridge to the west and it truncates against the Troms-Finnmark Fault Complex to the southeast. Veslemøy High divides the Tromsø Basin from the Bjørnøya Basin in the north (Gabrielsen et al., 1990) while south-western margin are Senja Fracture Zone and Harstad Basin. A series of salt structures and related flexures and faults defines the NNE-SSW axis orientation of the Tromsø Basin (Gabrielsen, 1984).

Salt flowage in the weak zones of overburden was triggered by the regional tectonic activities and has played an important role in structuring the Tromsø Basin (Øvrebø and Talleraas, 1977).

2.3.5 Hammerfest Basin

The Hammerfest Basin is a complicated sedimentary basin and it has been influenced by several tectonic phases. Hammerfest Basin has an area of 10,500 km^2 and has developed during Late Jurassic to Early Cretaceous (Berglund et al., 1986). Troms-Finnmark Fault Complex divides the Hammerfest Basin from Finnmark Platform to the south whereas Asterias Fault Complex separates the basin from Loppa High to the North. Western limit of Hammerfest Basin is defined by the southernmost segment of Ringvassøy-Loppa Fault

Complex whereas its eastern margin developed as a flexure against the Bjarmeland Platform (Gabrielsen et al., 1990).

Thickness variations are associated with basin-parallel structures with thinning trend towards the domal feature present in the central segment of the Hammerfest Basin (Faleide et al., 1993b). Hammerfest Basin consists of both listric and deep high angle faults in the central part and along the basin margin respectively. The eastern part of basin is distinctive sag basin and relatively less influenced by faulting during tectonic activities (Gabrielsen et al., 1990).

2.4 Stratigraphy

Stratigraphy of Barents Sea is mainly dominated by Carbonates and Clastic sediments. Carbonates belongs to Devonian, Carboniferous and Permian time period whereas clastic sediments represents the Mesozoic and Cenozoic time period. Furthermore, clastic sediments are divided into two distinct lithologies; sandstones in Kapp Toscana Group (Triassic and Jurassic) and shales in Adventdalen Group (Middle Jurassic to Middle Cretaceous). Permo-Carboniferous rocks are very similar to rocks exposed in the Svalbard and northeast Greenland (Ohm et al., 2008).

The deepest well in Johan Castberg Field is 7219/8-1 which is located in the southern part of Bjørnøya Basin and close to Veslemøy High. It has been penetrated up to Stø Formation of Middle Jurassic with total depth of 4611 meters. The shallowest well (7220/5-1) located on the western part of Loppa High whereas the other wells (7220/8-1, 7219/9-1) were drilled in the central part of Bjørnøya Basin. All wells have been penetrated to the target reservoirs Stø, Nordmela and Tubåen formations. Table 2.1 illustrates all Lithostratigraphic units with corresponding depth in well 7220/5-1.

Table 2. 1: Lithostratigraphic units with corresponding depth recorded at well 7220/5-1.

Total depth (m) RKB	Unit	Age	Group
428	Nordland Gp	Late Pliocene-Holocene	Nordland Gp
478	Torsk Fm	Palaeocene-Oligocene	Sotbakken Gp
1035	Kolmule Fm	Middle Cretaceous	Adventdalen Gp
1238	Knurr Fm	Lower Cretaceous	
1296	Hekkingen Fm	Lower Cretaceous	
1312	Fuglen Fm	Upper Jurassic	
1337	Stø Fm	Middle Jurassic	Kapp Tascana Gp
1415	Nordmela Fm	Lower Jurassic	
1578	Tubåen Fm	Upper Triassic-Lower Jurassic	
1695	Fruholmen Fm	Upper Triassic	

2.4.1 Kapp Toscana Group

The Late Triassic to Middle Jurassic Kapp Toscana group mainly consists of sandstone, siltstone and shales and well exposed on Spitsbergen, Edgeøya, Hopen, Kong Karls Land and Bjørnøya islands. It continues in the subsurface as well across the south-western Barents Sea to the Nordkapp and Hammerfest basins. Kapp Toscana Group is further divided into two subgroups (Figure 2.3); Storfjorden and Realgrunnen subgroups (Worsley et al., 1988).

2.4.1.1 Storfjorden Subgroup

Storfjorden subgroup mainly consists of shales and shallow marine deltaic sandstone of varying provenance. The lower part of Storfjorden subgroup is mainly dominated by organic rich shales deposited throughout the Ladinian age due to development of prodelta shales (Worsley, 2008). Snadd Formation in the southern Barents Sea has been interpreted as being deposited in lower delta plain on the basis of bioturbation, capped by coal layer and coarsening upward sequence (Riis et al., 2008).

2.4.1.2 Realgrunnen Subgroup

The Late Triassic to Middle Jurassic Realgrunnen subgroup contains shallow marine quartz rich, mature sandstone deposited in coastal plain and fluvio-deltaic environment (Mork et al., 1982). Thin coal layers and shale interval are common in the lower parts of Realgrunnen subgroup. The group was originally deposited on the Troms-Finnmark Platform and Loppa High and increases in thickness towards the Tromsø Basin (Dalland et al., 1988). The subgroup is thickest in the southern part of Bjørnøyrenna Fault Complex, thinnest on the Bjarmeland Platform and mostly eroded from the Loppa High (Halland, 2014). Realgrunnen Subgroup is divided into four formations: Fruholmen Fm., Tubåen Fm., Nordmela Fm., and Stø Fm.

Fruholmen Formation: Fruholmen Formation is dominated by grey to dark grey shale, sandstone and coal (Dalland et al., 1988). This formation is further divided into three members on the basis of lithology (Halland, 2014); shale dominated Akkar Member (lower), sandy Reke Member (middle) and more shale rich Krabbe Member (upper).

Tubåen Formation: This formation mainly comprises sandstones with subordinate shale and coal. Thickness of coal bed increased towards the southeast margin of Barents Sea. Upper and lower parts of Tubåen Formation mainly consist of sandstone .The middle part of this formation is dominated by shaly interval (Halland, 2014).

Nordmela Formation: Nordmela Formation consists of sandstone, siltstone, and shale with minor coals. The proportion of sandstone increased upward (Dalland et al., 1988).

Stø Formation: Early to Middle Jurassic Stø Formation mainly comprises moderate to well sorted and mature sandstone (Dalland et al., 1988). Minor amount of shale and siltstone in the Stø Formation indicates regional transgressive pulses. This formation is 78m thick in the well (7220/5-1) and has been subdivided into three depositional episodes based on transgression in the area (Halland, 2014). Prograding coastal regime depositional environment of sands in Stø Formation make it more stronger candidate of being good reservoir sandstone.

2.4.2 Adventdalen Group

Regional transgression in Middle to Late Jurassic led to deposition of organic rich shale dominated Adventdalen Group in the Barents Sea whereas sandstones were mostly restricted to the margins of highs and platforms close to the Jurassic/Cretaceous boundary (Worsley, 2008). Adventdalen subgroup comprises five formations; Fuglen Fm., Hekkingen Fm., Knurr Fm., Kolje Fm., and Kolmule Fm.

Fuglen Formation: Fuglen Formation contains dark, pyritic mudstones with subordinate limestone and sand, where sand is extremely bioturbated in the southern Barents Sea (Mørk et al., 1999).

Hekkingen Formation: This formation comprises mainly brownish-grey to dark grey shales and mudstones with subordinate thin limestone, dolomite, siltstone and sandstone (Dalland et al., 1988). Hekkingen Formation is an important source rock for hydrocarbons in the south-western Barents Sea (Bugge et al., 2002).

Knurr Formation: The Knurr Formation is composed of dark grey to greyish brown claystones with interbedded thinly limestone, sandstone and dolomite (Dalland et al., 1988). Sandstone is deposited in a massive turbidite sequence at the toe of slope fans along the margin of Loppa High (Sattar, 2008).

Kolje Formation: This formation mainly comprises dark brown/grey shales and mudstone indicating distal, open marine depositional environment with water circulation. Kolje Formation is between 15 and 403 m thick in the Barents Sea (Dypvik et al., 2010).

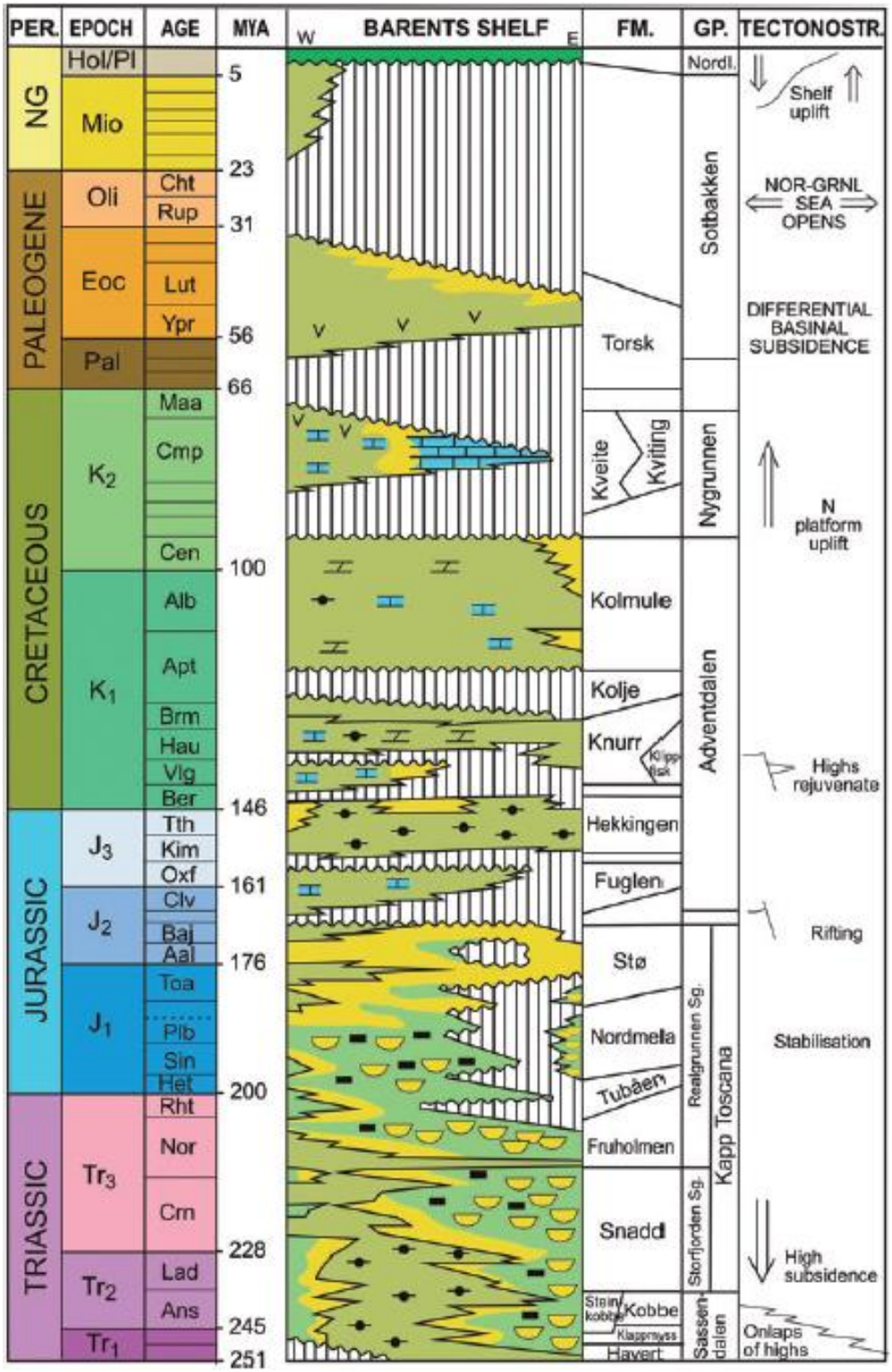

Figure 2.3: The Mesozoic and Cenozoic development of south-western Barents Sea (Worsley, 2008).

Kolmule Formation: Kolmule Formation is mainly dominated by dark grey/green claystones, silt and shale with subordinate limestone and dolomite. This formation is 945m thick in the type well whereas 530m thick in the reference well (Dalland et al., 1988).

2.5 Depositional Environment

Depositional environment and provenance of a sedimentary succession are highly demanded to specify the quality of reservoir rock. Petrophysical and mineralogical properties of sedimentary rocks depends on their depositional environment and distribution in the area and are important due to their potential for hydrocarbons accumulation.

Depositional age of Kapp Toscana Group is Carnian to Bathonian. Figure 2.4 shows that the Carnian prodelta area was shallow near the continent whereas remaining area towards the north is deep shelf.

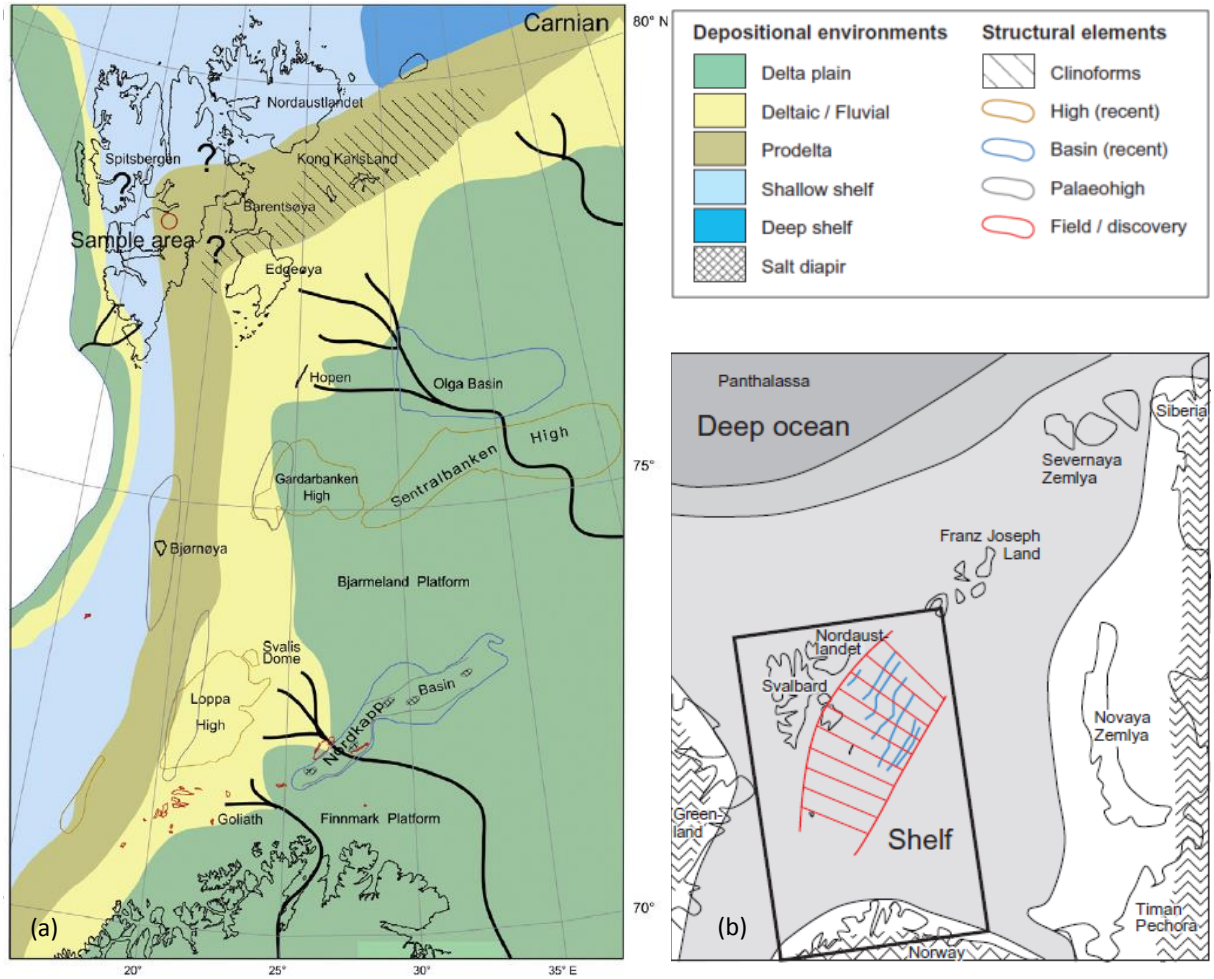

Figure 2.4: (a) Paleogeographic map illustrates progradation of Carnian Prodelta. (b) Overview map shows the study area in the Barents Sea (Riis et al., 2008).

Hammerfest Basin was the main depocenter in the southern Barents Sea and probably detached from the Nordkapp Basin during Early Jurassic. These sediments were derived from the Finnmark region together with land in the east and transported toward the north. During Middle Jurassic, the Loppa High subjected to uplifting and erosion, and sediments transported

to Hammerfest Basin. Norwegian Barents Sea was covered by vast alluvial plains within humid temperate climatic zone during Upper Triassic in contrast to North Sea and Norwegian Sea (Ramberg, 2008).

The Nordmela Formation represents deltaic environment in addition to lake, delta front, flood plain, and river channels (Figure 2.5). The sandstones of Nordmela Formation deposited by river channels whereas mud deposited on the flood plains between the channels (Berglund et al., 1986). Nordmela Formation also demonstrates tidal flat sequence with remarkable lateral extension of the facies (Olaussen et al., 1984).

Barents Sea started to submerge during Early Jurassic and sand was deposited along the coastal plain. Sedimentation was controlled by a complex interplay of tectonic subsidence, seal level changes and amount of sediments (Berglund et al., 1986). With time, coastal plains got submerged throughout the Hammerfest Basin due to continuous subsidence and sand deposited over the alluvial plains during Middle Jurassic. Latterly, this thick marine sand is termed as Stø Formation that was deposited in the shoreface area and in the shallow sea close to the coastline. Sedimentary structures observed in the lower part of Stø Formation indicate that sand was reworked by tidal and wave action. Phosphate nodules and extreme bioturbation in the upper part of Stø Formation demonstrates less sediments supply probably due to low topography of provenance areas (Ramberg, 2008). Trace fossils such as Planolites and Helminthopsis in Stø Formation indicates shallow marine conditions with increasing upward lagoonal conditions (Smelror et al., 2001).

2.6 Petroleum Systems

In the south-western Barents Sea, several petroleum systems and plays have been found and are described briefly in order to get better understanding of hydrocarbon generation, migration, accumulation and distribution in the area. The Barents Sea is well known for the existence of multiple source rocks and under-filled gas fields with an oil leg (Duran et al., 2013). Furthermore, the recent discoveries and presence of substantial amount of light hydrocarbons in the Barents Sea also confirmed the existence of large working petroleum systems (Fanavoll et al., 2014). Hydrocarbons are distributed into three major petroleum systems in the greater Barents Sea; Palaeozoic, Early-Middle Triassic and Late Jurassic (Figure 2.6). However, the petroleum systems in Bjørnøya Basin and Loppa High are Late Jurassic and Early-Middle Triassic respectively (Henriksen et al., 2011b).

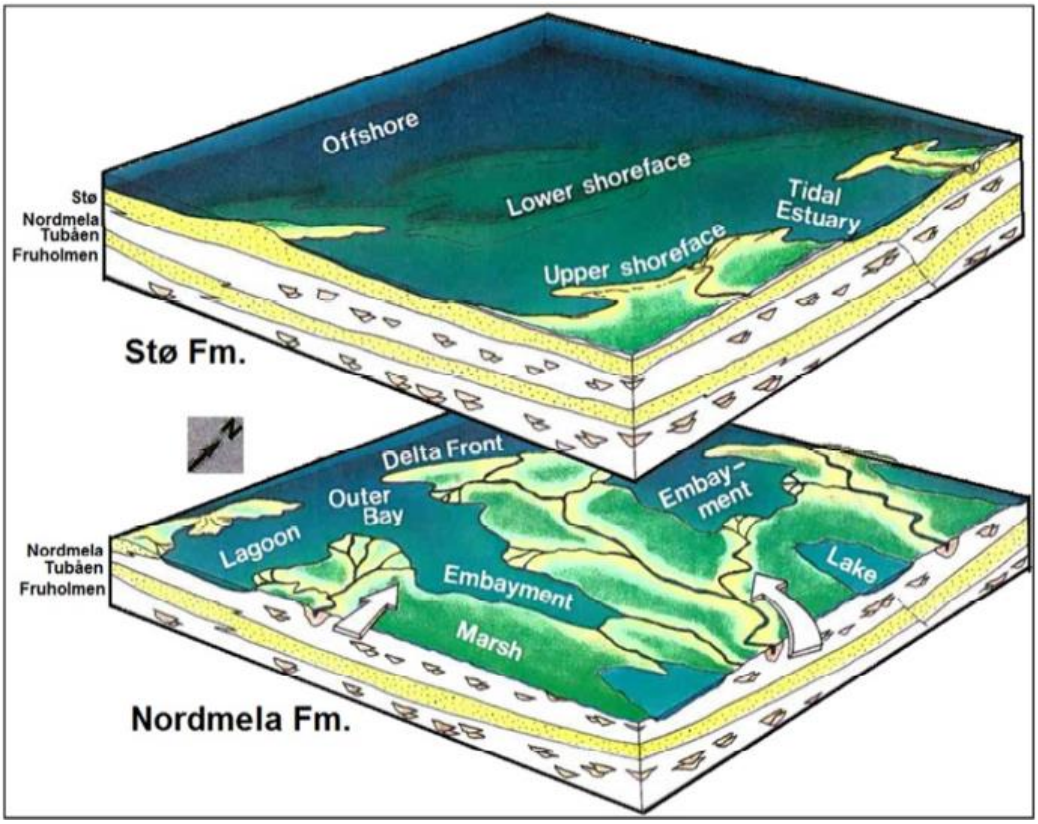

Figure 2.5: Model illustrates the depositional environment of Nordmela and Stø formations (Berglund et al., 1986).

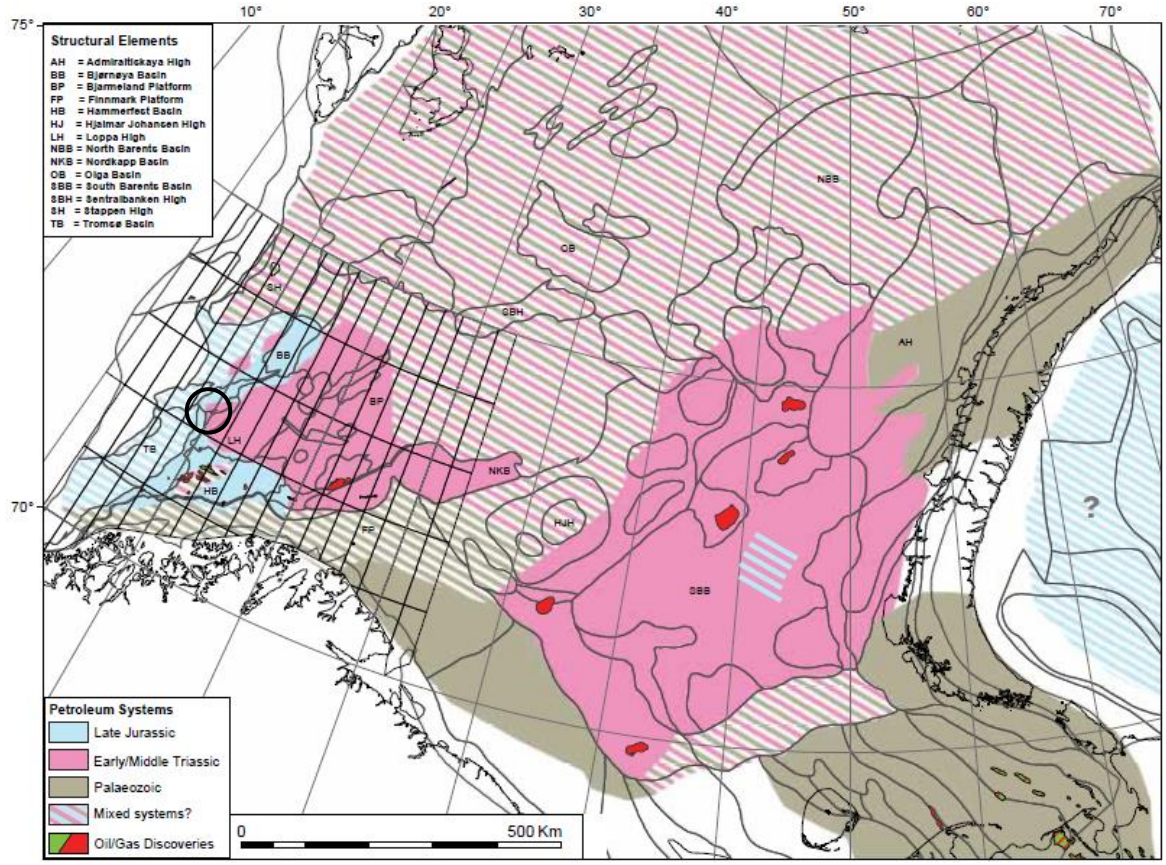

Figure 2.6: Major petroleum systems in the greater Barents Sea. Encircled area is the location of study area. Modified after (Henriksen et al., 2011b).

A petroleum system encompasses a pod of hydrocarbon source rock, migration pathway, reservoir rock, trap and seal. Essentially, it includes all the necessary parameters, processes and elements that are required for the existence of hydrocarbon accumulation (Magoon and Dow, 1994). Petroleum system in the Johan Castberg Field area consists of a source rock (Hekkingen Formation) of Late Jurassic to Early Cretaceous Age, reservoir rocks (Stø and Nordmela and Tubåen formations) with seals of Cretaceous and Upper Jurassic age.

2.6.1 Source Rock

Source rock is a viable element in the petroleum systems that can be defined as; any fine-grained organic rich rock that is capable of producing hydrocarbons at required temperature and pressure. Capability of a source rock depends on its volume, total organic content (TOC) and thermal maturity (McCarthy et al., 2011). A typical source rock mainly dominated by abundance of organic matter deposited in reducing environment. Kerogen expels to oil (60-120°C) and gas (100-200°C) during consequent burial and heating while gas and oil mostly generates from terrestrial and marine kerogen respectively (Doré, 1995).

Table 2. 2: Petroleum plays description for the south-western Barents Sea (Modified from Duran et al., 2013).

Name	Area	Reservoir rock	Source rock	Depositional environment	Trap	Fields/Discoveries
Palaeocene-Supra Palaeocene	Harstad and Sørvestnaget basins	Sandstone	Cretaceous shale	Shallow marine to moderately deep marine	Rotated fault blocks	No source and reservoir rocks have been drilled
Upper Jurassic to Lower Cretaceous	South-western Loppa high, Veslemøy High, Finmark Platform	Sandstone (deposited as lobes down flank from highs)	Upper Jurassic Hekkingen Formation	Shallow marine to moderately deep marine	Fault dependent and stratigraphic pinch-out	Discovery in Well 7120/1-2
Lower to Middle Jurassic	Bjørnøya, Hammerfest and Nordkapp basins	Sandstones of Early to Middle Jurassic	Upper Jurassic shales of Hekkingen Formation	Shallow marine, fluvial, deltaic and estuarine	Rotated fault blocks and horst structures	Johan Castberg, Snøhvit, Albatross, Askeladd and Goliat fields. Discoveries in wells 7120/12-2 and 12-3. 7120/1-2, 7220/5-1 and 7119/12-3
Triassic	Bjørnøya, Hammerfest and Nordkapp basins, Bjarmeland and Finnmark platforms	Sandstones of Upper and Lower Triassic in west and east respectively	Lower Carboniferous coal, Upper Permian shales and Lower Permian marls	Fluvial, deltaic, shallow marine, tidal and estuarine	Stratigraphic	Goliat field, Tornerose, Nucula and Obesum. Discoveries in wells 7226/11-1, 7228/7-1, 7222/11-1, 7125/1-1, 7224/6-1 and 7223/5-1

Several potential source rocks exist in the Barents Sea but the most important source rock with best quality is Hekkingen Formation (Figure 2.7). In the southern Barents Sea, source rock has different stages of maturity because of different burial depth. Hekkingen Formation is considered to be mature enough for generating hydrocarbons only in a narrow belt in Hammerfest Basin and around Loppa High. It is deeply buried in the Tromsø Basin and immature in the area between Hammerfest and Nordkapp basins, however, it has widespread distribution in the southern Barents Sea (Ohm et al., 2008, Doré, 1995).

In general, source rocks in the south-western Barents Sea mainly comprise kerogen Type II and III, with 8-15 wt% total organic content and high hydrogen index, and capable of generating oil and condensates (Fleet and Boldy, 1999). Triassic source rocks are considered to be more mature than Hekkingen Formation. Furthermore, mostly Triassic source rocks have entered to gas window whereas Hekkingen Formation lies in oil window in the south-western Barents Sea (Ohm et al., 2008).

Figure 2.7: Core photographs of black to dark brownish grey claystones of Hekkingen Formation from well 7219/8-1S with depth interval of 4275-4277m. Bioturbation is almost absent and dark black colour indicates that this source rock is deposited in strongly restricted marine basin with reducing environment conditions (www.npd.no).

2.6.2 Reservoir Rock

Stø Formation is the most important reservoir rock in the south-western Barents Sea with excellent porosity, high permeability and higher proportion of clean sand (Ramberg, 2008). According to Riches et al. (1986), Jurassic sandstones possess best potential for hydrocarbon accumulation because these are deposited during a transgressive cycle passing through tidal flat sediments (Nordmela Formation) up into the coastal sands (Stø Formation). The lower Jurassic Nordmela and Tubåen formations also retain hydrocarbons with good quality reservoir sandstone. Nevertheless, 85% of the Norwegian Barents Sea resources 1ie within Stø Formation (Doré, 1995).

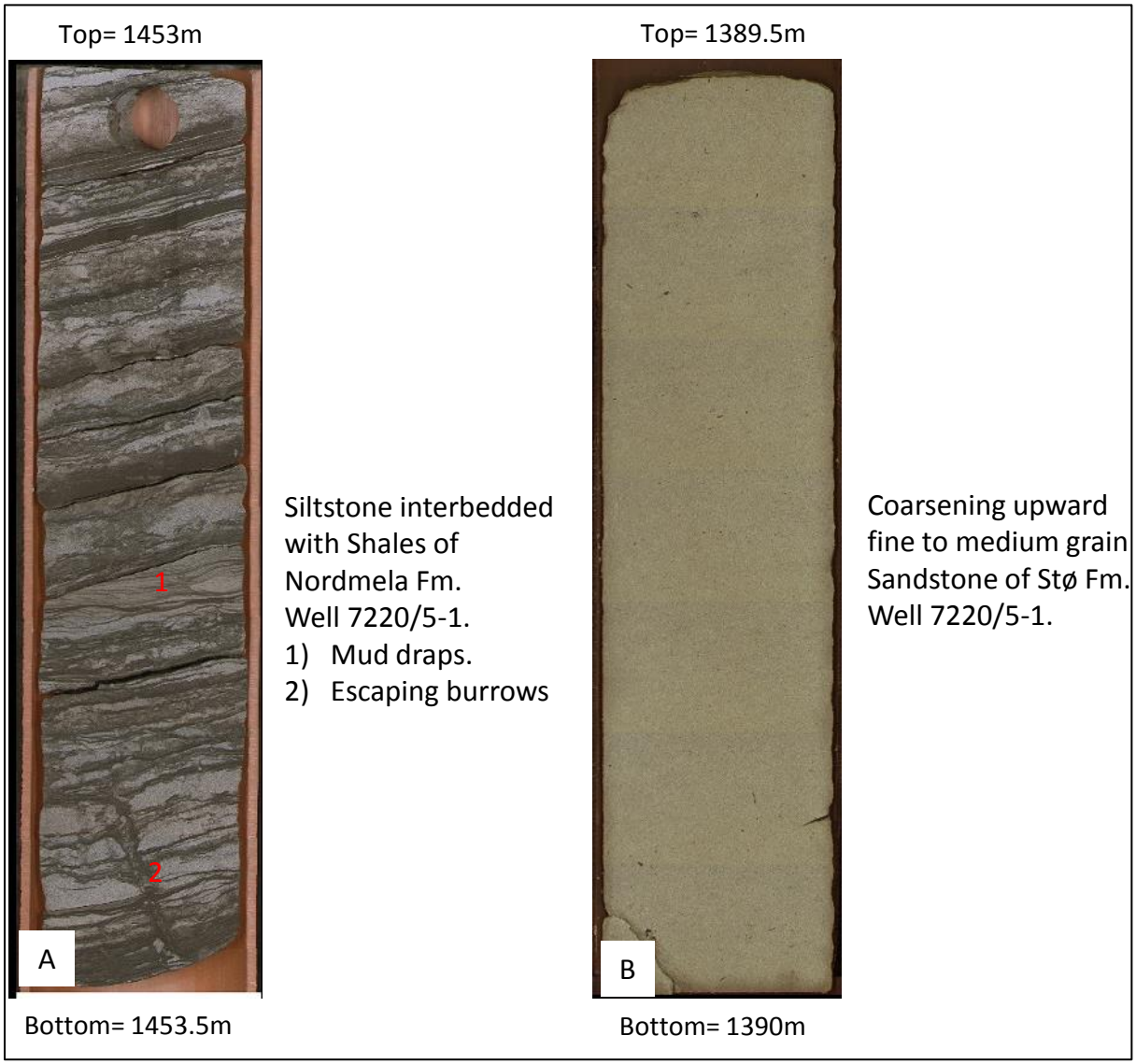

Figure 2.8: Core photographs showing the variation in depositional environments from tidal (A) to coastal plain sediments (B).

The Stø Formation encompasses higher net to gross ratio as compared to Nordmela and Tubåen formations. The Nordmela Formation is dominated by more complex facies and lithologies. Additionally, porosity and permeability is good in the upper part as compared to lower part of Nordmela Formation. In general, sandstones of Stø Formation are coarser in grain size than those of Nordmela Formation. Whereas sandstone of Tubåen Formation deposited by transgressive episodes has average net to gross ratio of 75% in the uppermost part, and it decreases in the middle part (Linjordet and Grung Olsen, 1978, Ramberg, 2008, Gao, 2013).

2.6.3 Sealing and Trapping Mechanism

The south-western Barents Sea is mainly characterized by NE-SW trending faults system. Therefore, most hydrocarbon traps are generally fault bounded positive blocks. There is also possibility of stratigraphic onlaps and pinch-out traps along the basin margins. Upper Jurassic and Lower Cretaceous shales acts as a super-seal in Bjørnøya and Tromsø basins due to excellent sealing capacity (Johansen et al., 1992, Doré, 1995). Intensive tectonic activities in the Barents Sea resulted in fault-bounded and dome-like structural traps that are significantly good for hydrocarbon accumulations (He et al., 2012).

2.6.3.1 Effect of Uplifting on Reservoir Quality and Sealing Mechanism

The Barents Sea has been subjected to tectonic uplift for several times in the geological history. Therefore, maximum burial depth experienced by reservoir should be taken into account for estimating reservoir quality. The amount of uplift calculated in the south-western Barents Sea ranges from 500 m in the west and 1500 m in the east (Henriksen et al., 2011b). The filling mechanism of hydrocarbons in the Stø Formation is influenced by tectonic uplift during Lower Tertiary when the main loss occurred due to spilling out of hydrocarbons from the trap (Figure 2.8) linked with gas expansion and tilting of structure (Duran et al., 2013). Exploration risks have been increased enormously in the Barents Sea leading to the high number of dry wells. Uplifting and erosion has influenced the strength of cap rock in the basin and has increased the chances of escaping hydrocarbons from the structure. Hydrocarbon generation also stopped locally due to significant decrease in temperature and heat produced as a result of uplift and erosion in the south-western Barents Sea (Ben-Awuah, 2013).

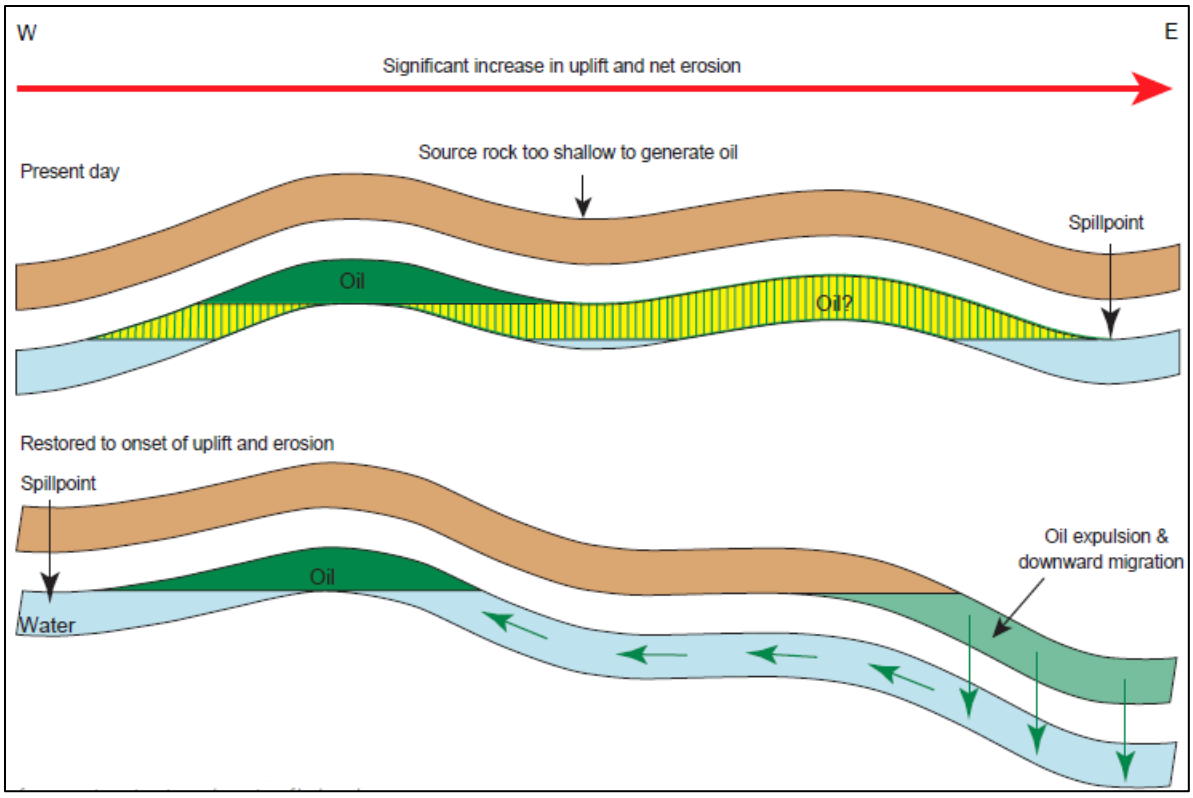

Figure 2.9: Effect of uplifting on structures and hydrocarbon generation, migration and accumulation (Henriksen et al., 2011b).

CHAPTER 3

THEORETICAL BACKGROUND

- PREDICTION OF RESERVOIR QUALITY
- DIAGENESIS
- COMPACTION PROCESSES
- QUARTZ CEMENTATION
- POROSITY PRESERVING MECHANISMS

3.1 Introduction

Sandstones are the dominant reservoir rocks on the Norwegian continental shelf and almost 60% of the petroleum reservoirs are sandstone in the world except in the Middle East. The properties of sandstones are mainly associated with primary composition, which is a function of source area, shallow and deep diagenetic processes, and depositional environment (Bjørlykke and Jahren, 2010). Sandstones have capability to preserve porosity and permeability significantly at greater depths under certain conditions that can add values to the commercial production and economic base for hydrocarbon accumulations.

This chapter deals with diagenetic and compaction processes that are responsible for the alteration of reservoir properties after deposition. The alteration of reservoir properties occurs continuously with depth and time due to combined effect of overburden, temperature, pressure, fluids and chemical processes. Controlling factors and processes are discussed to enlighten their effect on sandstone reservoir properties.

3.2 Prediction of Reservoir Quality

The appropriate reservoir quality is very important in petroleum plays and prospects particularly in which sandstone reservoirs have been subjected to higher temperature (>100°C) and pressure at greater depth for a long time period (Taylor et al., 2010). At shallow depths, sandstone reservoir properties are mainly controlled by sorting, grain size, clay content and mineralogy while in deeply buried sandstones (>4km), major controlling processes are quartz overgrowth, precipitation of quartz cement, illitisation and stylolization. At greater depths, different types of grain coatings are very important in order to preserve porosity and inhibit precipitation of quartz cement (Marcussen et al., 2010). An adequate change in porosity and permeability can be estimated, if all the controlling factors and the processes that can change these parameters are well understood during exploration and production of a hydrocarbon field (Bjørlykke and Jahren, 2010).

According to Manacherry S. (2008) the reservoir quality is mainly controlled by four factors:

1. Depositional porosity and permeability.
2. The degree of mechanical and chemical compaction
3. The amount and type of pore-filling cement.

All the processes that can alter the reservoir quality are discussed below:

3.3 Diagenesis

The sandstone diagenesis is a function of burial rate, sediment composition and texture, sedimentary and tectonic environment, hydrodynamic and geothermal gradients, and chemical reactions. Diagenesis can decrease effective intergranular macro-porosity and permeability but on the other hand, it can also create void spaces through dissolution of soluble components of the rock. Mechanical compaction, chemical compaction and cementation are the three main diagenetic processes responsible for the modification of intergranular porosity during burial of sandstones (Pittman, 1979, Menacherry, 2008). Early diagenetic processes starts at a very shallow depth (<1-10m), where sediments have maximum possibility to react with atmosphere and infiltrated meteoric water close to the ground surface. Diffusion and advection processes are more effective near the surface, so as a result, the potential for sediments to change their bulk composition is much higher at shallow depths than at greater depths (Bjørlykke and Jahren, 2010).

The mineral dissolution at shallow burial depths due to meteoric waterflow plays an important role in the primary clastic composition of sandstone reservoirs (Figure 3.1). Carbonic acid and sulphuric acid generated by acidic rainwater speed up the weathering reactions. At the same time, silicate minerals like feldspar neutralize this acidity by weathering reactions. The precipitation of kaolinite is resulted by the dissolution of feldspar and micas with meteoric water. Cations like Na^+ and K^+ from potassium feldspar and micas brought into solution and therefore, precipitation of kaolinite need constant supply of freshwater because the reaction products K^+ and Na^+ requires to remove from feldspar and mica (Bjørlykke and Jahren, 2010). These reactions can be written as below:

$$\underset{\text{Feldspar}}{2K\,(Na)AlSi_3O_8} + 2H^+ + 9H_2O \longrightarrow \underset{\text{Kaolinite}}{Al_2Si_2O_5(OH)_4} + \underset{\text{dissolved silica}}{4H_4SiO_4} + \underset{\text{dissolved cations}}{2K+\,(2Na^+)}$$

$$\underset{\text{Muscovite}}{2KAl_3Si_3O_{10}\,(OH)_2} + 2H^+ + 3H_2O \longrightarrow \underset{\text{Kaolinite}}{3Al_2Si_2O_5\,(OH)_4} + \underset{\text{dissolved cations}}{2K^+}$$

This above reaction produces secondary porosity by dissolving soluble components of rock but conversely, precipitation of kaolinite reduces the porosity and permeability as pore-filling mineral (Bjørlykke and Jahren, 2010).

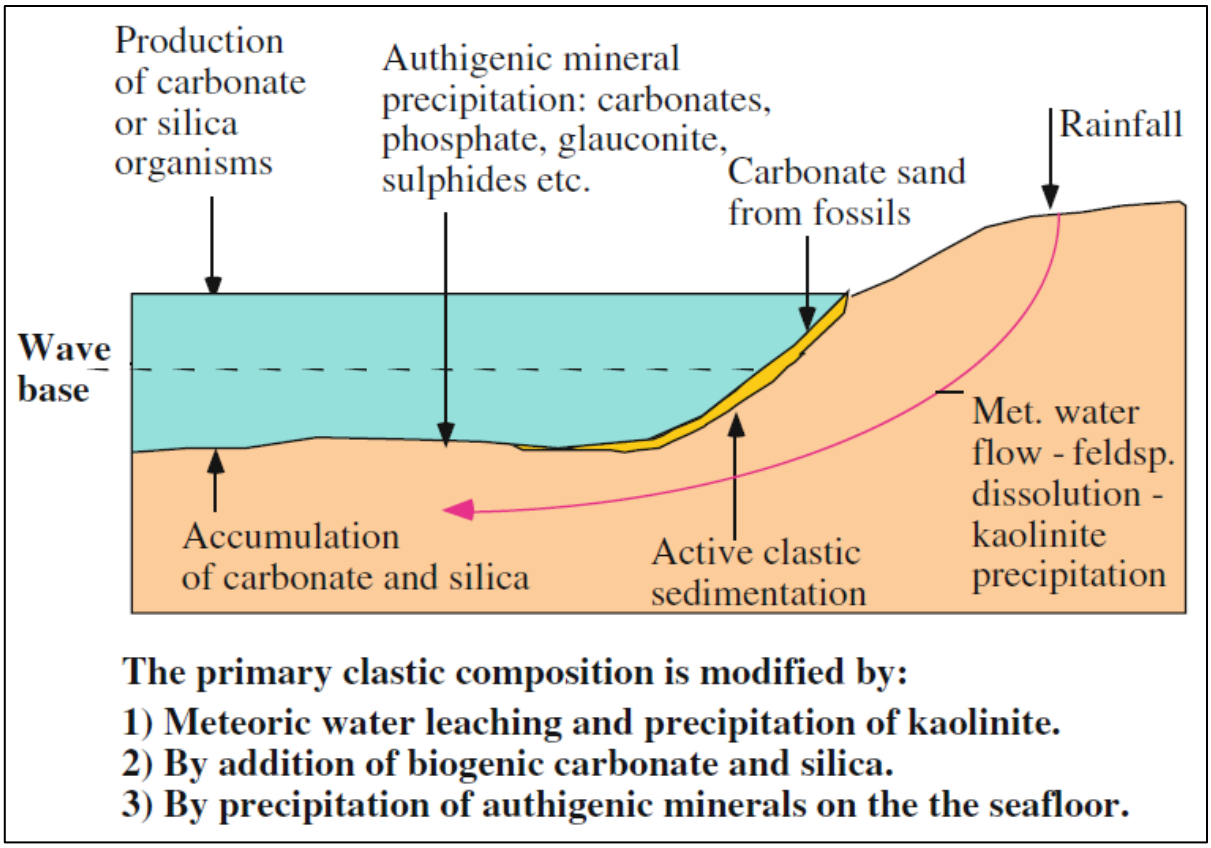

Figure 3.1: Schematic illustration of diagenetic processes in the shallow marine environment (Bjørlykke and Jahren, 2010).

Furthermore, this precipitated kaolinite is exposed to illitisation process at greater depth (3.5-4 km) and above 130°C whereas illitisation of smectite takes place at relatively lower temperature range (65-100°C). The presence of K^+ ions from the dissolution of K-feldspar is necessary for the precipitation of illite. Occasionally, illitisation is not coherent with petrographical observations which indicate existence of kaolinite mineral together with K-feldspar in a partly illitized sandstones (Meunier and Velde, 2004).

$$KAlSi_3O_8 + Al_2Si_2O_5(OH)_4 \longrightarrow KAl_3Si_3O_{10}(OH)_2 + 2SiO_2 + H_2O$$

K-Feldspar Kaolinite Illite Quartz

Authigenic illite replaces kaolinite from the pore spaces and has fibrous and bridging morphology that influences strongly on the reservoir quality in the sandstone. The probability of illite precipitation from smectite in semi-arid to arid environment is relatively higher than humid environment. However, smectite can act as the precursor for chlorite coatings in semi-arid to arid environments (Chuhan et al., 2000, Maast, 2013)

3.4 Compaction Processes

Bulk volume reduction in the rock due to grain rearrangement, plastic deformation, dissolution, and brittle deformation is known as compaction. Compaction processes are controlled by burial history and lithology of sediments and are divided into mechanical and chemical compaction (Menacherry, 2008).

3.4.1 Mechanical Compaction

The mechanical compaction is defined by the rearrangement of newly deposited loosely packed sediments at shallow depth into densely rigid compacted sediments as a result of grain slippage, twisting, rotation and brittle fracturing (Menacherry, 2008, Burley and Worden, 2009).

In general, well-sorted sand still behave as loose sand up to depth of 2 km if it is not calcite-cemented. However, experimental data shows that sands reduced porosity from 40% to 25% during mechanical compaction at lithostatic pressure of 25 MPa (Figure 3.2). Temperature is relatively less involved in mechanical compaction as compared to chemical compaction (Bjørlykke and Jahren, 2010).

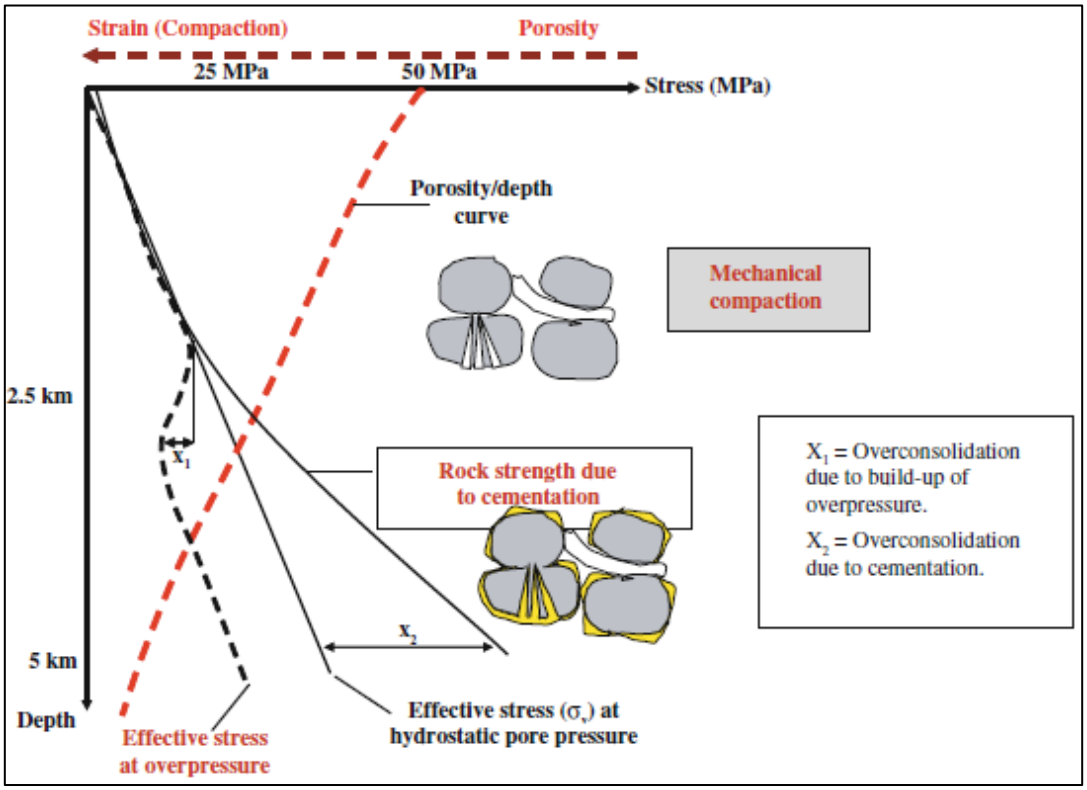

Figure 3.2: Mechanical compaction of sandstone as a function of effective stress by grain reorientation and grain breakage. Quartz cementation makes the sandstone more stiffer at higher depth (Bjørlykke and Jahren, 2010).

3.4.2 Sandstone Reservoirs Buried to Intermediate Depth

Quartz cementation start at intermediate depths and further compaction processes are mainly controlled by mineral dissolution and precipitation (figure 3.3). Experimental data shows that quartz cementation generally takes place above 75-80 °C on the Norwegian continental shelf (Bjørlykke and Jahren, 2010, Walderhaug, 1994).

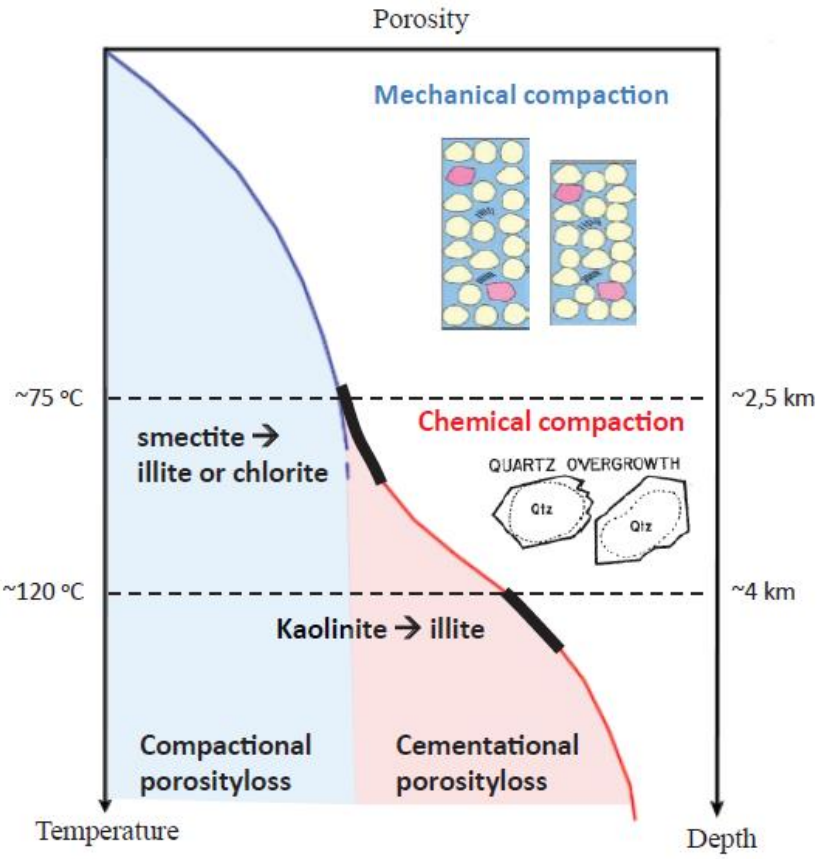

Figure 3.3: Important diagenetic processes in clastic sandstone reservoirs (Maast, 2013).

3.4.3 Deeply Buried Sandstones (>3.5-4 km, >120°C)

Quartz cementation is the main cause of porosity loss in deeply buried quartzose sandstone reservoirs in different basins. Porosity and permeability decreases significantly in sandstone reservoirs from burial depth of 3.5 to 4.5 km and at temperatures higher than 120°C. Furthermore, quartz cementation continues until nearly all the porosity is lost or temperature drops below 70 - 80°C due to erosion or uplifting of the area (Figure 7.1).

The quartz cementation may increase by 30-40% between the burial depth of 3 to 4 km and the rate of precipitation may increase four times due to higher temperatures (100-140°C). At more than 6-7 km burial depth (200-300°C), sandstones are metamorphosed to a well-cemented hard quartzite and available porosity is filled by quartz cementation (Bjørlykke and Jahren, 2010).

Pressure solution is a key process in deeply buried sandstone reservoirs. In fact, this is a deformation mechanism that encompasses dissolution of quartz at grain-to-grain contacts into liquefied material under higher stresses (Robin, 1978).

Stylolites are saw-like dissolution surfaces formed by pressure solution within sandstone reservoirs (Figure 3.4). Stylolites have significant impact on the reservoir quality because of their control on precipitation, deformation, dissolution and fluid transport in deeply buried sandstone reservoirs (Aharonov and Katsman, 2009). The dissolution of quartz and diffusive transportation of silica into the interstylolite volume creates supersaturation of silica, where it precipitates as cement. Furthermore, the concentration of silica along the stylolite would be highest and may decrease away from the stylolites showing degree of transport (Wangen, 1998, Bjørlykke and Jahren, 2010).

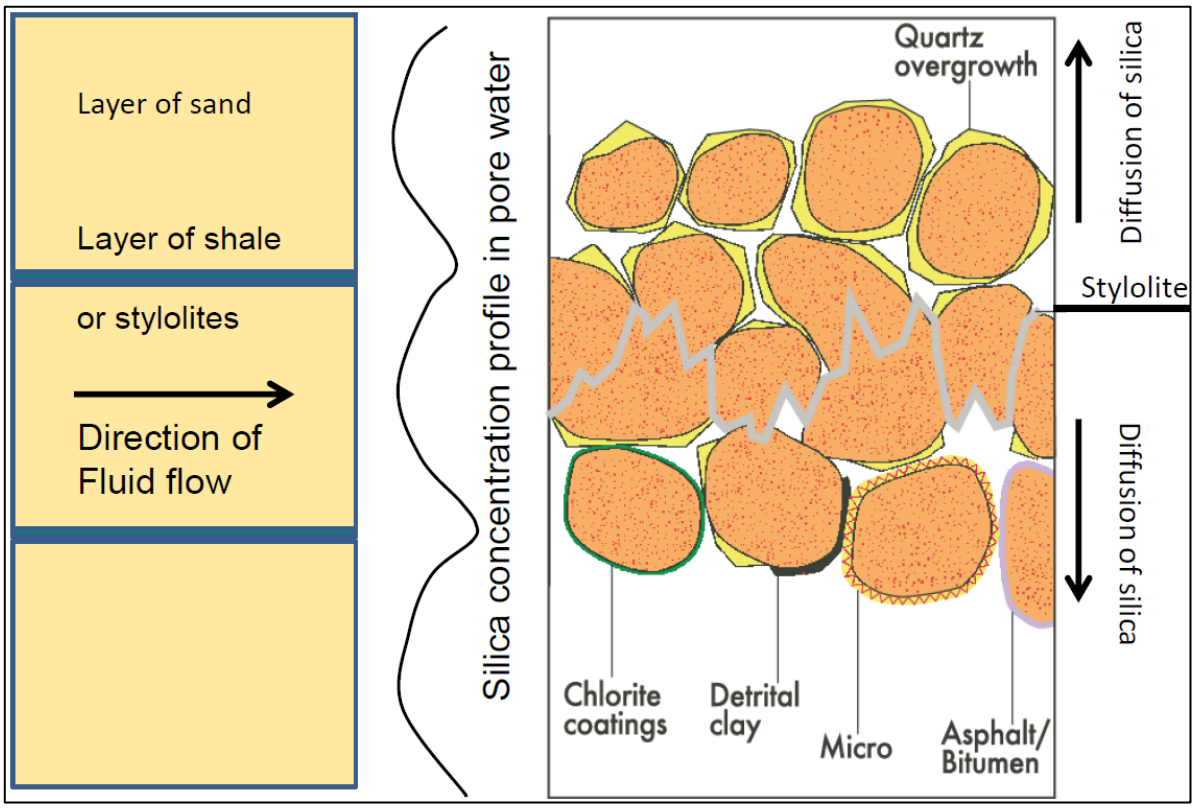

Figure 3.4: Schematic illustration of a stylolite. Diffusion of silica occurs away from the clay rich stylolite. Different types of grain coatings such as chlorite, detrital clay, micro-quartz and asphalt to retard quartz cementation (Bjørlykke and Jahren, 2010).

According to Walderhaug and Bjørkum (2003), the Lower-Middle Jurassic sandstones of Stø Formation have good reservoir quality than other sandstones with similar temperature histories because of less quartz cementation and low abundance of stylolite.

3.4.4 Quartz Cementation

Quartz is the most dominant diagenetic mineral in sandstones and quartz cementation is the main controlling process responsible for the changes in the physical properties of sandstones during burial history. In addition, petrographic and geochemical information acquired from quartz cementation process helps for the better understanding of burial and diagenetic history of sandstone reservoirs (Harwood et al., 2013, Worden and Morad, 2000).

Quartz cementation destroys porosity significantly in relatively well-sorted quartz arenites and feldspathic sandstones. The amount of precipitated quartz cement depends on the time-temperature integral and the grain surface available for quartz cementation. The amount of quartz cementation will be higher in the areas with high geothermal gradients and slow subsidence rates. The rate of quartz cementation increases by a factor of 1.7 for every 10°C increase in temperature. However, it is also function of time and available surface area for precipitation (Walderhaug, 1994, Bjørlykke and Jahren, 2010). Figure 3.5 delineates that the shrinkage of volume or porosity loss (compaction) will be higher and fast at higher temperatures than at lower temperature.

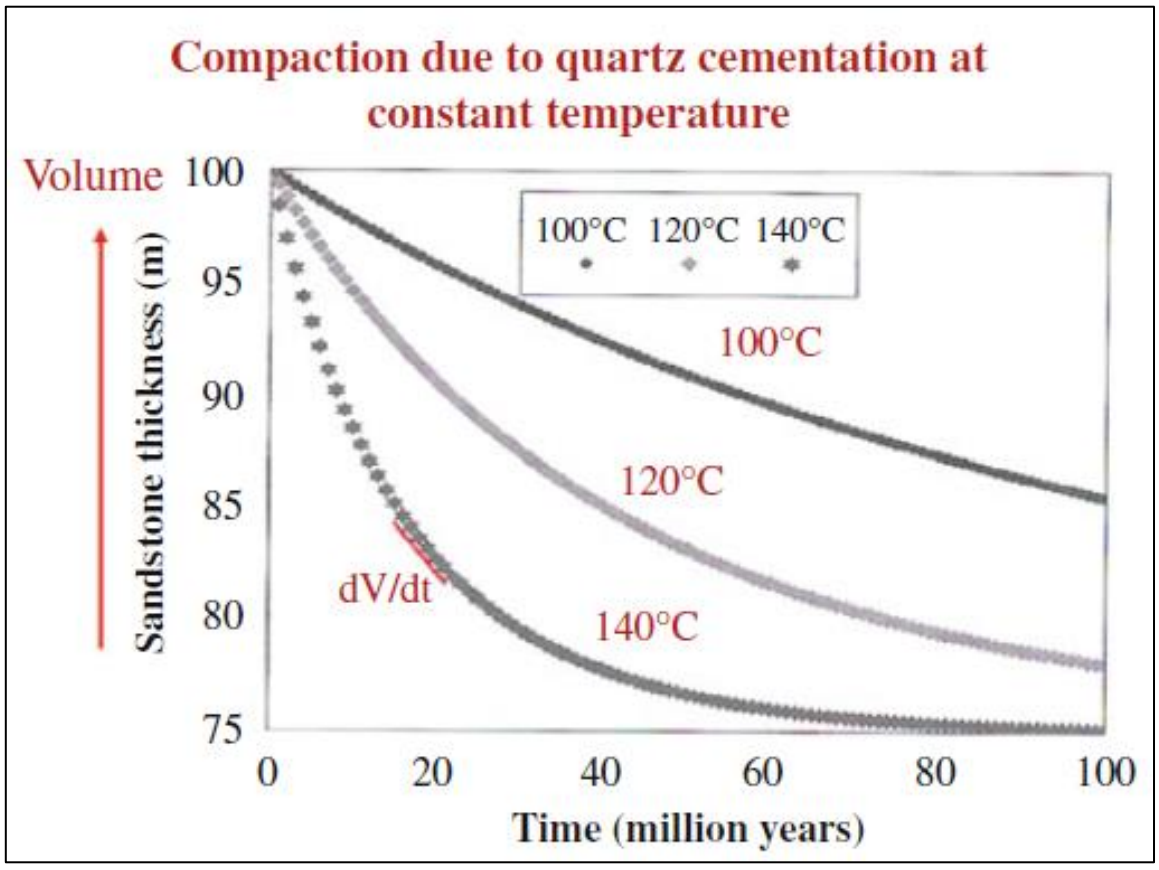

Figure 3.5: Quartz cementation and chemical compaction due to quartz cementation as a function of temperature and time (Walderhaug et al., 2001).

3.5 Porosity Preserving Mechanisms

Porosity preserving mechanisms such as different grain coatings are very important to preserve quality of deeply buried (>3-4 km) sandstone reservoirs. In general, grain coatings have the capability to stop quartz over-growth if developed on the grain surfaces prior to quartz cementation (Hussain, 2012). Different mechanisms that can help in preserving porosity and permeability in deeply buried sandstones are described below.

3.5.1 Grain Coats

Grain coats have a critical control on quartz cementation in sandstones and form on the framework grain (Figure 3.6). The effectiveness of grain coats in order to retard quartz cementation depends on their; 1) origin, 2) thermal history and grain size, 3) completeness and 4) the abundance of quartz grains. Grain coatings commonly include clays and microcrystalline quartz. However, it has very less effect in sandstones with less quartz cement (Bloch et al., 2002).

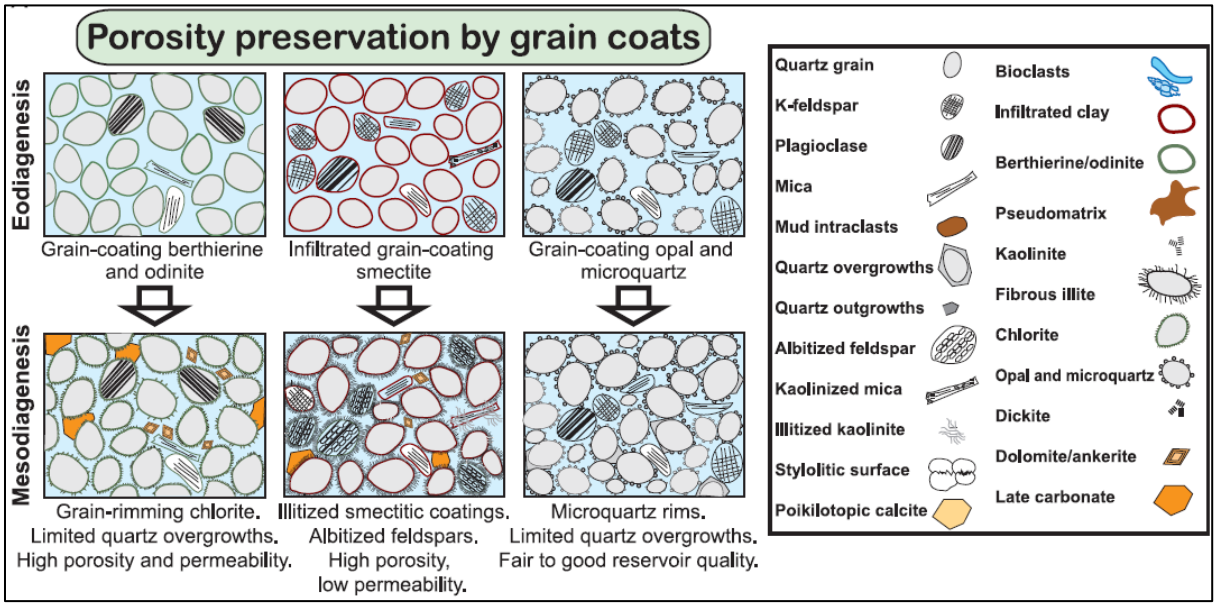

Figure 3.6: Diagram showing porosity preserving mechanisms by grain coatings during diagenetic processes (Morad et al., 2010).

3.5.1.1 Clay coating

Authigenic clay coatings such as chlorite and illite have long been recognized as a more effective coating in deeply buried sandstone reservoirs. In general, sandstones with insufficient clay coating have poor reservoir quality due to intensive quartz cementation but

on the other hand, complete coating of clay minerals preserves very good reservoir quality even in deeply buried sandstones (Maast, 2008).

Chlorite coating is the most important and effective clay coating in order to retard quartz cementation in sandstones because it has the tendency to develop continuous layering around detrital quartz grains. Authigenic chlorite coats have several origins due to differences in provenance and composition (Taylor et al., 2010, Bloch et al., 2002). According to Ehrenberg (1993), iron-rich chlorite coating present in the Lower-Middle Jurassic sandstones of Norwegian continental shelf is deposited in shallow marine environments.

3.5.1.2 Microcrystalline Quartz

Micro-quartz coating acts the same as clay coating that forms on the surface of detrital quartz grains. Normal quartz overgrowth follows the crystallographic orientation of the parent detrital grain whereas micro-quartz overgrowths occur in the random orientation and hinder the formation of normal quartz overgrowths (Pittman, 1972, Bloch et al., 2002).

The precipitation of micro-quartz usually occurs at lower temperature (60-80°C) when porewater is supersaturated with respect to quartz. Micro-quartz precipitation occurs in thin layers at high silica supersaturation sourced from organic silica (sponges). The permeability and porosity values are mostly higher if all the grains in the sandstone are coated with micro-quartz cement (Bjørlykke and Jahren, 2010, Aase et al., 1996).

According to Ramm et al. (1997), it is well noticed that "*The early deposition of small quartz crystals on grain surfaces was an important factor in the porosity preservation. These crystals provided cement when primary porosity was high, but only occupied a small proportion of the porosity. With further burial the crystals inhibited the deposition of larger pore-filling quartz and feldspar overgrowths*".

3.5.2 Hydrocarbon Emplacement

According to Walderhaug (1996), quartz cementation depends on the wettability of reservoir and may stop in an oil-wet hydrocarbon filled reservoir while it will continue in water-wet reservoir. In the oil-wet scenario, precipitation of quartz cement hindered because the silica-bearing water cannot access to detrital quartz grain surface. The tendency to stop quartz cementation and dissolution increases with increasing oil-wetting conditions, the more oil-wet system, the less quartz cementation occurs (Bloch et al., 2002, Worden et al., 1998).

CHAPTER 4

DATA AND METHODS

- WELL DATA CORRELATION AND PETROPHYSICAL EVALUATION
- PETROGRAPHIC EVALUATION
  - OPTICAL MICROSCOPY AND POINT COUNTING
  - THIN SECTION OBSERVATIONS
  - SCANNING ELECTRON MICROSCOPE (SEM)
  - X-RAY DIFFRACTION (XRD)
  - CORE ANALYSIS

4.1 Introduction

Several techniques have been applied on the 15 samples from the well 7220/5-1 to estimate mineralogy, quartz over growth, sorting and porosity within the Stø and the Nordmela formations using XRD (X-ray diffraction), thin section microscopy and SEM (Scanning electron Microscopy) analysis. Core photos are also studied for sedimentological interpretation from depth 1458m to 1337m and the well information has been obtained from the Norwegian Petroleum Directorate (Table 4.1).

Table 4. 1: General information of the well 7220/5-1 (www.npd.no).

Well 7220/5-1	
Type	Exploration
Purpose	Appraisal
Main area	Barents Sea
UTM Zone	33
Wellbore contents	Oil and Gas
Bottom hole temperature (˚C)	52
Water depth	388m
Total Depth (MD)	1740m
Deepest penetrated age	Late Triassic
Oldest penetrated Fm.	Fruholmen Fm.

The following workflow chart describes the processes carried out during this research work.

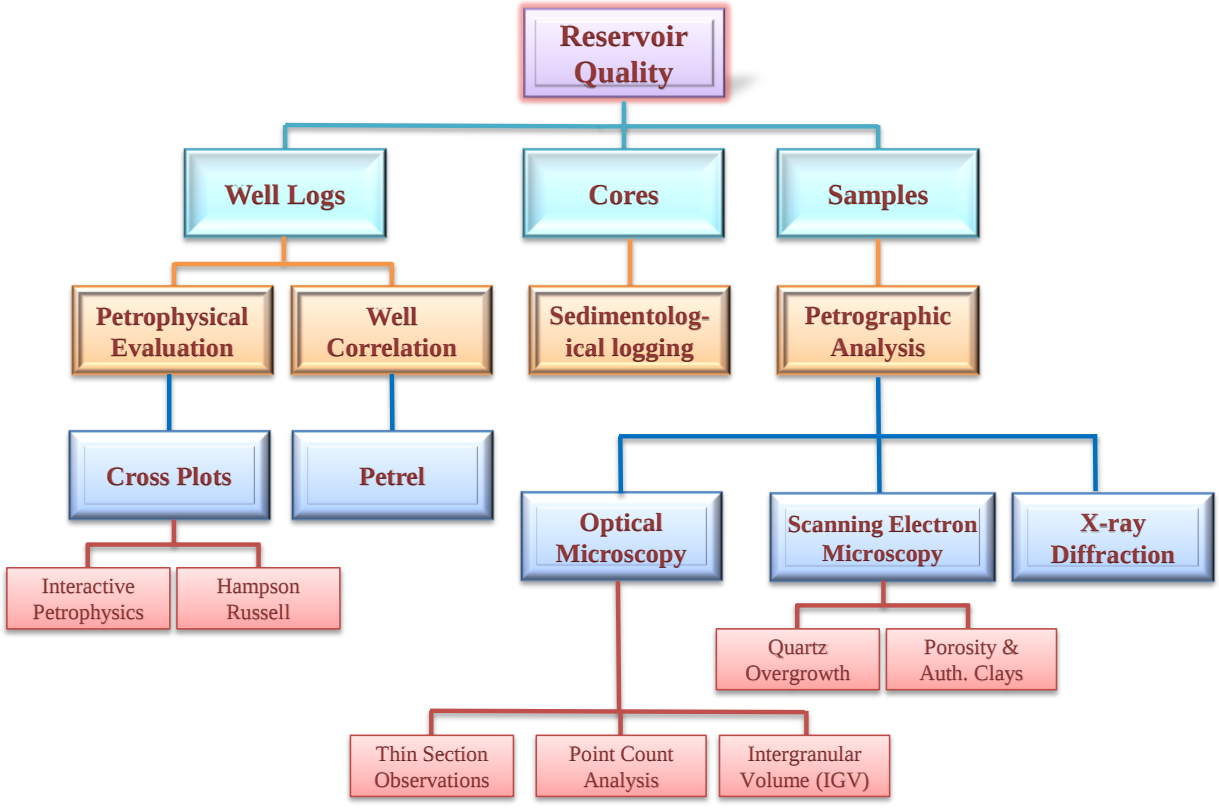

Figure 4. 1: Workflow chart of this study.

4.2 Well Log Correlation and Petrophysical Evaluation

Stratigraphic correlation of closely spaced three wells (7220/5, 7, 8-1) in the Johan Castberg Field has been performed to distinguish different lithologies. The main purpose of well correlation is to correlate the Lower-Middle Jurassic sandstones across the three wells. Different lithostratigraphic units are identified on the basis of gamma ray (GR), bulk density (RHOB) and neutron porosity (NEU) logs.

Well log correlation is very useful in identification of cap rock and reservoir rock. Cap rock (usually shales) gives higher GR values whereas reservoir rock shows lower GR values. The geological and tectonic setting of an area can be predicted by thickness correlation of same lithostratigraphic unit in different wells. Well log correlation of lithostratigraphic units is very important in order to understand:

1. Facies distribution.
2. Lateral and vertical variations of lithostratigraphic unit.
3. Geological and depositional setting.
4. Hydrocarbon rich zones (especially from neutron porosity-density crossover).

Well correlation, Histograms and cross-plots of different logs were made using Petrel 2013, Interactive Petrophysics V4.3 and Hampson-Russell V2.1. These well logs are used as additional tool for SEM, thin section microscopy and XRD analysis. Furthermore, interpreted well tops are exported from Petrel to Hampson-Russell and Interactive Petrophysics for more comprehensive analysis of reservoir quality. Total and effective porosities have been calculated from density logs.

4.2.1 Temperature Gradient:

Temperature gradient has been calculated for the estimation of maximum temperature experienced by reservoir sandstones. It is derived from bottom hole temperature (BHT) in wells 7220/5-1 and 7220/7-1. The formula used for the estimation of temperature gradient can be written as:

$$m = \frac{y-c}{x} \quad \ldots\ldots\ldots\ldots\ldots\ldots\ldots\ldots\ldots\ldots\ldots\ldots \quad (3.1)$$

Where, m is the geothermal gradient, y is the bottom hole temperature (BHT), c is the mean annual surface temperature and x is the total depth. Mean surface temperature has been considered 4 ^{o}C in this study.

4.2.2 Estimation of Uplift

The amount of uplift has been calculated in wells 7220/5, 7, 8-1 to obtain adequate maximum burial depth of reservoir sandstones prior to uplift. It is estimated by comparing Vp with published reference curve by Mondol (2009).

4.3 Petrographic Evaluation

Petrographic analysis is performed by using X-ray Diffraction (XRD), (Scanning Electron Microscopy (SEM) and Optical Microscopy on 15 samples from the well 7220/5-1 (table 4.2).

Table 4.2: Table illustrates the depth and formations of samples used in petrographic analysis.

Sample	Depth	Formation
1	1340.15	Stø Formation
2	1345.05	Stø Formation
3	1349.36	Stø Formation
4	1356.07	Stø Formation
5	1363.03	Stø Formation
6	1369.77	Stø Formation
7	1373.10	Stø Formation
8	1379.50	Stø Formation
9	1420.70	Nordmela Formation
10	1425.76	Nordmela Formation
11	1431.72	Nordmela Formation
12	1436.20	Nordmela Formation
13	1439.80	Nordmela Formation
14	1444.36	Nordmela Formation
15	1449.35	Nordmela Formation

4.3.1 Optical Microscopy and Point Counting

Point counting is a statistical technique that involves recording of different information at each point under the optical microscope. It has been carried out on all 14 samples for quantitative volume analysis of minerals, matrix and porosity under microscopic study. All these parameters are estimated by 300 point counts for each thin section.

4.3.1.1 Intergranular Volume (IGV)

Intergranular volume (IGV) can be defined as a sum of intergranular porosity, cements and detrital clay matrix (Walderhaug and Bjørkum, 2003). These parameters have been calculated by point counting. Intergranular volume (IGV) gives clues about degree of compaction in the sandstone reservoirs. Furthermore, it is an indicator of diagenesis that can provide important

information about porosity loss in sandstone reservoirs when plotted against depth (Szabo and Paxton, 1991).

4.3.2 Thin Section Observation

The reservoir properties of the Stø and the Nordmela formations have been examined extensively using thin section observations under a Nikon Optiphot-Pol petrographic microscope. The information acquired from thin section observations include grain size, mineralogy, micro-quartz overgrowth, grain coating, cementation, grain shape and sorting.

4.3.3 Scanning Electron Microscopy (SEM)

Scanning Electron Microscopy (SEM) is a technique for high-resolution imaging of surfaces. It can provide much more detailed images with better resolution than an optical scope due to relatively shorter wavelength. In this technique, samples are placed both in low and high vacuum to investigate heavy and light minerals with high-resolution. Cathode luminescence (CL) responses are used for differentiating authigenic quartz from detrital quartz grain.

JEO2 JSM-6460LV Scanning Electron Microscope (SEM) with a LINK INCA Energy Dispersive X-Ray (EDX) system has been used for studying both gold mounted stubs and carbon coated thin sections. Quartz overgrowth, illitisation, porosity and cementation are very easy to observe in Scanning Electron Microscope (SEM).

4.3.4 X-Ray Diffraction (XRD)

XRD technique has been implemented in combination with other techniques to obtain a comprehensive and integrated approach to petrographic evaluation. It provides reliable results for mineral identification and is useful for identifying fine-grained minerals and mixtures of minerals. Moreover, XRD can provide quantitative volume fractions of minerals in a sample.

Bulk analysis by XRD has been performed on 15 samples for the quantitative determination of minerals. Numerical calculation includes a data table with weight percent mineralogy. In this analysis, firstly 5 grams of each sample is crushed and then pulverized in a pulverizing mill for 12 minutes until a homogenous powder is obtained. Then this homogenous powder is placed against glass to provide stable surface analysis. At the end, these prepared samples are placed in the XRD machine and final results are interpreted by using DIFFRAC.EVA V2.1 and Profex softwares (see Appendix B 11).

Following minerals have been identified and quantified.

- ***Quartz:*** The XRD response at 3.34 Å with (001) basal reflection.
- ***Clay Minerals:***
  - Illite/Mica: 001 reflection identified at 10.0 Å.
  - Kaolinite: XRD response of Kaolinite at 7.15 Å with basal (001) reflection. While it has (002) reflection at 3.58 Å.
- ***Feldspars:***
  - Microcline: The 001 Reflection at about 3.24 Å is used.
  - Plagioclase/Albite: The 001 reflection at about 3.19 Å is used.
- ***Carbonates and Evaporates:***
  - Calcite: XRD response at about 3.03 Å is used.
  - Halite: XRD response at about 2.82 Å is used.
  - Gypsum: XRD response at about 3.07 Å is used.
- ***Iron and Zinc Sulfides:***
  - Pyrite: The 001 reflection at about 2.71 Å is used.
  - Sphalerite: The 001 reflection at about 3.12 Å is used.

4.3.5 Core Analysis

Core logging of well 7220/5-1 (116m) was carried out by Saad Ullah Nisar at the Weatherford laboratories in Stavanger and later on it has been modified by core photos provided by the TullowOil Norge. A standard logging sheet was used for logging at a scale of 1:100 (appendix A1). Observation of grain size, shape and sorting were made by using hand lens whereas all other sedimentary structures like ripple marks, cross bedding, and bioturbation are directly observed and plotted on the logs by using SedLog software. In addition, different facies have been identified on the basis of core logging. The depositional environment of Lower-Middle Jurassic sandstone reservoirs has been determined on the basis of sedimentological features.

CHAPTER 5

WELL LOG CORRELATION AND PETROPHYSICAL EVALUATION

- INTRODUCTION
- WELL LOG CORRELATION
- PETROPHYSICAL ANALYSIS
- DECLARATION OF HYDROCARBONS
- HISTOGRAMS AND CROSS PLOTS
- OVERPRESSURE
- EXHUMATION

5.1 Introduction

Main objective of this chapter is to evaluate petrophysical properties of Stø and Nordmela formations in wells (7220/5, 7, 8-1). These three wells are closely spaced in the west of Loppa High and Bjarmøyrenna Fault complex. Well 7220/5-1 is used for petrophysical analysis and it is located 3km to the north of wildcat well 7220/8-1. In fact, this well was drilled to upraise Skrugard Discovery 7220/8-1 (www.npd.com).

The Skrugard structure is separated into three different parts by erosion features and has a saddle point that further isolates three gas-oil contacts. The appraisal well 7220/5-1 is located in the middle part while the wildcat well 7220/8-1 is situated in the southern part of Skrugard structure. General information's of these three wells are mentioned in the table 5.1.

Table 5. 1: Summary sheet of wells used for well correlation and petrophysical analysis.

General Information	Well 7220/5-1	Well 7220/8-1	Well 7220/7-1
Type	Exploration	Exploration	Exploration
Purpose	Appraisal	Wildcat	Wildcat
Wellbore contents	Oil and Gas	Oil and Gas	Oil and Gas
Bottom hole temperature (˚C)	52	N/A	72
Water depth	388m	374m	365m
Total Depth (MD)	1740m	2222m	2230m
Deepest penetrated age	Late Triassic	Late Triassic	Late Triassic
Oldest penetrated Fm.	Fruholmen Fm.	Snadd Fm.	Fruholmen Fm.

5.2 Well Correlation

Well log correlation has been carried out on the basis of depositional sequences. Clean sandstone, silty sandstone, sandy silt and shale facies are identified on the basis of gamma ray values. These facies are deposited as a result of progradational, aggradational and retrogradational episodes. The Lower-Middle Jurassic Tubåen, Nordmela and Stø formations of Kapp Toscana group have been correlated using neutron-density crossover, facies, and gamma ray logs (Figure 5.1). Furthermore, neutron-density crossover shows that the Stø Formation consists of more clean and thick sandstone throughout the area. The sandstone proportion increases upward in the Nordmela Formation while the lower part majorly consists of shales with gamma ray values greater than 100API.

Tubåen Formation consists of alternating beds of shales and sandstones with upward increasing shale content. The formations tops are shallower in wells (7220/5, 8-1) located in the eastern part of Bjørnøya Basin while it deepens towards west in the well (7220/7-1).

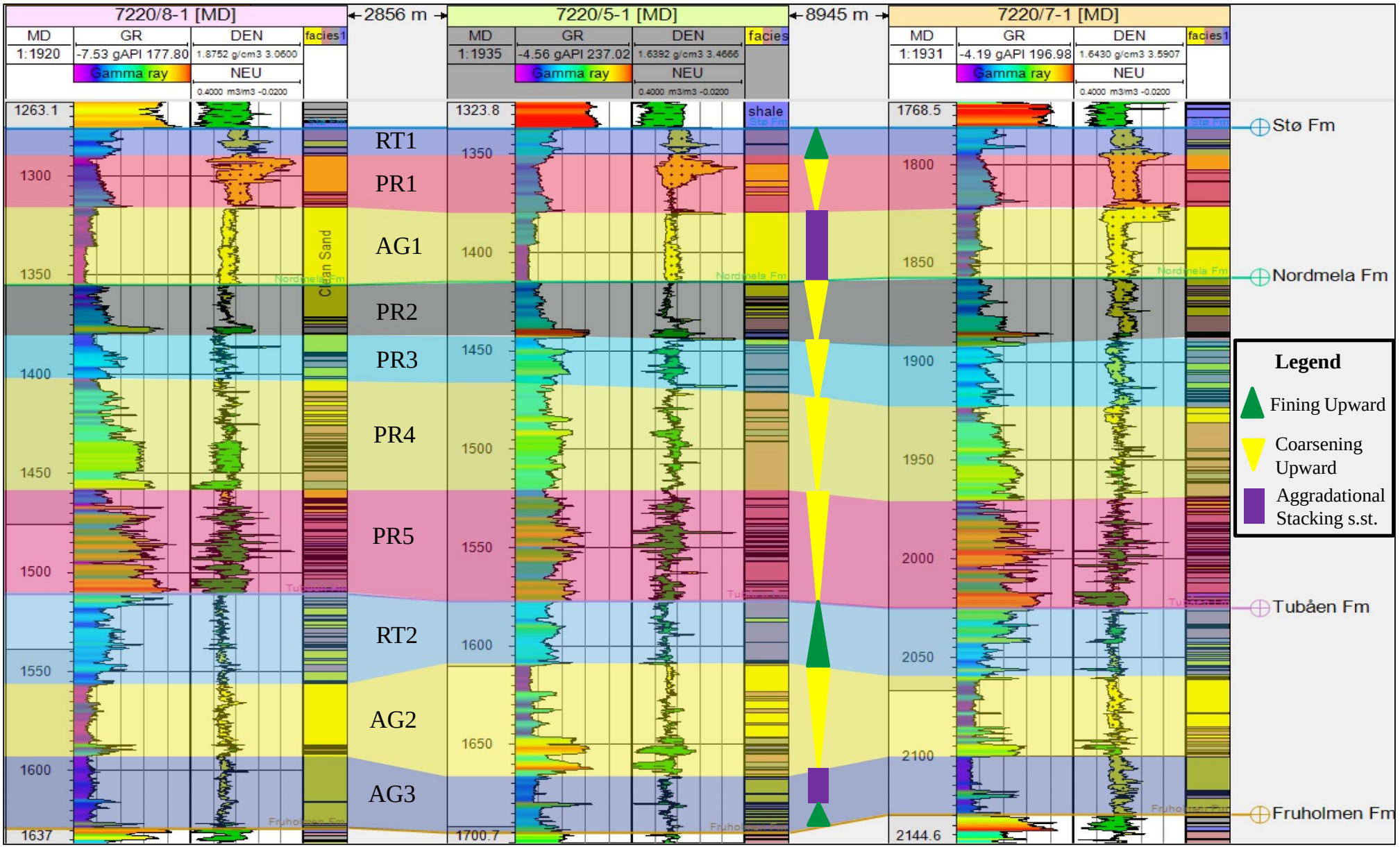

Figure 5. 1: Well correlation of depositional sequences within of Lower-Middle Jurassic Tubåen, Nordmela and Stø formations (RT: retrogradational, PR: progradational and AG: aggradational parasequences).

In addition, well logs have been integrated with core photos, thin sections and SEM results to obtain adequate conclusions (figure 5.2). For example, gamma ray log with a value of 30 API at 1356m depth indicates clean sandstone that is further confirmed by thin section microscopy, core photos and SEM analysis.

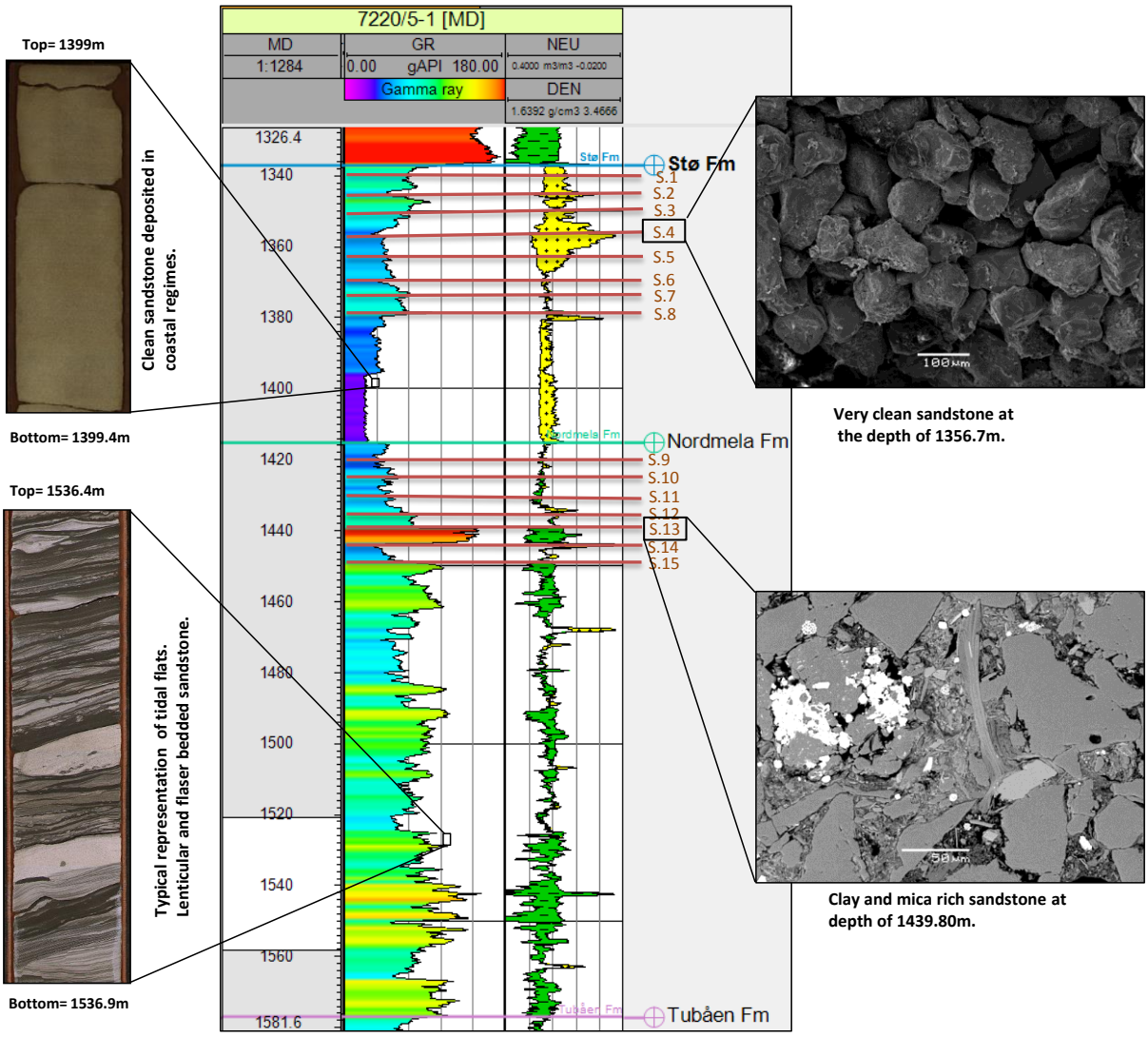

Figure 5. 2: Integrated study of well logs together with core photos and SEM images.

5.3 Petrophysical Analysis

Petrophysical analysis has been carried out in the key well (7220/5-1) to obtain reservoir properties such as porosity and volume of shale. The porosity values are derived from density and sonic logs. Lithologies have been differentiated and sandstone intervals are characterized using gamma ray, V_shale, and neutron porosity logs.

5.3.1 Declaration of Hydrocarbons

The hydrocarbon zones are identified on the basis of deep resistivity, gamma ray log and neutron-density crossover in the well 7220/5-1 from 1414m to 1337m (Figure 5.3). These logs confirm the presence of hydrocarbons within Stø Formation. Moreover, porosity logs have been generated by using standard formulas to extract more detailed information within the reservoir area.

Volume of shale has been calculated by using Larionov (1969) equation for the older rocks (Schön, 2011). The Lower V_shale values and the higher effective porosity values are indicative of good quality reservoir sandstones in the Stø Formation (figure 5.3). The higher resistivity values in the clean sandstone units of lower Stø Formation indicate presence of hydrocarbons. The lower part has comparatively good reservoir quality than the upper part of Stø Formation because of fining upward trend. There is almost no effective porosity just above the reservoir that indicates appropriate seal for the hydrocarbon accumulation.

The sandstone reservoir has been divided into two parts on the basis of resistivity and type of hydrocarbons. The lower part contains oil and consists of very clean sand with less than 40gAPI values. Effective porosity values are higher (18-26%) in the lower part of reservoir whereas these values are less than 18% in the upper part due to presence of shale. The upper part of reservoir contains gas and consists of silty sandstones.

5.3.2 Histograms and Crossplots

Several well logs have been used for histogram and crossplots to get a great deal of information from the well 7220/5-1.

5.3.2 .1 Gamma Ray Histogram

The gamma ray log is lithological indicator and histogram of gamma ray values has been created to differentiate shale from sandstone in the Lower to Middle Jurassic formations. Figure 5.4 shows gamma ray cutoff values used for the differentiating lithologies i.e. clean sand (20-45 API), silty sand (45-70), sandy silt (70-100) and shales (100-150). Histogram shows that the sandstone proportion is higher than the shales in the Lower-Middle Jurassic Tubåen, Nordmela and Stø formations.

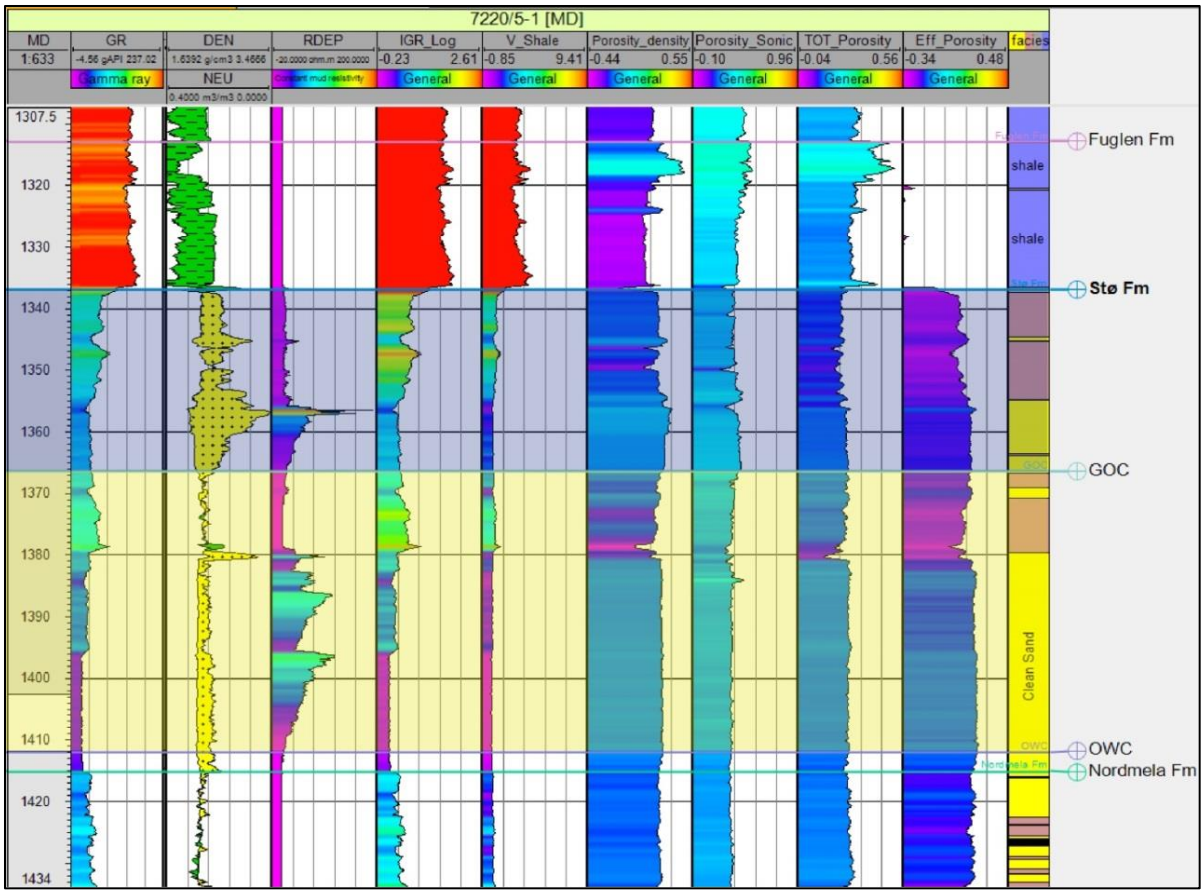

Figure 5. 3: Illustration of porosity logs derived from density and sonic logs in the well 7220/5-1.

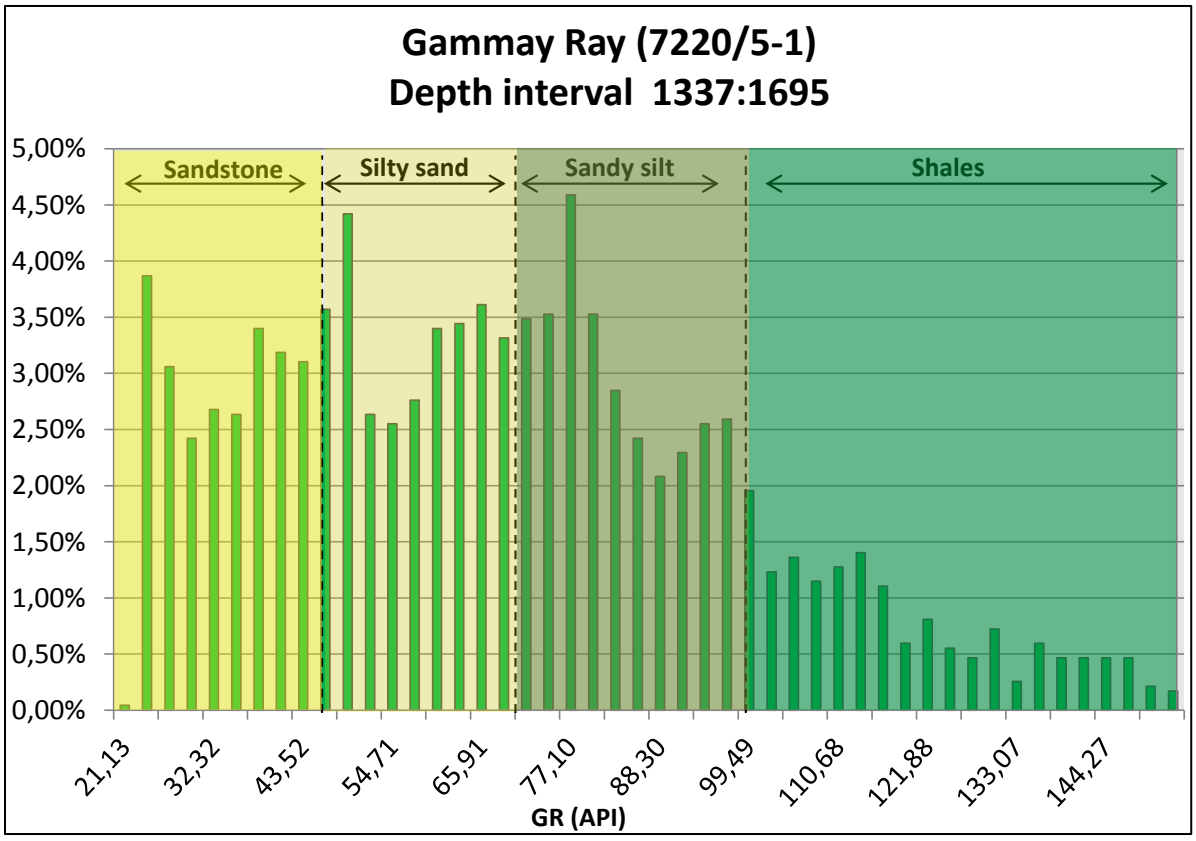

Figure 5. 4: Gamma ray distribution for the lithology identification within Tubåen, Nordmela and Stø formations.

5.3.2 .2 Gamma Ray Vs Resistivity Crossplot

Hydrocarbon and water bearing sands are differentiated by cross plotting gamma ray values against deep resistivity values and color coded with depth (Figure 5.5). Shale has lower resistivity values whereas sand containing hydrocarbons has higher resistivity values than the brine sand.

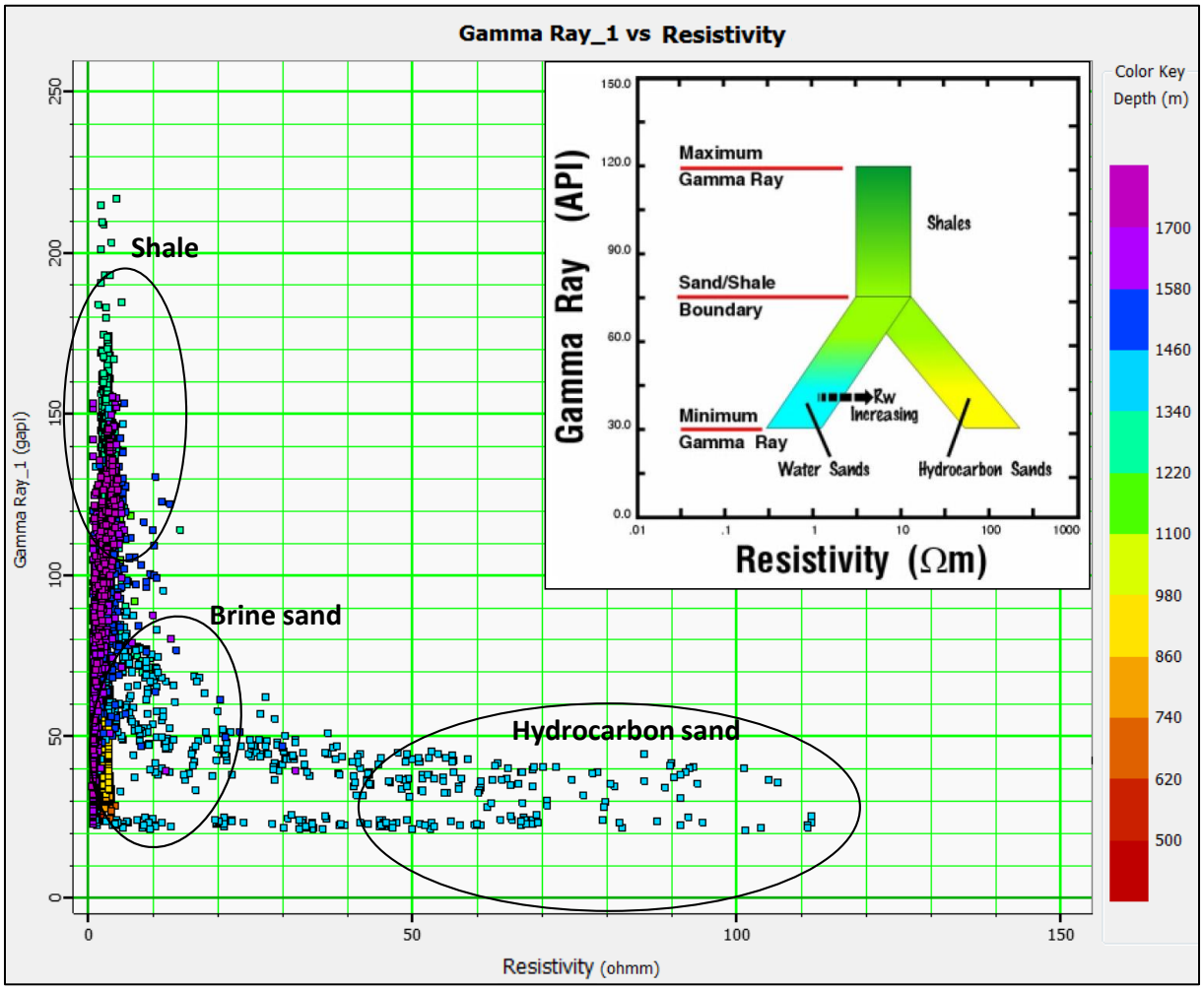

Figure 5. 5: Resistivity Vs Gamma ray cross plot color coded with depth in the well 7220/5-1 and reference trend is taken from (Heslop and Heslop, 2003).

5.3.2 .3 Histogram of Different Porosities

The histogram of different porosity logs has been created to obtain general trend of porosities in Lower-Middle Jurassic formations. Figure 5.6 shows that the most of porosity values ranges between 5 and 30%. The effective porosity values are negative within shale rich horizon intervals such as 1438-43m. Whereas, the porosity values derived from the sonic log are comparatively higher due to shale effect.

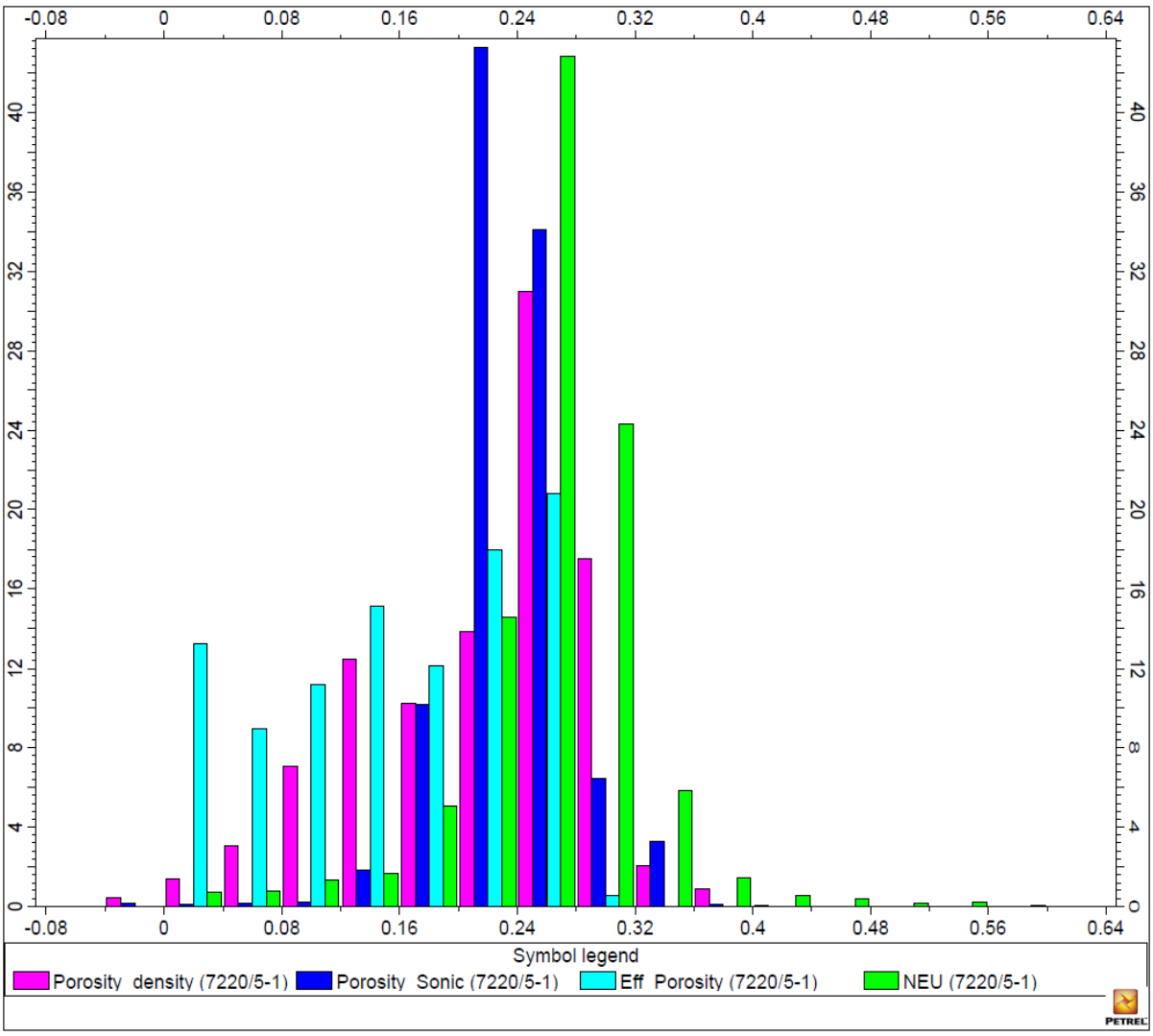

Figure 5. 6: Histogram delineates different porosities distribution in the reservoir sandstone.

5.3.2.4 Density Vs Gamma Ray Crossplot

Density log is cross plotted against gamma ray log and color coded with the porosity values (figure 5.7). This cross plot shows that the sand containing gas has lowest density and GR values. While porosity values decreases with increasing GR values in the Lower-Middle Jurassic formations.

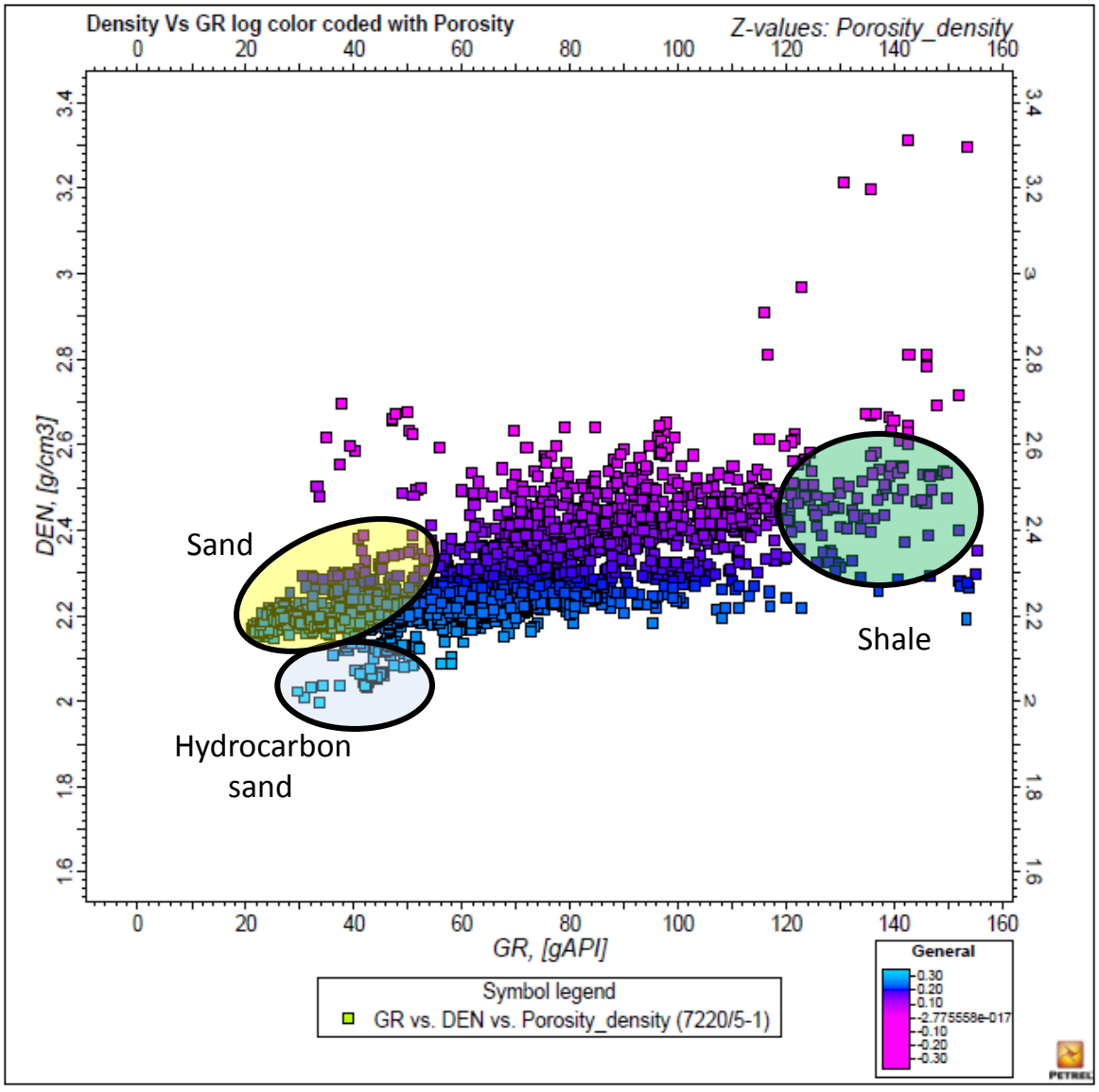

Figure 5. 7: Cross plot between gamma ray and density logs color coded with porosity calculated from density.

5.3.2.5 Neutron Porosity Vs P-Impedance Crossplot

Neutron porosity log is plotted against P-wave impedance and color coded with gamma ray log to get a variety of information at a glance (figure 5.8). The shales with higher GR values (>100gAPI) have higher neutron porosity but less P-wave impedance. Whereas clean sandstones with less GR values (<50gAPI) shows higher P-wave impedance except the sandstones containing gas. Gas sand shows lower neutron porosity values due to gas effect in the reservoir zone. The sand gas has more hydrogen atoms that captures the neutrons and the two detectors will detect fewer neutrons for hydrogen index resulting lower neutron porosity values.

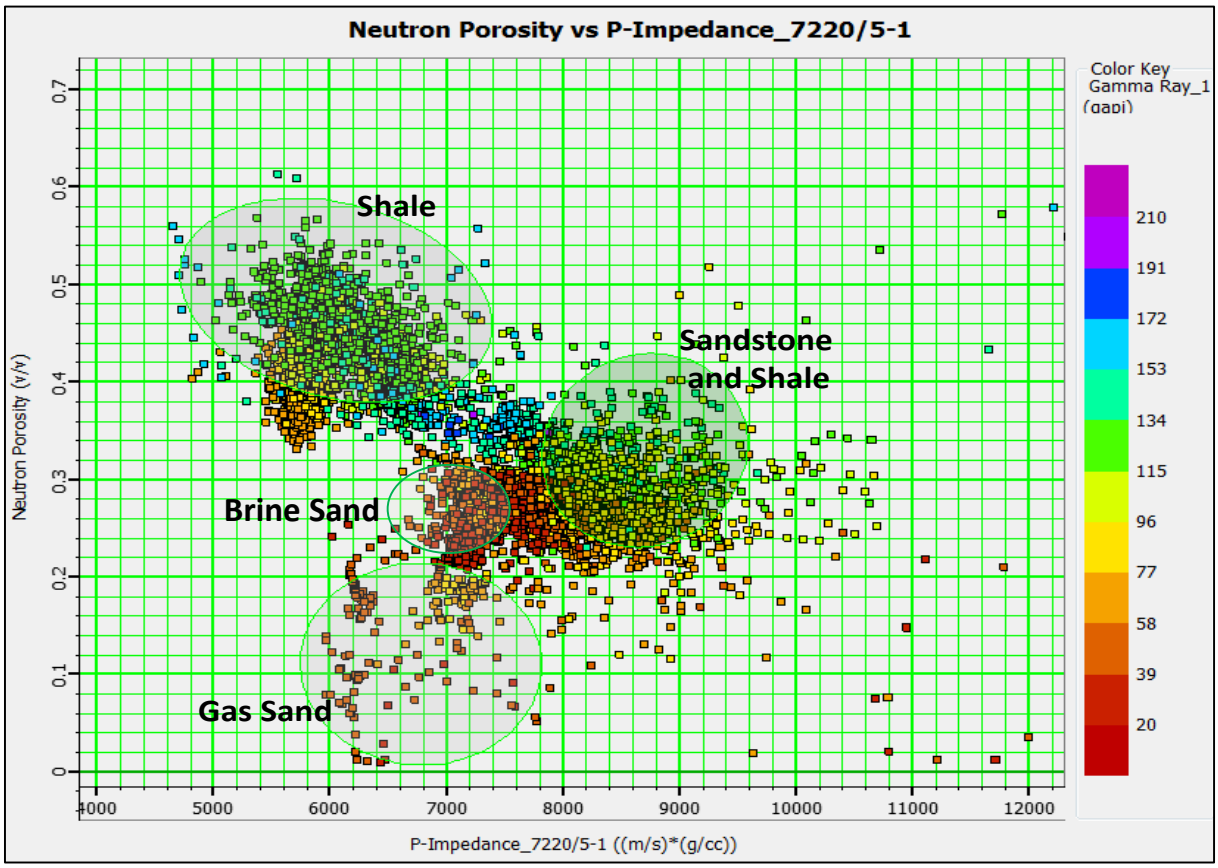

Figure 5. 8: Neutron Porosity log vs P-wave impedance color coded with gamma ray values.

5.3.3 Overpressure Zone

Overpressure zone has been investigated on the basis of P-wave velocity and density values in the well 7220/5-1. The velocity of a bulk rock is related to lithology, density, porosity and the type of fluid present in the pore spaces. The bulk rock density can decrease due to the presence of light hydrocarbons such as gas in the pore spaces. Accordingly, the presence of light hydrocarbons also has a strong effect on the velocity. The velocity has been plotted against the depth and color coded with the formations for estimation of overpressure zone (figure 5.9). Velocity data indicates that the overpressure gradually increases from reservoir top to upper part of Fuglen Formation. Overpressure increases to upper part of Fuglen Formation and it decreases in the Hekkingen Formation. The sudden change in the velocities at 1240 m depth may happen at lithological boundary.

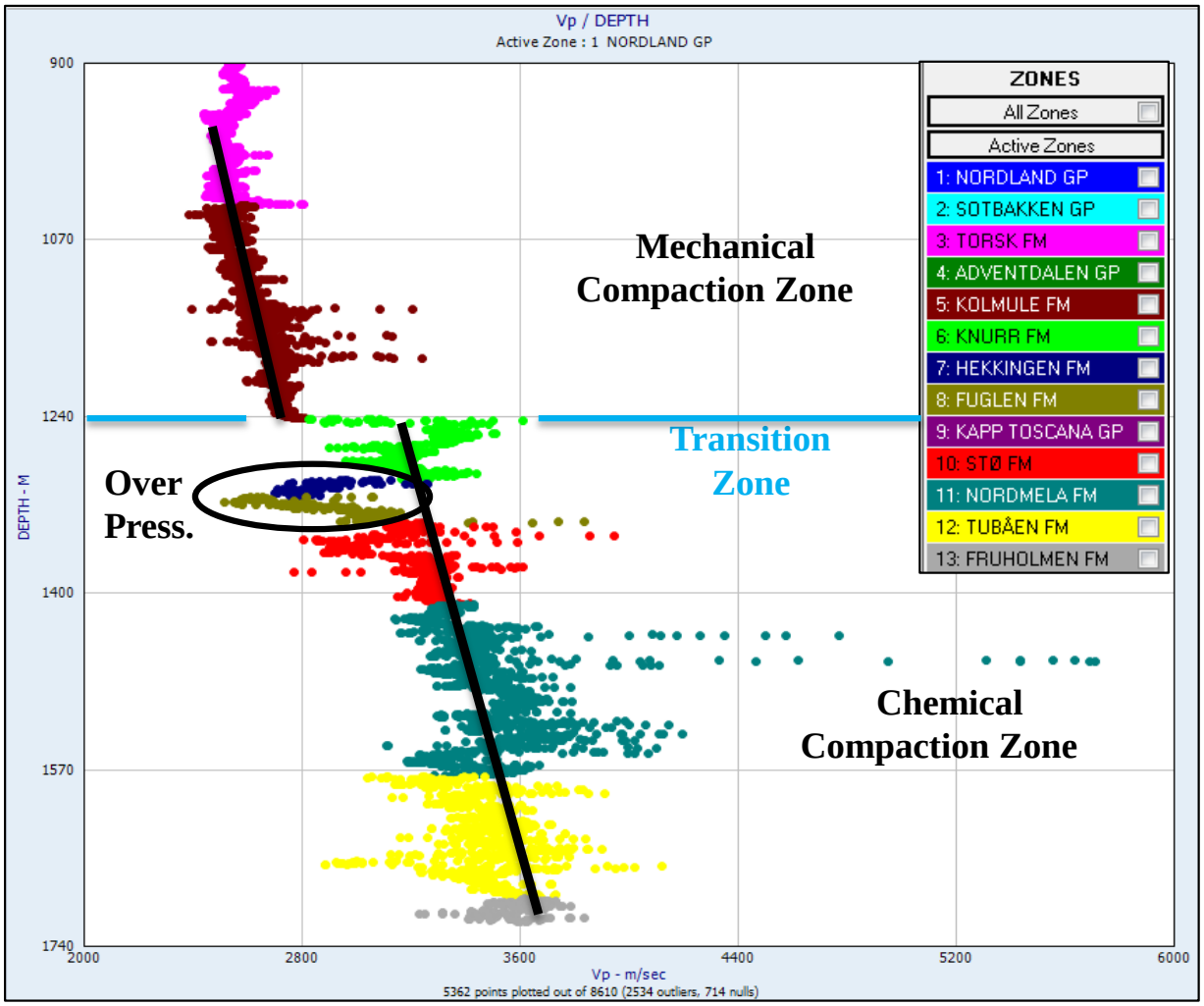

Figure 5. 9: Vp versus depth illustrating overpressure in the well 7220/5-1. The general trend line in black color is not for a particular lithology but for the entire well data.

5.3.4 Exhumation

The exhumation is estimated to acquire maximum burial depth of reservoir sandstones prior to uplift. The uplift estimation has been carried out by plotting P-wave velocity against the depth and comparing cross plot with standard compaction curve for the known lithology kaolinite:silt (50:50) published by Mondol (2009). Figure 5.10 illustrates the P-wave velocity against the depth for the estimation of uplift in the well 7220/5-1.

Well information from the table 5.1 has been used in the equation 3.1 for the calculation of temperature gradient. Measured temperature gradient values are 27 ^{o}C/km and 31 ^{o}C/km in the wells 7220/5-1 and 7220/7-1 respectively. However, average temperature gradient 29 ^{o}C/km has been used for the calculation of maximum temperature experience by reservoir sandstones.

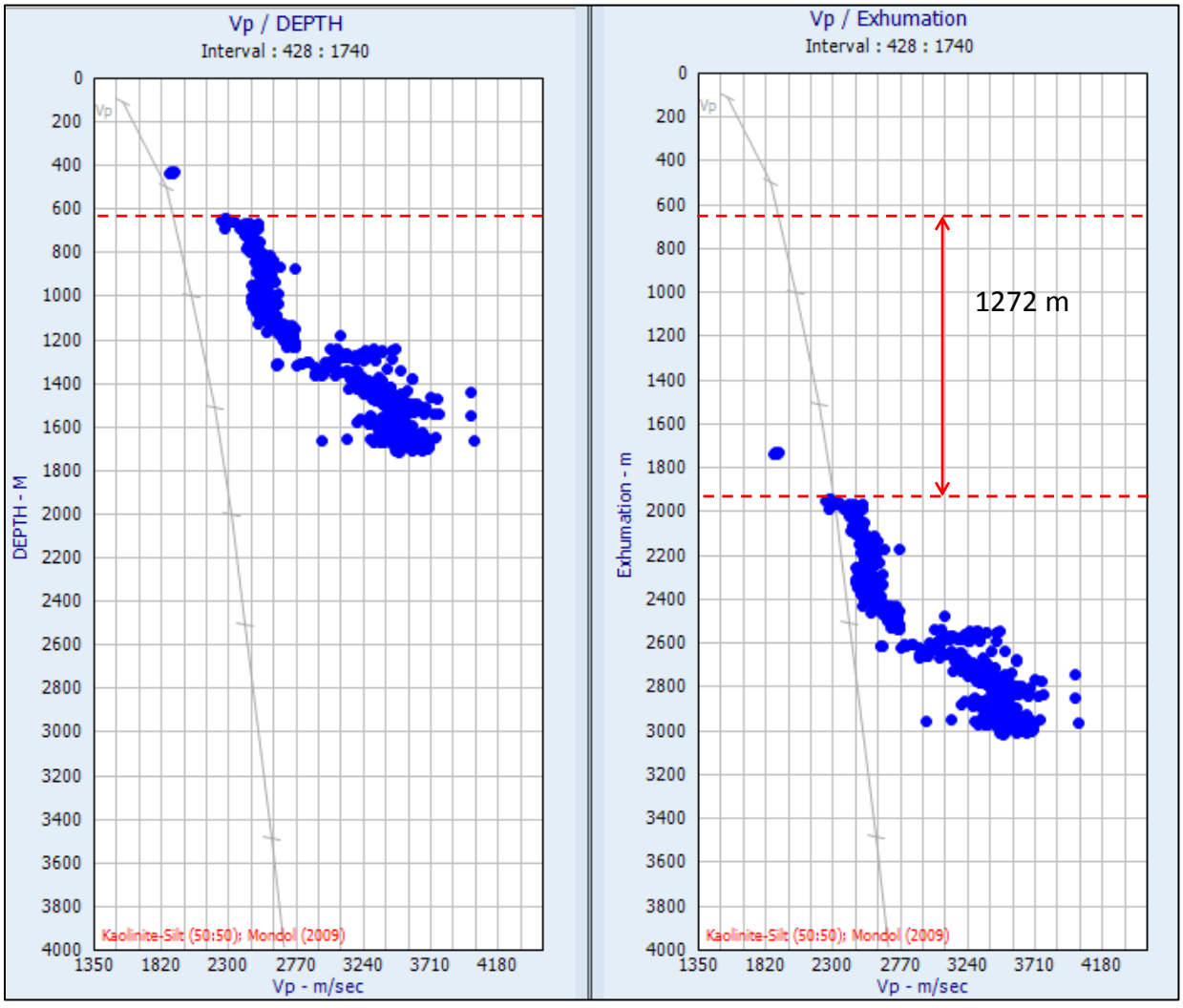

Figure 5.10: Vp-depth crossplot of well data 7220/5-1 with experimental reference curve published by Mondol (2009) showing exhumation estimation in the area.

CHAPTER 6

PETROGRAPHICAL ANALYSIS

- POINT COUNT ANALYSIS
- THIN SECTION MICROSCOPY
- SCANNING ELECTRON MICROSCOPE (SEM)
- X-RAY DIFFRACTION (XRD)
- CORE ANALYSIS

6.1 Introduction

A petrographic and mineralogical study has been carried out using SEM (Scanning Electron Microscope), XRD (X-ray Diffraction) and Optical microscopy. Thin sections petrography gives two dimensional whereas SEM gives three dimensional understanding of features and structures. All 15 samples have been studied using XRD and SEM techniques whereas thin section petrography has been carried out on 14 samples.

Main focus of petrographic analysis is to investigate the processes involved during deposition, diagenesis, compaction, quartz overgrowth and the formation of authigenic clays in Lower-Middle Jurassic sandstones.

Results

6.2 Point Count Analysis

Fourteen thin sections, seven from each formation (Nordmela and Stø) have been point counted using a point counter and stage. This technique was applied to get a quantitative analysis of detrital quartz, matrix, cement, primary and secondary porosity, intergranular Volume (IGV), authigenic clay and rock fragments employing 300 points per sample. In addition, sorting and roundness observation of the grains has been made on the basis of standard scale published by (Pettijohn, 1987). Sorting of grain is sets to three classes; poor, moderate and well sorted sandstones. Sorting is an arrangement of rock grains on the basis of grain size and well sorted sandstones are composed of similar grain size.

During point count analysis, highly altered minerals without any specific structure and dispersed clays have been point counted as matrix. In addition, illite and mica have been point counted together as mica. The primary and secondary porosities have been point counted separately but the combined (total) porosity has been used in the further analysis. Similarly, sphalerite, barite and pyrite have been point counted separately and named as heavy minerals in the results and discussions. Both polycrystalline and monocrystalline quartz grains have been counted as quartz during point count analysis. Quartz is the predominant framework constituent in all samples with an average of 92% among the rock forming minerals and 62.7% of the total bulk volume of rock including matrix and porosity. The results of point count analysis are shown in table and figure 6.1.

Table 6. 1: Point count results of Nordmela and Stø formations in the well 7220/5-1.

Fms.	Depth (m)	Quartz	Feldspar	Lith. Fragments	Mica	Auth. Clay	Heavy Min.	Matrix	Tot. porosity	Qtz. Overgrowth	IGV	G. Size (mm)	Sorting	Roundness
Stø	**1340,15**	59,3	5,9	3,9	1,6	7,6	2,3	2	17,3	0	28,5	0,14	Mod.-Well	Sub Rounded
	1345,05	62,6	5,2	2,6	4,3	9,6	1,9	3,3	10,3	0,3	26,8	0,22	Poor-Mod.	Sub Angular
	1349,36	72	2,9	0	2,3	7,3	0,6	1,3	13,3	0,3	25,2	0,27	Poor-Mod.	Angular
	1356,07	67,3	2,9	2,3	1,3	4,6	1	1,6	19,2	0	26,1	0,22	Mod.	Sub Rounded
	1369,77	64,6	4,3	2,3	1,9	4,3	0,6	5,3	16,6	0,3	28,4	0,19	Mod.	Sub Angular
	1373,10	58,3	4,2	1,6	2,3	6,3	1,3	6,3	19,6	0,3	34,5	0,15	Well	Sub Rounded
	1379,50	62,3	5,2	1,3	3,3	7,3	1,6	5,6	12,9	0,3	28,8	0,16	Mod.-Well	Sub Angular
Nordmela	**1420,70**	61,6	2,6	3	1,3	3	2	2,6	23,6	0,6	30,1	0,18	Well	Rounded
	1425,76	62,6	1,6	3	1,3	3,3	2,3	3,6	21,3	1	30,2	0,2	Well	Sub Rounded
	1431,72	65,6	1,6	1,6	0,6	2,6	1,3	2,3	23,6	1	29,5	0,21	Mod.-Well	Sub Rounded
	1436,20	62,3	2,9	1,3	1,3	3,3	1,6	0,6	24,9	1,6	30,4	0,22	Well	Sub Rounded
	1439,80	56,3	6,3	0,6	7,6	10,6	3,6	8,3	6	0,6	33,1	0,15	Mod.-Well	Sub Angular
	1444,36	66,3	1,6	1	0,6	2,6	1,3	1,3	23,9	1,3	29,1	0,26	Mod.	Sub Rounded
	1449,44	57	6,2	0,6	0,6	6,3	1,9	0,6	26,3	0,6	32,4	0,19	Well	Sub Rounded

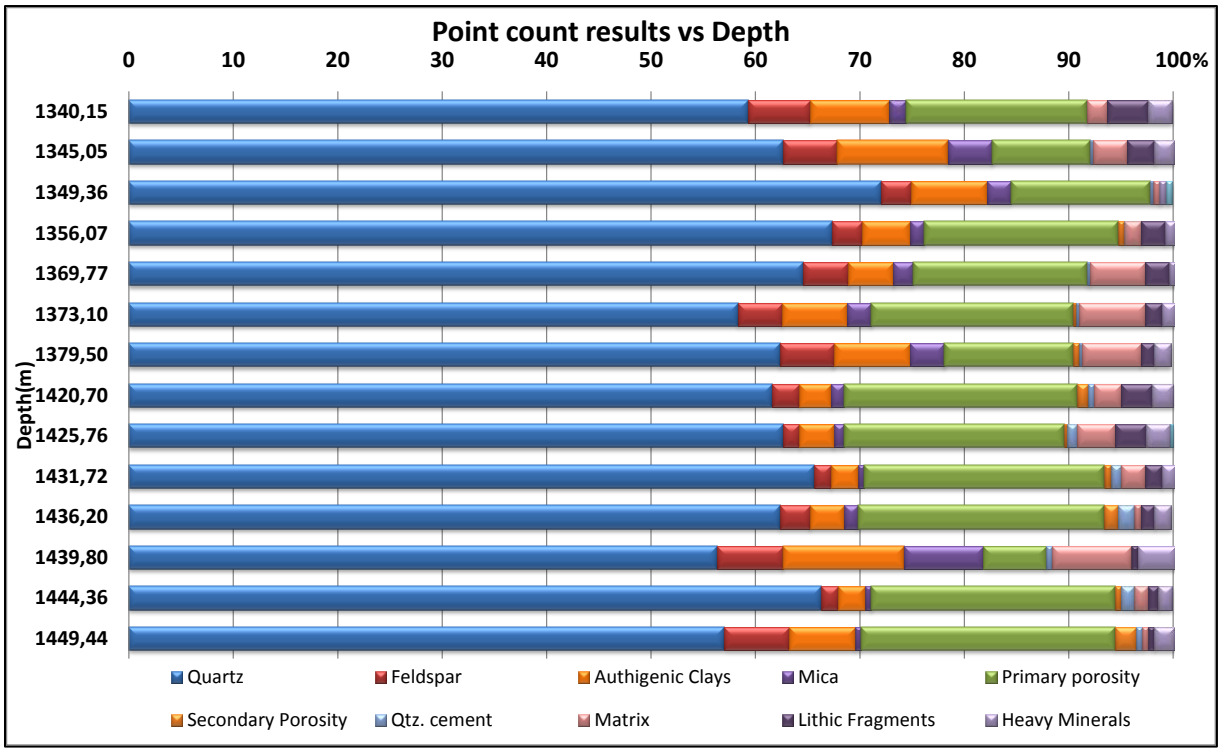

Figure 6. 1: Bar chart illustrates the point counting results against depth.

6.2.1 Petrographic Classification

Petrographic classification has been performed to determine the type of sandstones. To obtain adequate results, quartz, feldspar and lithic fragments have been added together and their percentages are calculated with respect to their sum (Table 6.2). These percentages are further plotted on a petrographic classification diagram to acquire sandstones type (Figure 6.2). Eight samples out of fourteen contain feldspar in between 5 and 10% and are classified as subarkosic sandstones. Three of the samples have quartz more than 95% and are termed as quartzarenite, whereas all other samples have relatively higher content of lithic fragments and are grouped under sublitharenitic sandstones.

Table 6. 2: Percentages of quartz, feldspar and lithic for the sandstone classification.

Fms.	Depth (m)	Quartz	Feldspar	Lith. Fragments	Total (Q+F+L)	Quartz%	Feldspar %	Lithic%	Sand st. Type
Stø	**1340,15**	59,30	5,90	3,90	69,10	85,87	8,54	5,64	Subarkosic
	1345,05	62,60	5,20	2,60	70,40	88,92	7,39	3,69	Subarkosic
	1349,36	72,00	2,90	0,00	74,90	96,13	3,87	0,00	Quartzarenite
	1356,07	67,30	2,90	2,30	72,50	92,83	4,00	3,17	Subarkosic
	1369,77	64,60	4,30	2,30	71,20	90,73	6,04	3,23	Subarkosic
	1373,10	58,30	4,20	1,60	64,10	90,95	6,55	2,50	Subarkosic
	1379,50	62,30	5,20	1,30	68,80	90,55	7,56	1,89	Subarkosic
Nordmela	**1420,70**	61,60	2,60	3,00	67,20	91,67	3,87	4,46	Sublitharenite
	1425,76	62,60	1,60	3,00	67,20	93,15	2,38	4,46	Sublitharenite
	1431,72	65,60	1,60	1,60	68,80	95,35	2,33	2,33	Quartzarenite
	1436,20	62,30	2,90	1,30	66,50	93,68	4,36	1,95	Sublitharenite
	1439,80	56,30	6,30	0,60	63,20	89,08	9,97	0,95	Subarkosic
	1444,36	66,30	1,60	1,00	68,90	96,23	2,32	1,45	Quartzarenite
	1449,44	57,00	6,20	0,60	63,80	89,34	9,72	0,94	Subarkosic

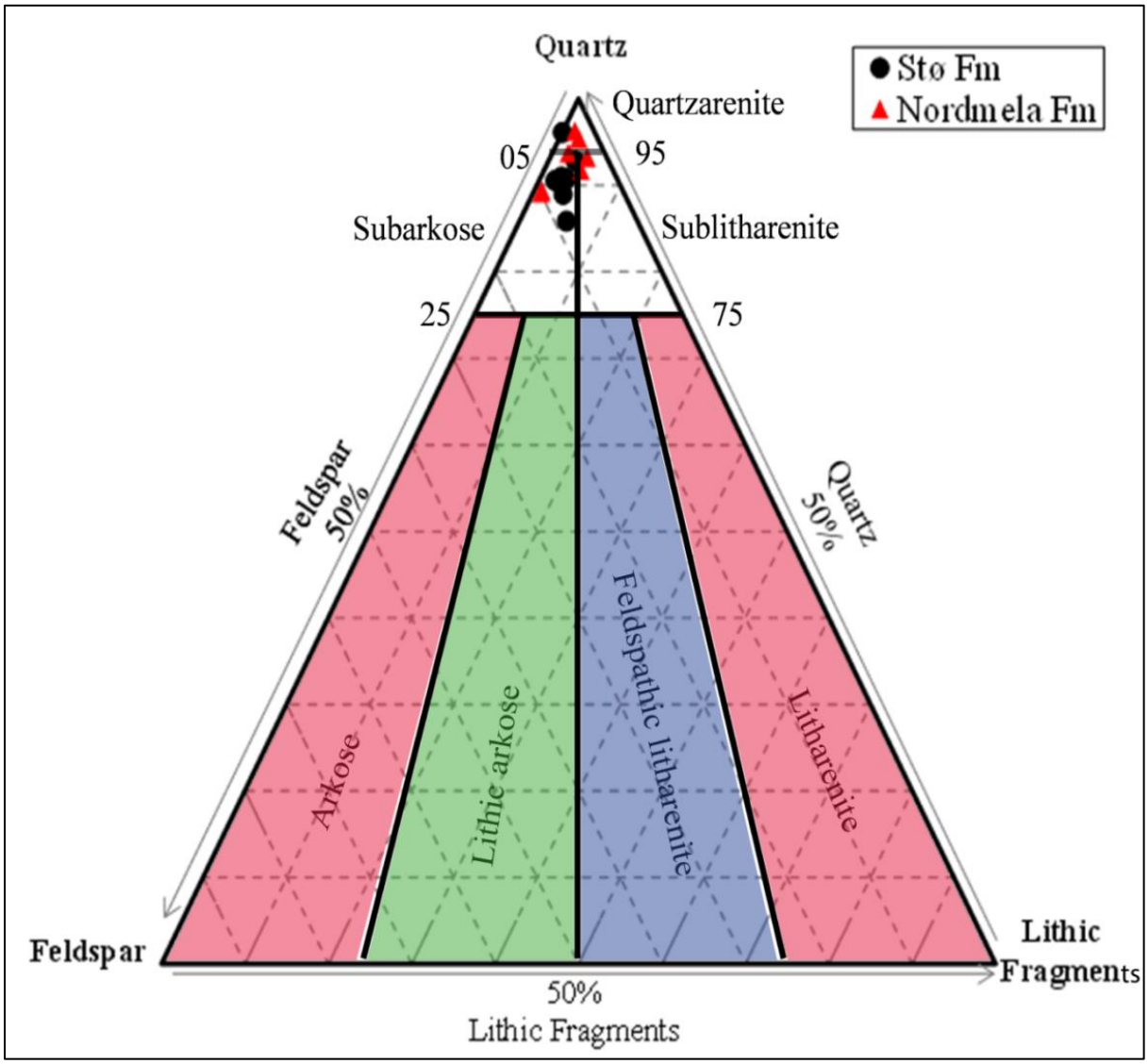

Figure 6. 2: Petrographic classification of sandstones (Pettijohn, 1987).

6.2.2 Provenance Analysis

Provenance analysis of sandstones is the reconstruction of the parent rock assemblage together with the depositional environments under which sandstones were formed (Weltje and von Eynatten, 2004). The provenance analysis has been carried out by plotting all samples on the QFL ternary diagram. Figure 6.3 show that sandstones of the Nordmela and the Stø formations have cratonic source of continental settings. The tectonic setting of the source area plays an important role in the sandstone composition. In addition, depositional environments, climate and transportation of sediments are important as secondary factors (Dickinson et al., 1983).

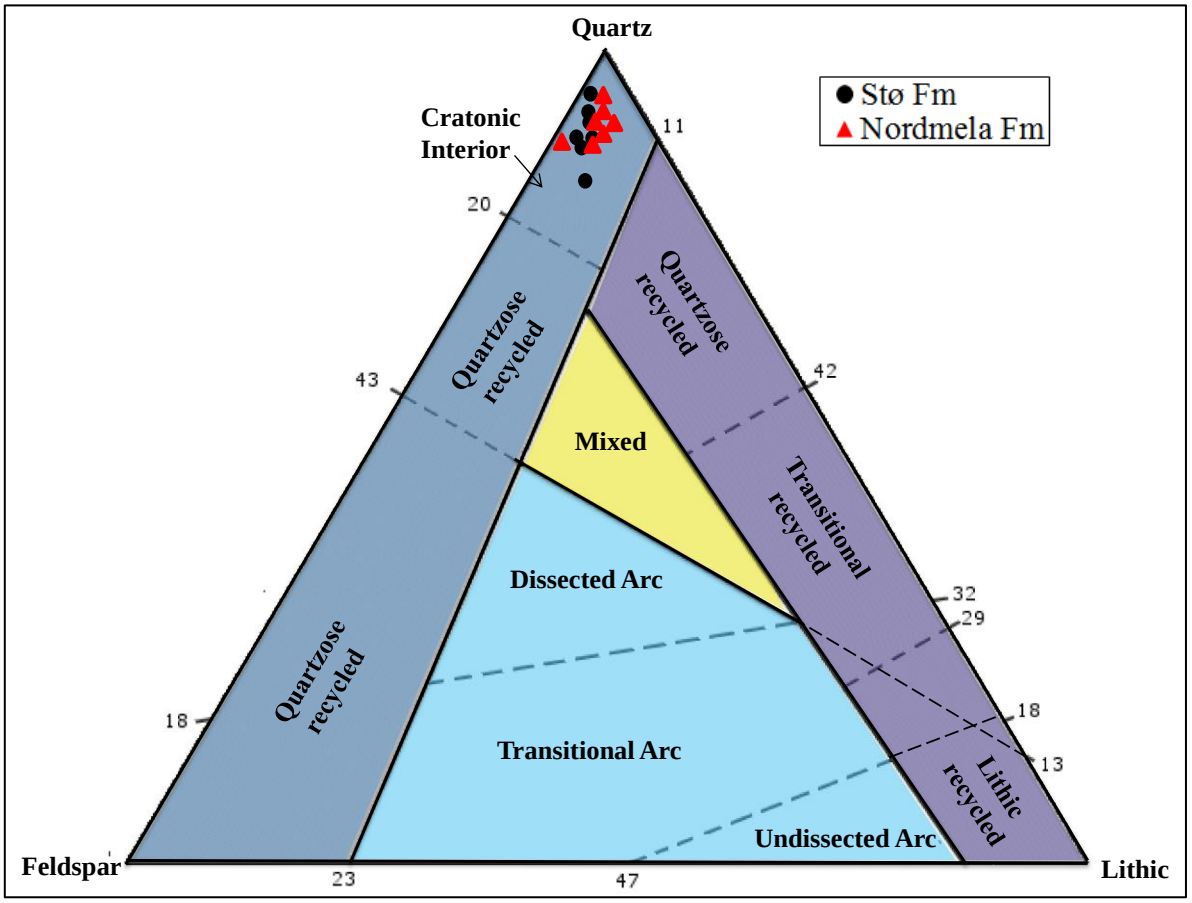

Figure 6. 3: Provenance of Jurassic sandstones based on the point count analysis. General diagram is from (Dickinson, 1985).

6.2.3 Total Porosity

Total porosity is the sum of primary (intergranular) and secondary (intragranular) porosities. Secondary porosity is higher in the Nordmela Formation as compared to the Stø Formation. However, it is negligible relative to primary porosity. The histogram gives the overview of total porosity in Nordmela and Stø formations (Figure 6.4). The porosity counts vary from 9.3% to 26.3%. The Nordmela Formation has comparatively higher total porosity values than the Stø Formation. The average porosities of Nordmela and Stø formations are 21.3% and 15.5% respectively.

Diagenesis and pore-filling materials are the main causes of porosity reduction in the sandstone reservoirs buried to intermediate depth. The counted percentages of porosity, matrix and quartz cementation are displayed in the histogram to observe their relationship within these sandstones (Figure 6.5). It is evident that porosity is dependent on the amount of matrix.

In general, the amount of quartz cementation increases with depth and is higher in Nordmela Formation as compared to Stø Formation. At some places in Stø Formation quartz overgrowth is completely absent whereas it is point counted up to 1.6% in the Nordmela Formation.

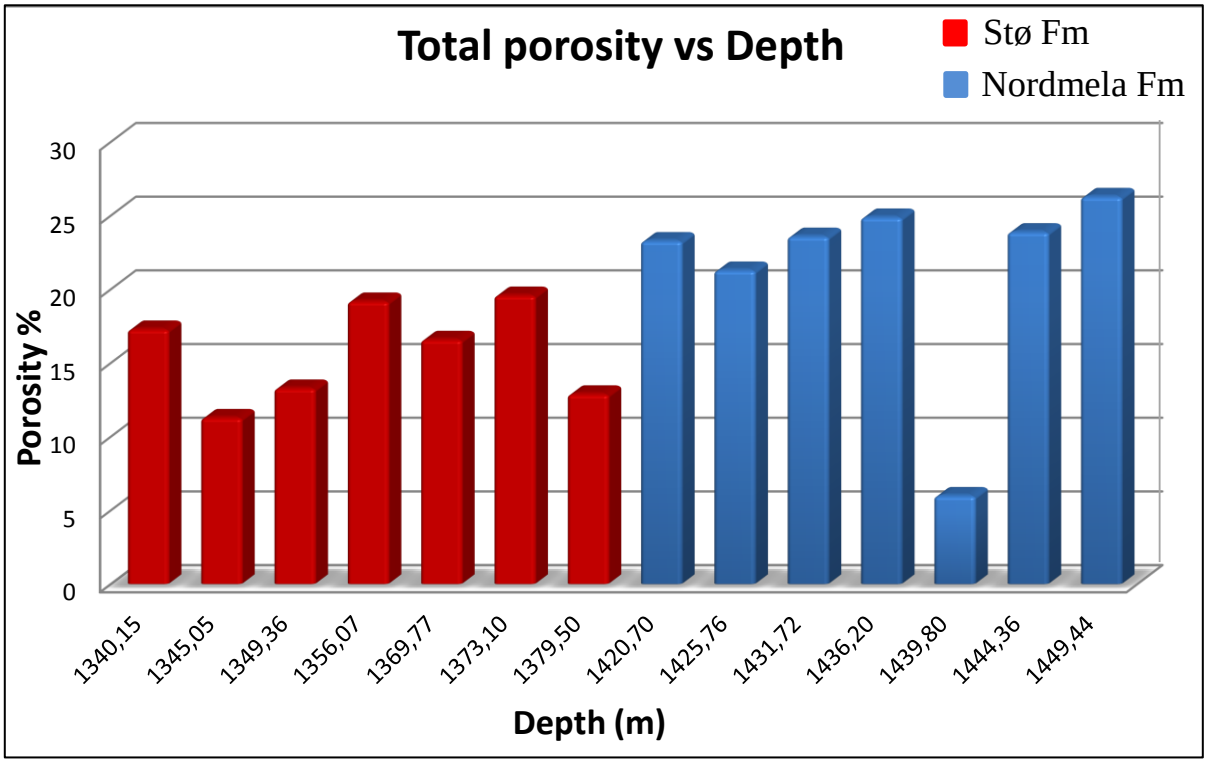

Figure 6. 4: Histogram of the counted percentage for total porosity against depth.

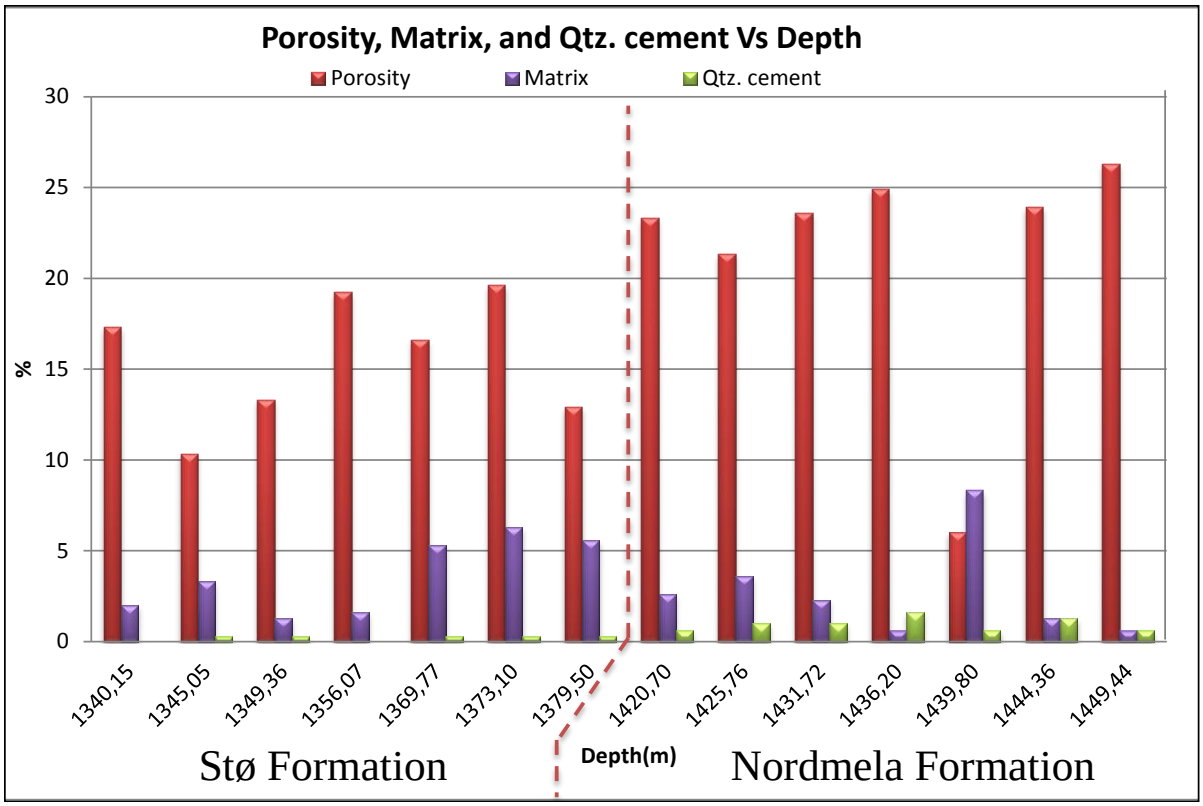

Figure 6. 5: Histogram of the total porosity, quartz cement and matrix against depth.

6.2.4 Authigenic Clays

Kaolinite is dominant among the authigenic clays found during point count analysis. Kaolinite exists as a pore-filling mineral and significantly reduces porosity and permeability in these sandstones. The counted percentage of authigenic clays and porosity are displayed in the histogram (figure 6.6) to get their relationship in these sandstones. Most of the kaolinite observed in thin sections is formed by authigenic processes apparent from their morphologies.

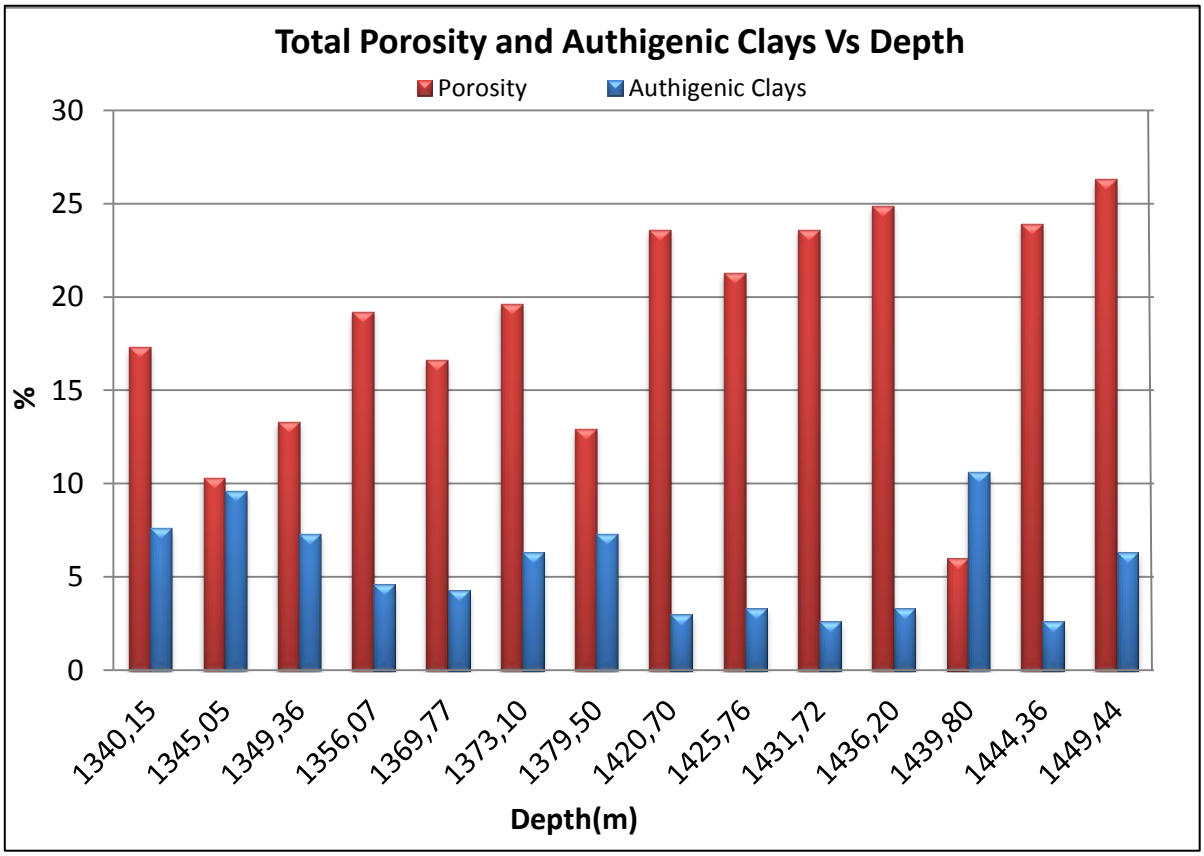

Figure 6. 6: Histogram of point counted percentage of total porosity and authigenic clays against depth.

6.2.5 K-Feldspar ($KAlSi_3O_8$) and Albite ($NaAlSiO_8$)

Both alkali (microcline) and plagioclase (albite) feldspars have been point counted during point count analysis. The point count percentages of microcline and albite range in between 1.6% to 6.2% and 0% to 2.3% respectively (Figure 6.7). The percentage of albite is very low and therefore microcline and albite are collectively named as Feldspar in further analysis.

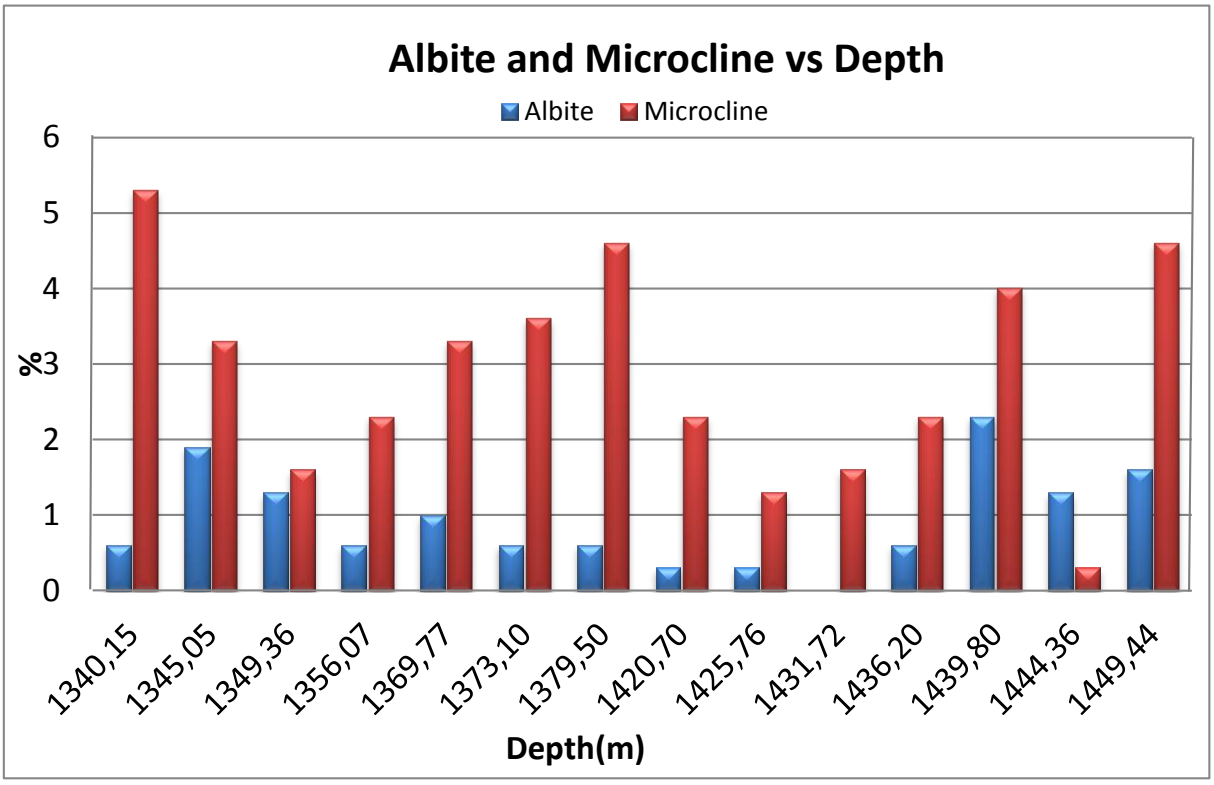

Figure 6. 7: Point count percentages of albite and microcline against depth.

6.2.6 Ductile Components

Ductile components including platy minerals like mica, authigenic clays mostly kaolinite, matrix, and rock fragments play an important role in controlling reservoir quality. Figure 6.8 illustrates the relationship between ductile components and porosity. The amount of ductile components varies from 5.5% to 27.1% within sandstones of Nordmela and Stø formations.

Furthermore, the presence of ductile components reduces porosity and permeability of sandstone reservoirs more rapidly during mechanical compaction. However, the amount of porosity reduction is strongly related to distribution, orientation and quantity of ductile components. Figure 6.9 demonstrates an inverse relationship between ductile components and porosity within sandstones of Nordmela and Stø formations.

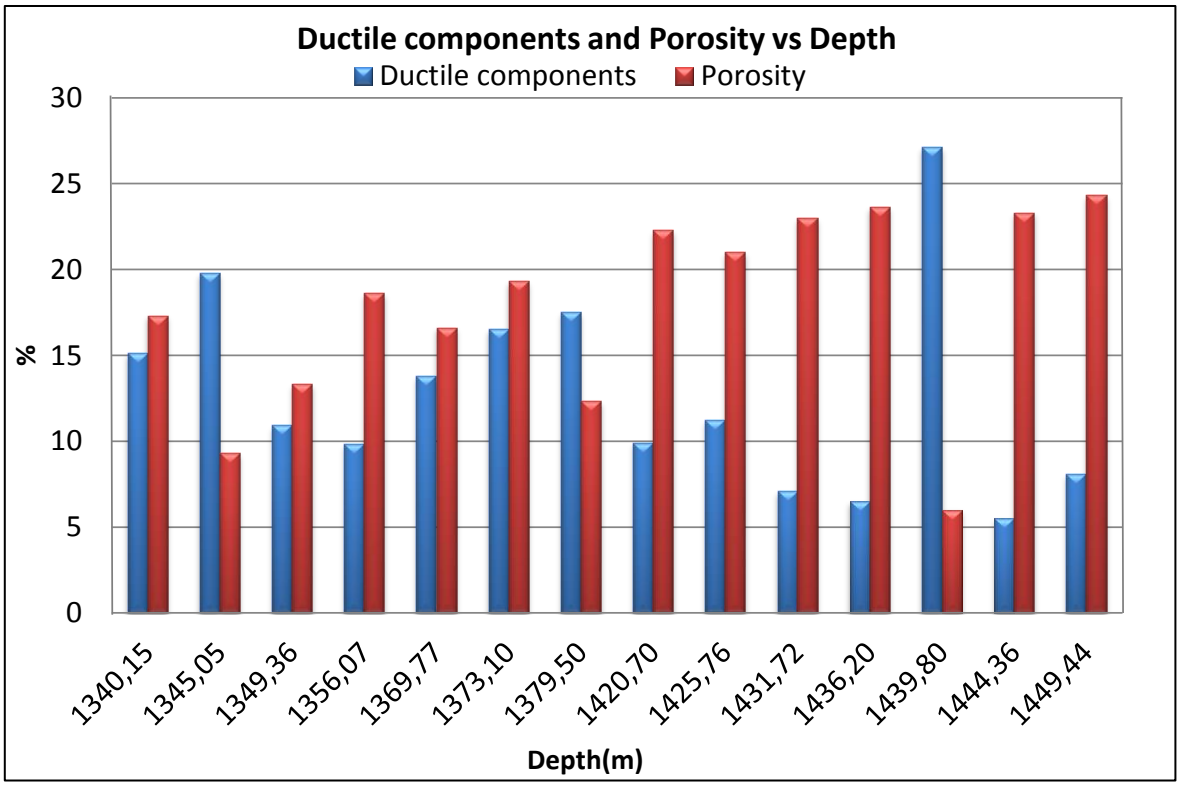

Figure 6. 8: Histogram illustrating point count percentages of ductile components (mica, matrix, clay and lithic fragments) and porosity against depth.

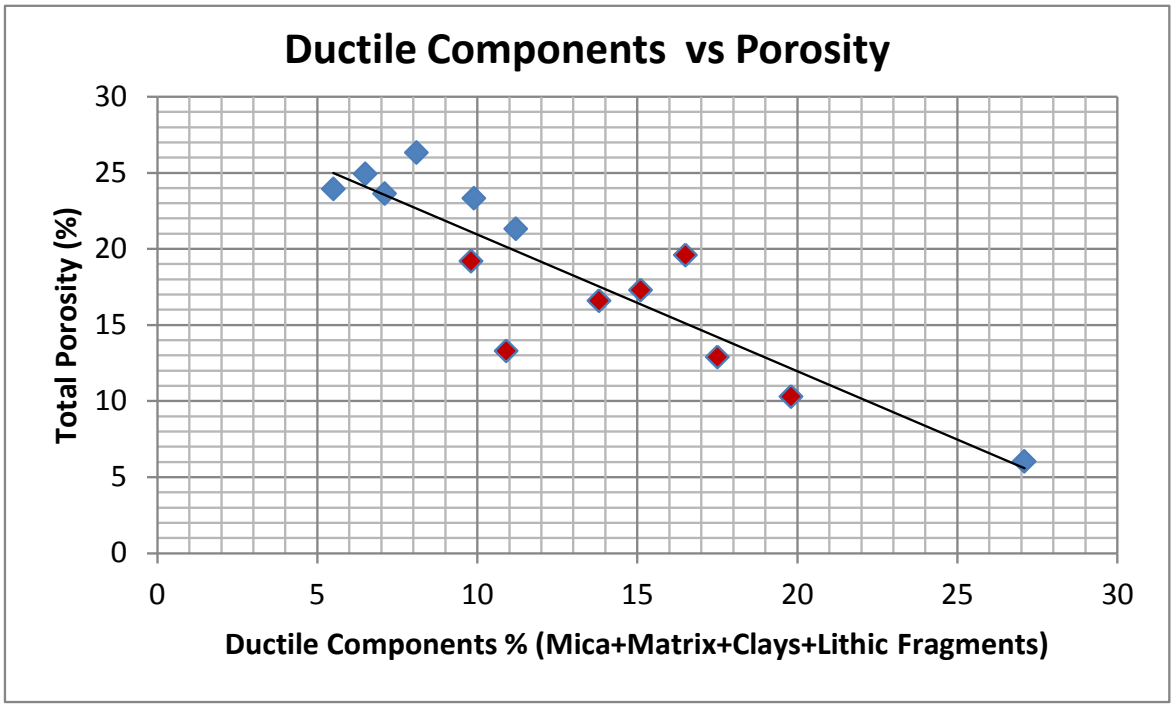

Figure 6. 9: Effect of ductile components on the porosity. Red and light blue colors illustrate Stø and Nordmela formations respectively.

6.2.7 Mica and Heavy Minerals

The mica sheets are dispersed within pore spaces and vary in amount from 0.6 to 7.6% with an average of 2.2%. Sphalerite and pyrite have been counted as heavy minerals and present in between 0.6 and 3.6% with an average content of 1.66%.

6.2.8 IGV (Intergranular Volume)

The estimation of intergranular volume is important in order to find out the porosity loss as a result of quartz cementation. Intergranular volume has been calculated by adding quartz cement, matrix, authigenic clays and primary porosity. Authigenic clays like kaolinite and illite are present as a pore-filling material and have been included in the intergranular volume.

The IGV values ranges between 25.2% and 34.5% with an average content of 28.23% within Stø Formation whereas it ranges from 29.1% to 33.1% with an average of 30.64% within Nordmela Formation (figure 6.10).

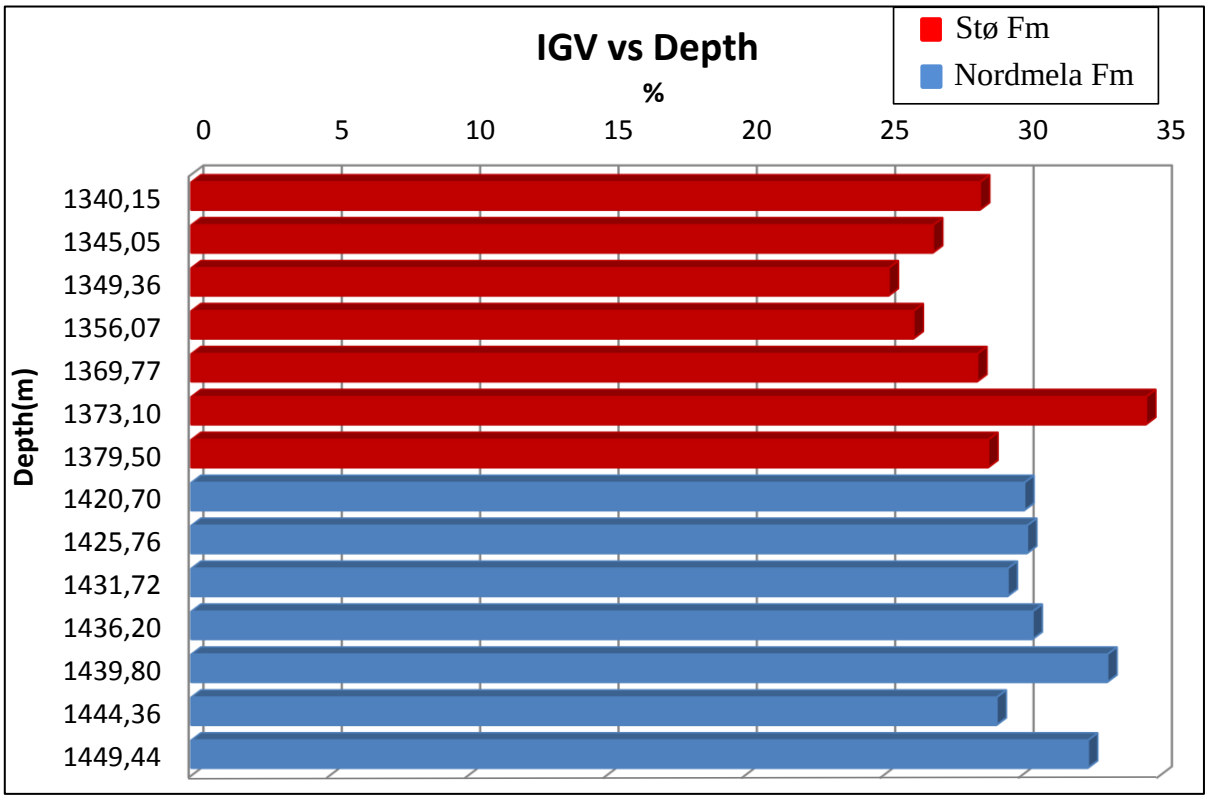

Figure 6. 10: Calculated intergranular volume (IGV) is plotted against depth.

6.2.9 Textural Characteristics

The reservoir quality is highly dependent on the textural characteristic of sandstones. It is obvious from the table 6.1 and figures 6.11, 12 and 13 that well-rounded, well-sorted and fine-grained sandstones occupies greater intergranular volume (IGV). The same results have been used for the determination of sandstones maturity. Well-sorted and well-rounded clean sandstones exhibit significant amount of porosity and higher permeability than less sorted silty sandstones. Fine-grained sandstones have higher IGV values than the medium-grained sandstones (figure 6.11).

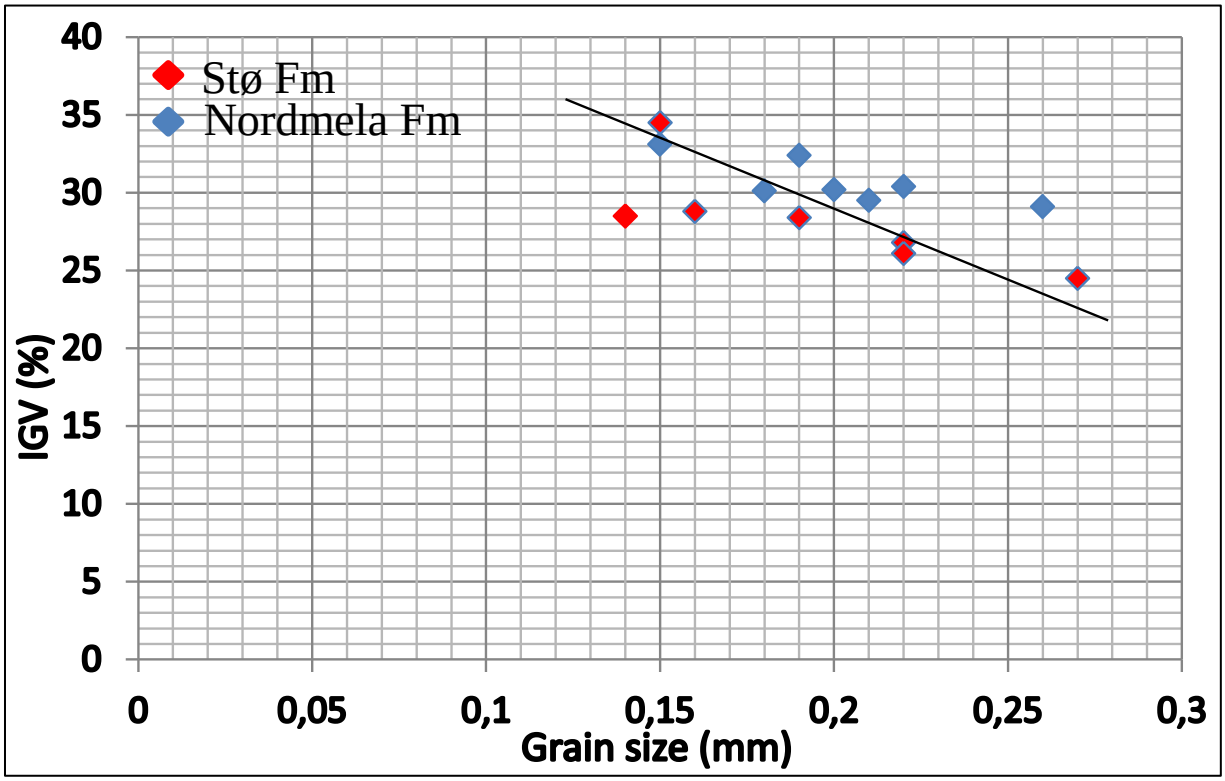

Figure 6. 11: Diagram illustrates relationship between grain size and IGV.

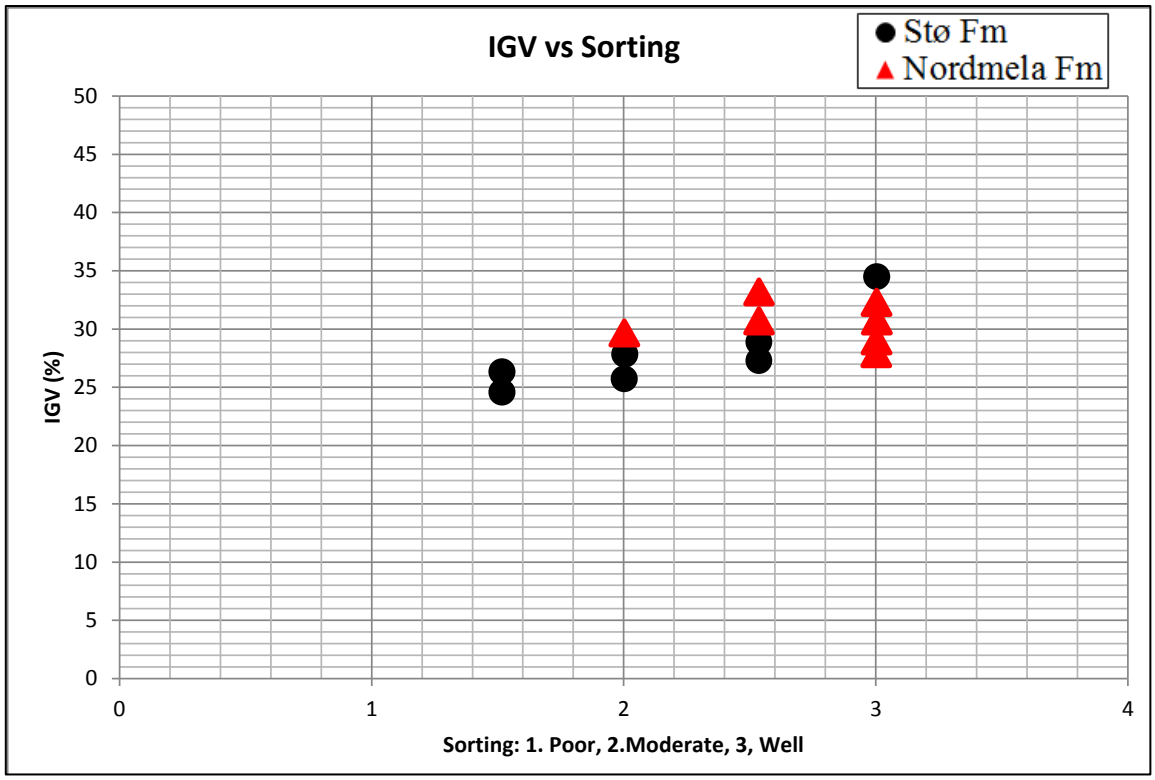

Figure 6. 12: Diagram illustrates relationship between degree of grain sorting and IGV.

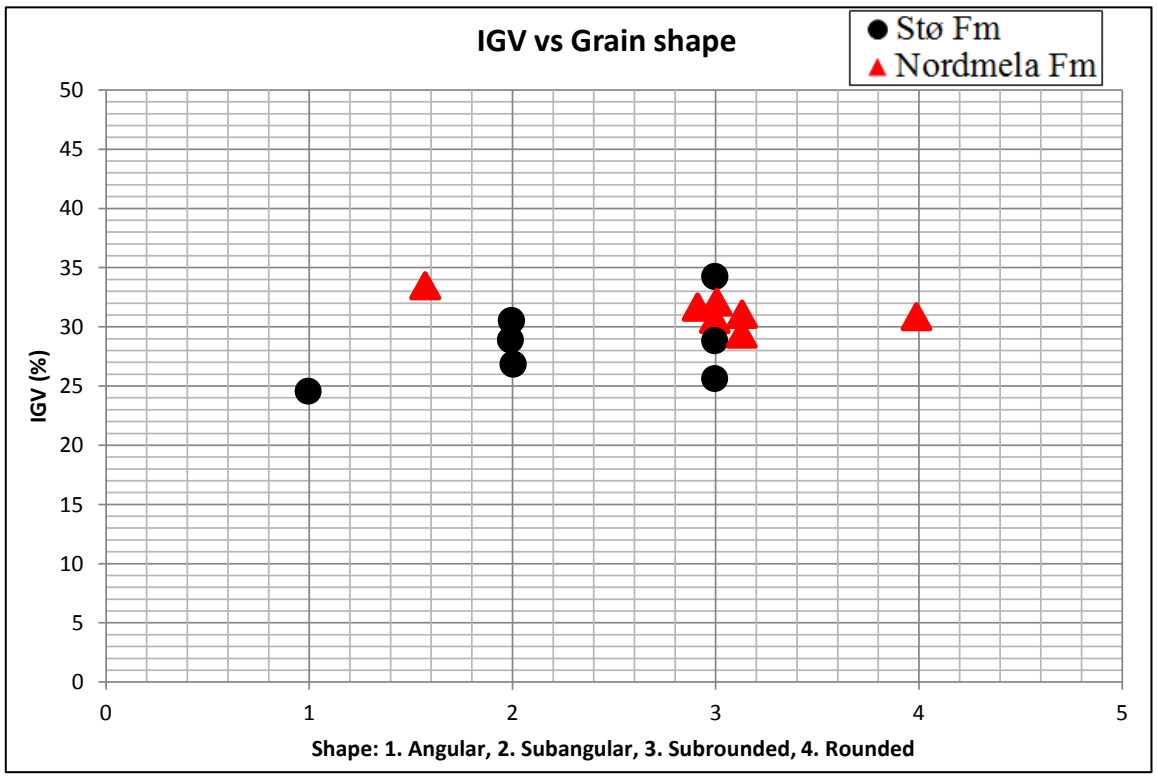

Figure 6. 13: Diagram illustrates relationship between degree of grain roundness and IGV.

6.2.10 Textural Maturity

Textural maturity of Nordmela and Stø formations has been determined on the basis of clay amount, grain shape and sorting of sandstones. Textural maturity determines the stability of sandstones and reveals adequate properties of sandstone reservoirs. According to Folk (1951), the maturity of sandstone can be classified in to four different stages (Table 6.3).

Table 6. 3: Four stages of textural maturity of sandstone reservoirs.

I. Immature Stage	II. Submature stage	III. Mature stage	IV. Supermature stage
Sediments consist of considerable clay and mica and sand grains are poorly sorted and angular.	Sediments contains very little amount of clay and mica but sand grains are still poorly sorted.	Sediments consist of no clay and well sorted but the grains are still sub-angular.	Sediments contain very clean sand without clay and well sorted. Sand grains are rounded.

All samples have been analyzed for the textural maturity of Nordmela and Stø formations (Figure 6.14). Most of the sandstones are texturally matured and one of them is very clean, rounded and well sorted sandstone and therefor it is classified as super-mature sandstone. While two samples are grouped as sub-mature due to higher proportion of clay than the rest of sandstones.

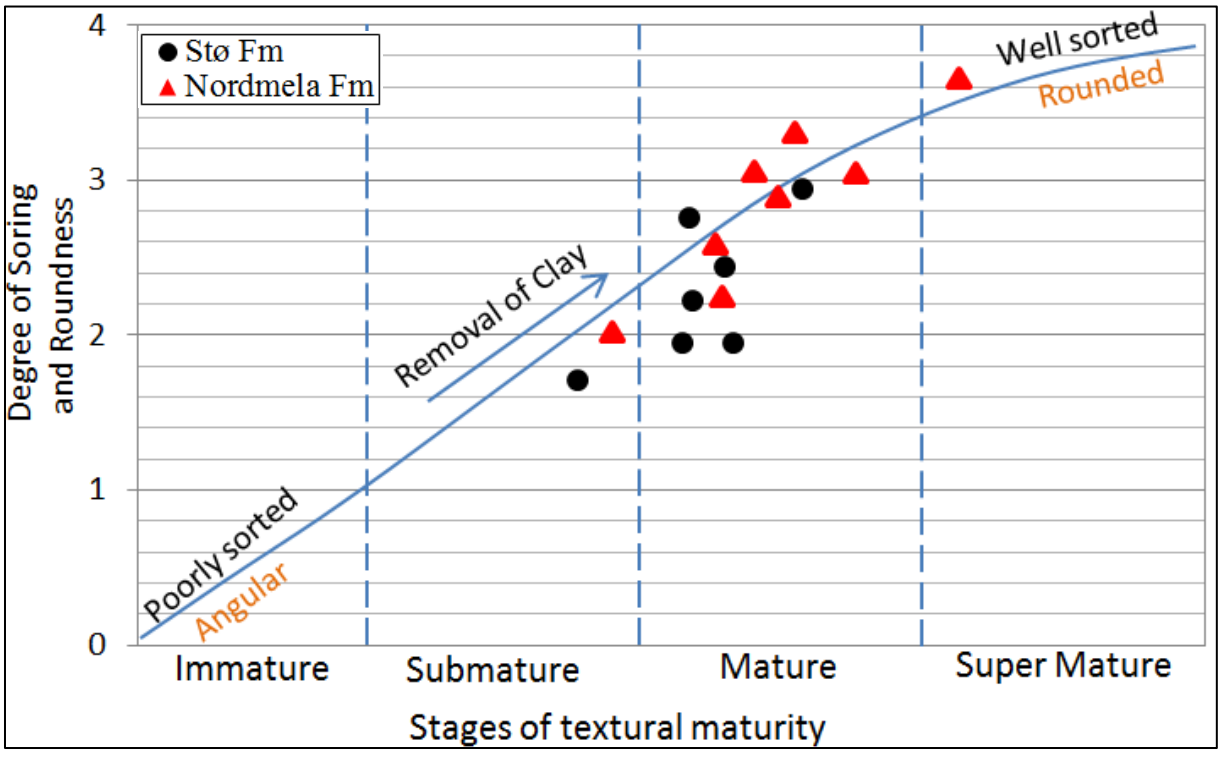

Figure 6. 14: Diagram illustrates textural maturity of sandstones of Nordmela and Stø formations. Modified from (Folk, 1951).

6.3 Thin Section Observation

Thin section observations have been made using optical microscope. Some interested observations are captured by attached camera with optical microscope (figures 6.15 and 6.16).

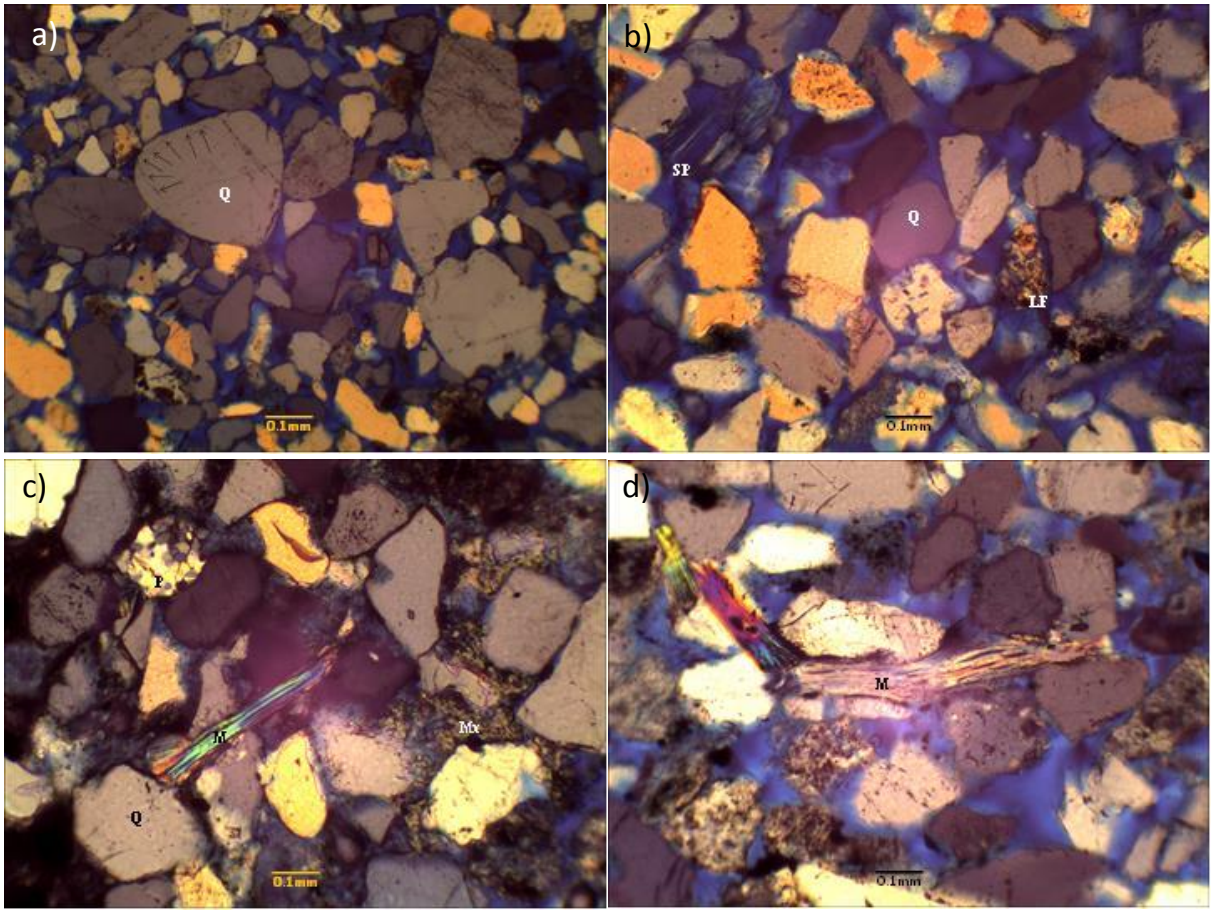

Figure 6. 15: Poorly sorted sandstone at 1349.36 m depth. b) Lithic fragment (LF) and secondary porosity (SP) within dissolved feldspar grain at 1356.07 m depth. c) Polycrystalline (P) and monocrystalline (Q) quartz with kaolinized mica (M) and matrix (Mx). Porosity is very less due to matrix and dispersed clay at 1349.36 m depth. d) Weathered feldspar and mica hindering the permeability within sandstone at 1449.35 m depth.

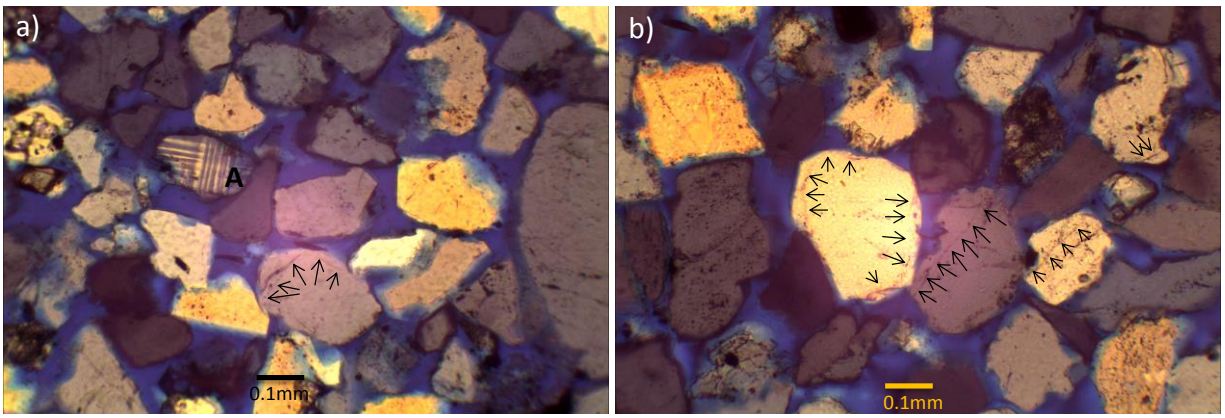

Figure 6. 16 : Quartz overgrowth (↗) increases with depth. a) Lesser amount at shallow 1369 m depth. b) Higher amount at greater 1436 m depth (A: Albite).

6.4 Scanning Electron Microscopy (SEM)

SEM technique has been employed on gold coated stubs and carbon coated thin sections for further investigation. The main objective of SEM analysis is to estimate porosity, authigenic clays, sorting, cementation, quartz overgrowth and mineralogy.

6.4.1 Quartz Overgrowth

Both macro-quartz and micro-quartz overgrowth have been observed during SEM analysis (figures 6.17 & 6.18). The effect of quartz overgrowth on the porosity has been analyzed both in stubs and thin sections during SEM analysis. In general, quartz overgrowth increases with depth and the amount of quartz cementation is higher in Nordmela Formation than Stø Formation.

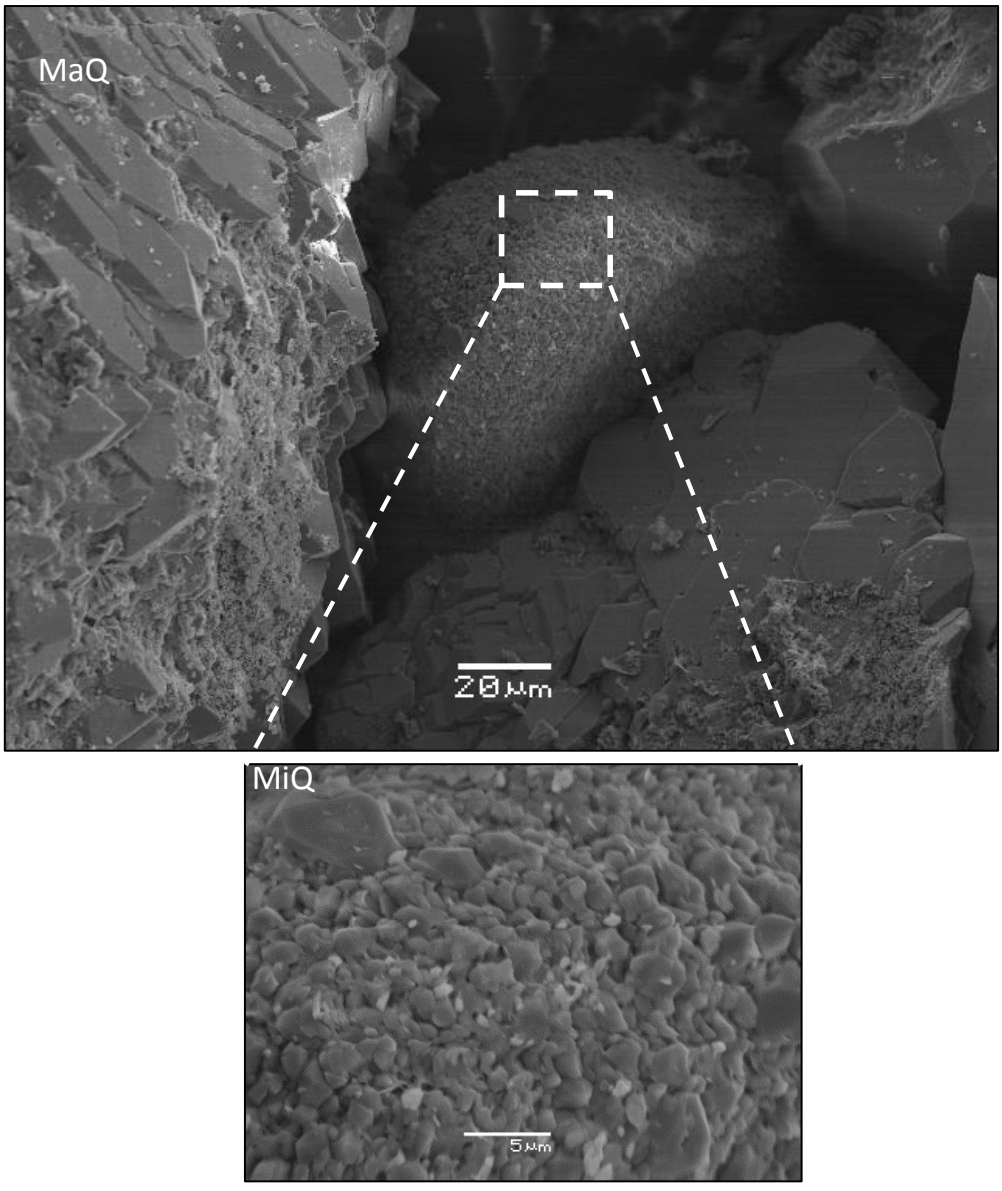

Figure 6. 17: SEM microphotographs of micro-quartz (MiQ) and macro-quartz (MaQ) overgrowth at 1444.36 m depth.

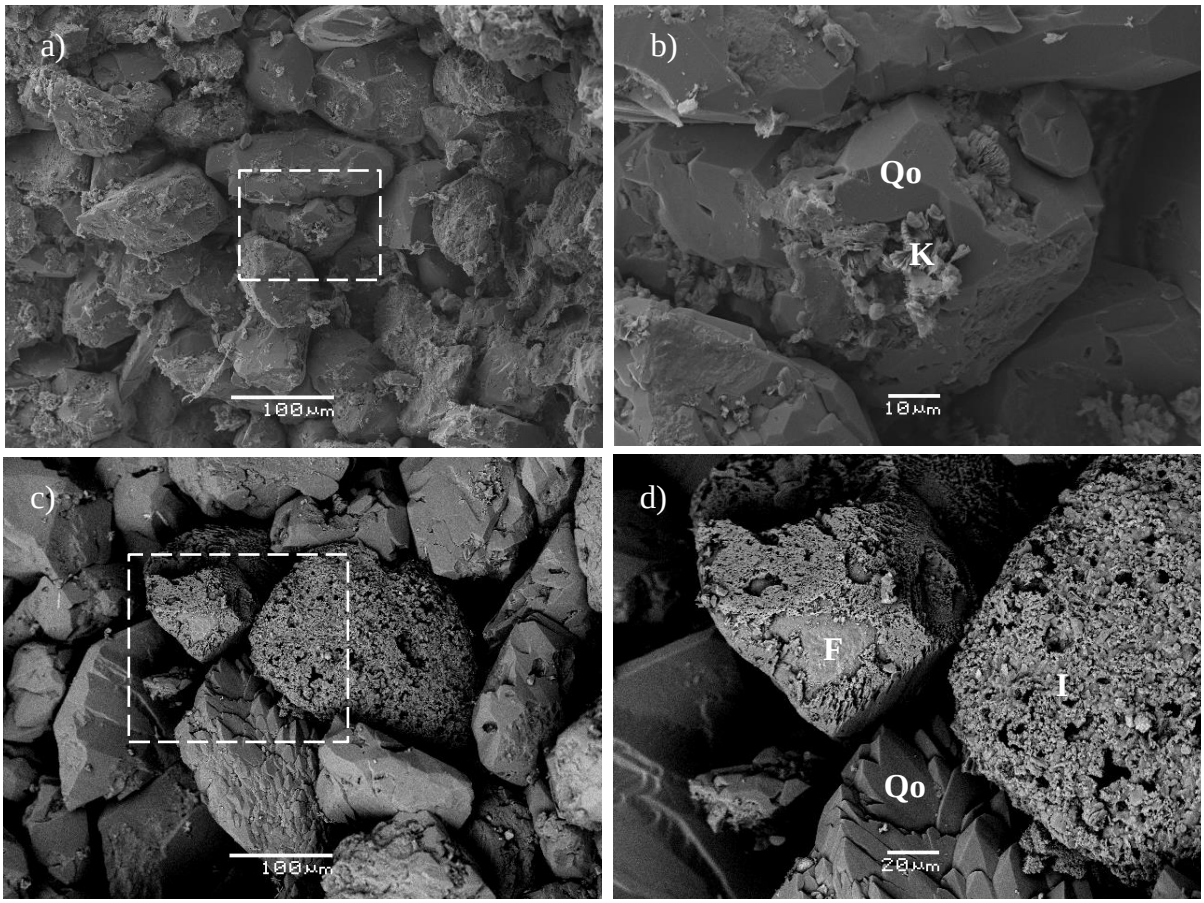

Figure 6. 18: Quartz overgrowth (Qo) increases with depth. a) SEM image from the depth 1373.10 m showing some amount of quartz overgrowth. b) The close-up view of the quartz overgrowth surrounds the kaolinite (K). c) SEM image for the depth of 1425.76 m showing relatively more quartz overgrowth. d) Enlarged part of the image shows that quartz overgrowth as well as K-feldspar grain (F) surrounded by illite coating (I).

The quartz cementation has also been confirmed by the carbon coated thin sections. Eleven carbon coated thin sections have been examined using cathode luminescence and back scattered electron mode during SEM analysis. The cathode luminescence proved to be very useful for the identification of quartz overgrowth. The quartz overgrowth has been distinguished from the detrital quartz grain on the basis of color difference. Quartz with authigenic growth appears as dark black areas around variously colored detrital grains (figure 6.19).

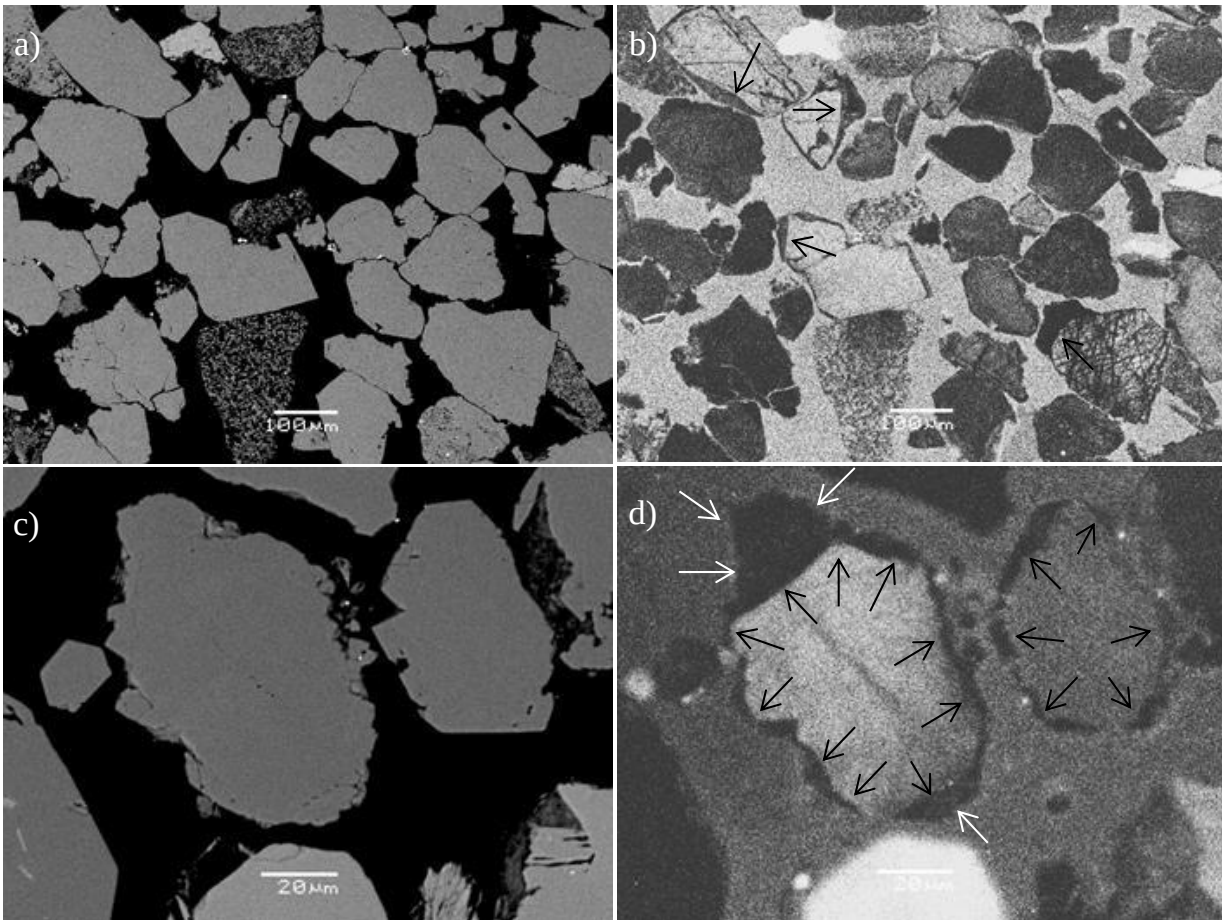

Figure 6. 19: Quartz overgrowth in carbon coated thin sections. Back scattered (left) and cathode luminescence (right) images of clean sandstones at 1444.36 m and 1373.10 m depths respectively. Black and white arrows mark the boundary of detrital and authigenic quartz grains respectively.

6.4.2 Authigenic clay and porosity

During SEM analysis, kaolinite, chlorite and illite have been found as pore-filling clays. Authigenic clays play a vital role in reducing porosity within sandstone reservoirs buried to intermediate depth. Kaolinite exists as vermicular and blocky shapes (figures 6.20) and has been identified in all samples. Illite and chlorite are also present as pore-filling material (See appendices B4). Illite occurs as cluster and platy/wavy shape on K-feldspar grains whereas chlorite is observed as hexagonal crystal close to the albite.

In addition, authigenic clays particularly vermicular kaolinites are also observed in carbon coated thin sections (figure 6.21). Thin sections also provide evidence of porosity and permeability reduction due to presence of authigenic clays (figure 6.22).

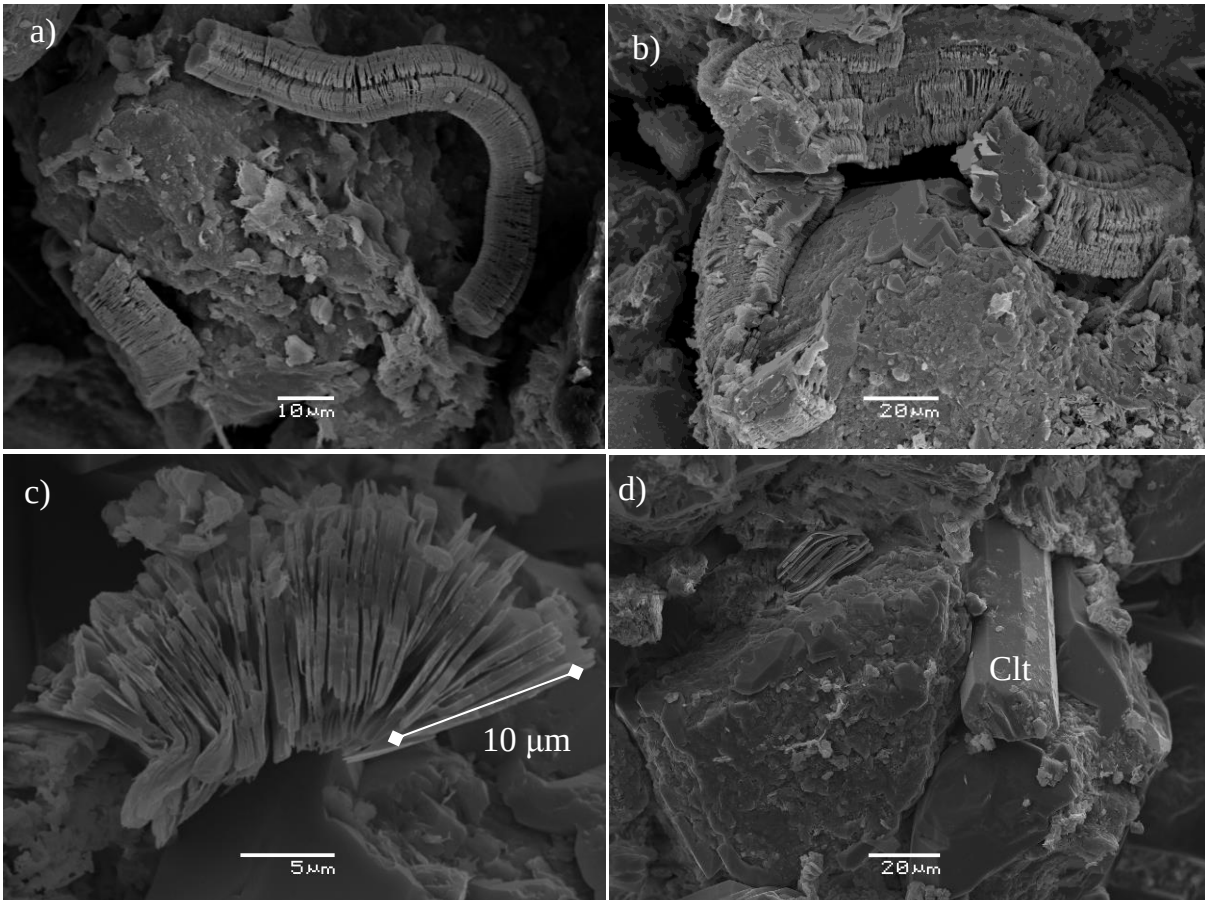

Figure 6. 20: SEM photomicrographs showing typical authigenic clays present in the primary pore spaces. a&b) vermicular kaolinite present at 1349.36 m depth. Small amount of quartz overgrowth also occurs in b. c&d) Flower like cluster of kaolinite clay (left) and hexagonal crystal structure of chlorite (Clt) (right) in the sandstone buried to 1340.15 m depth. Pore spaces between the kaolinite crystals are very small.

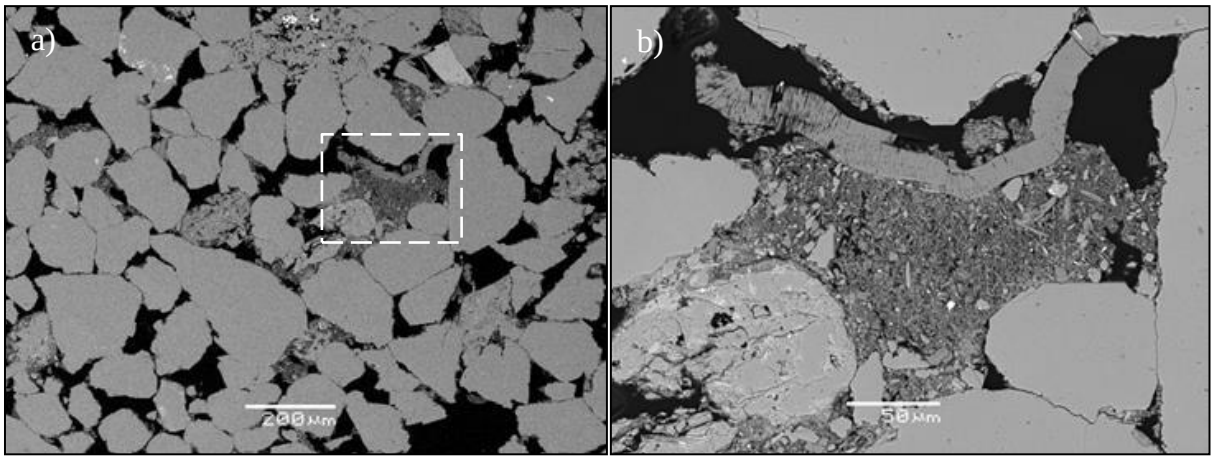

Figure 6. 21: Vermicular kaolinite present within pore spaces of sandstones at 1345.05 m depth.

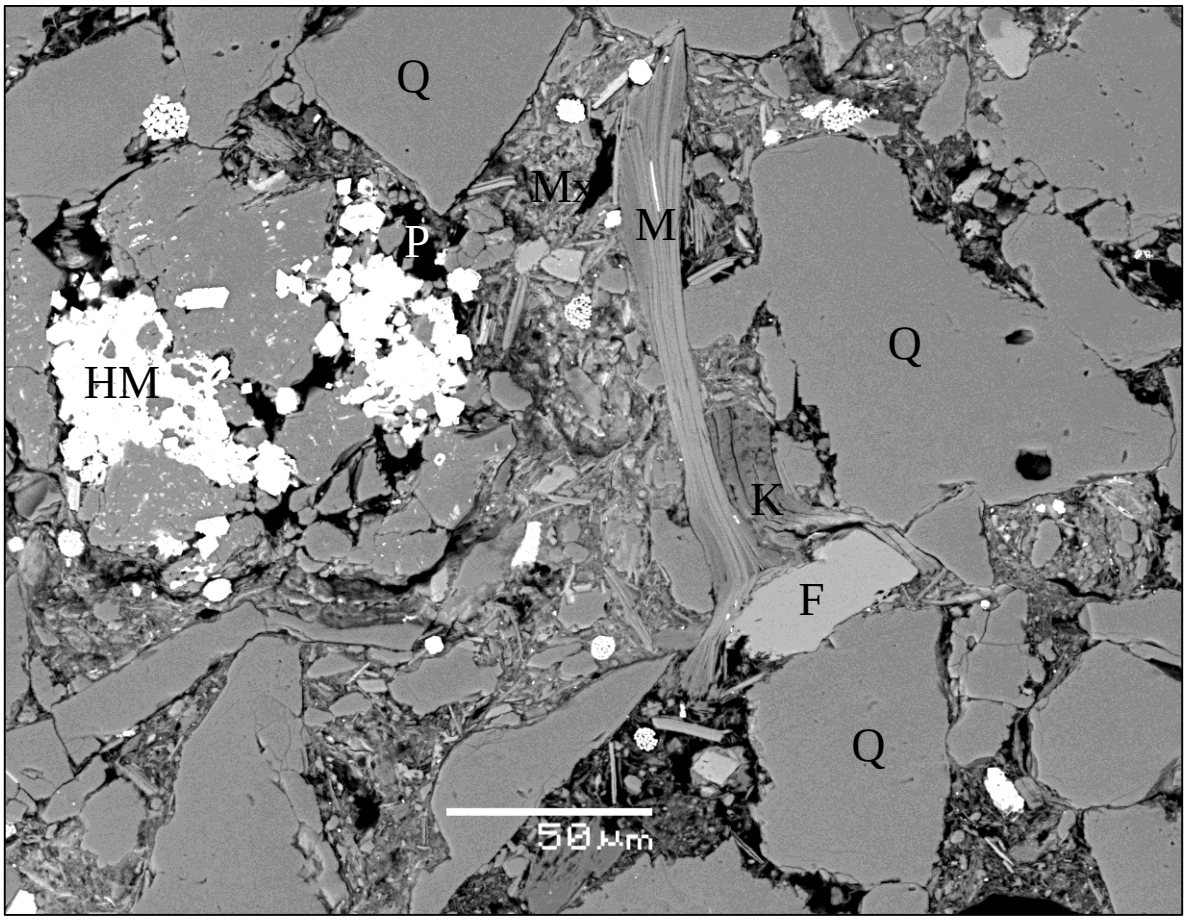

Figure 6. 22: Backscatter electron micrograph of thin section of argillaceous sandstone at 1439.80 m depth illustrating porosity and permeability reduction by authigenic clays. Minerals are labelled as Q for quartz, M for Mica, K for kaolinite, Mx is Matrix, P is porosity, F is feldspar and HM is heavy minerals.

6.4.3 Illite-Smectite Conversion

Pore-filling illite is probably altered from smectite in the presence of K-feldspar (figure 6.23). It is mostly observed to be present on the K-feldspar grains due to weathering of feldspar.

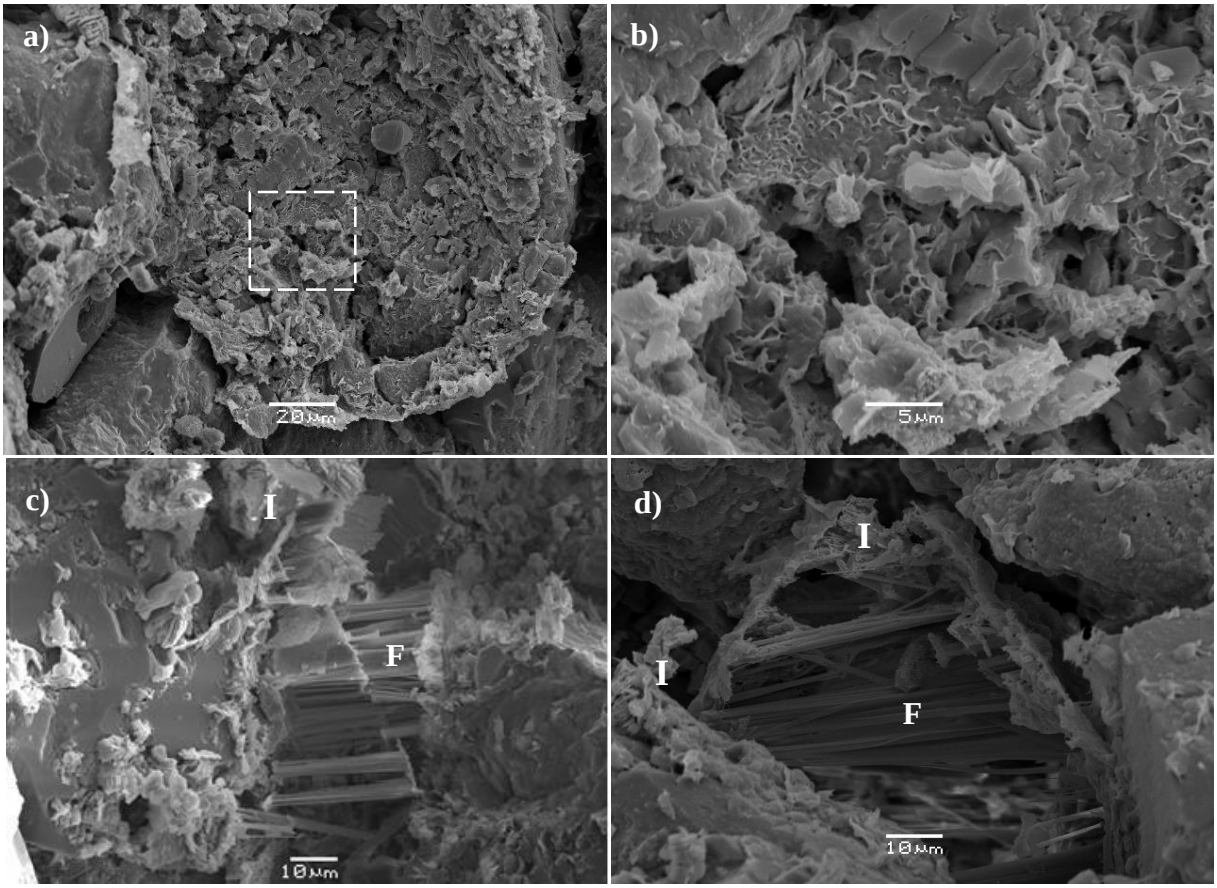

Figure 6. 23: SEM photomicrographs showing illite altered from smectite on the K-feldspar (F) grains. a) Illitisation from smectite and K-feldspar at 1349.36 m depth. b) Enlarged part of figure "a". c) Illitisation of K-feldspar at 1369.77 m depth. d) Illite (I) on the K-feldspar grain at 1349.36 m depth. Significant amount of secondary porosity can be observed within K-feldspar grains in c and d.

6.4.4 Feldspar and Porosity

Albite and microcline have been observed within primary pore spaces of sandstone during the SEM analysis (see Appendix B3). The amount of K-feldspar is comparatively less than the authigenic clays. The feldspar is commonly found as large dissolved grains with the replacement of k-feldspar with albite. Albitization and dissolution of K-feldspar have been identified both on stubs and carbon coated thin sections (figures 6.24 & 6.26). Albite appears as darker patches on light grey k-feldspar. Feldspar overgrowth has been also observed during SEM analysis (figure 6.25).

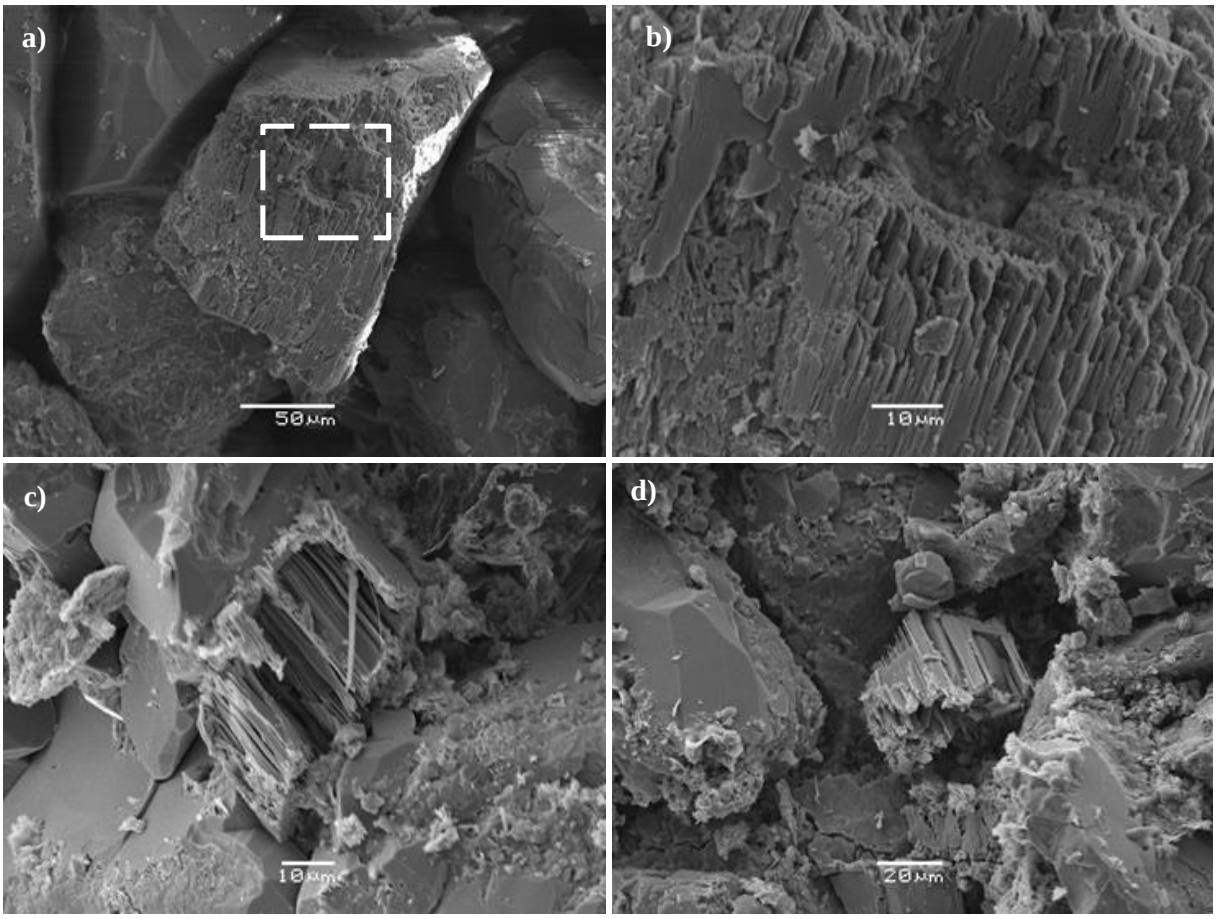

Figure 6. 24: SEM photomicrographs of K-feldspar within primary porespaces of sandstones. a) Pillar/needle like K-feldspar at 1444.36 m depth. b) Enlarged part of figure "a". c) Dissolved K-feldspar with illite clusters on the left at 1373.10 m depth. d) K- feldspar with quartz overgrowth on the left at 1379.50 m depth.

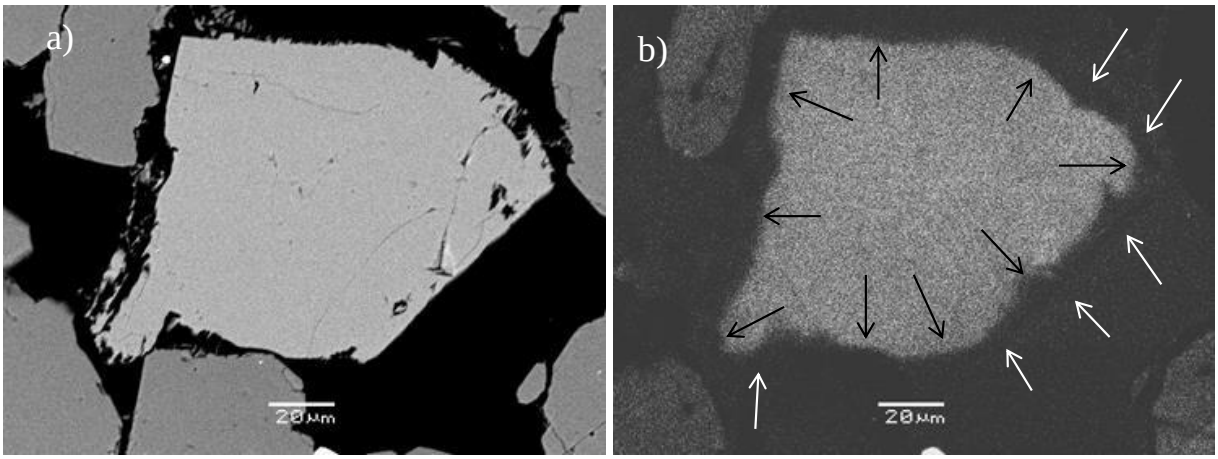

Figure 6. 25: Back scattered (left) and cathode luminescence (right) SEM images of K-feldspar overgrowth at 1420.70 m depth. Black and white arrows mark the boundary of detrital and overgrowth feldspar respectively.

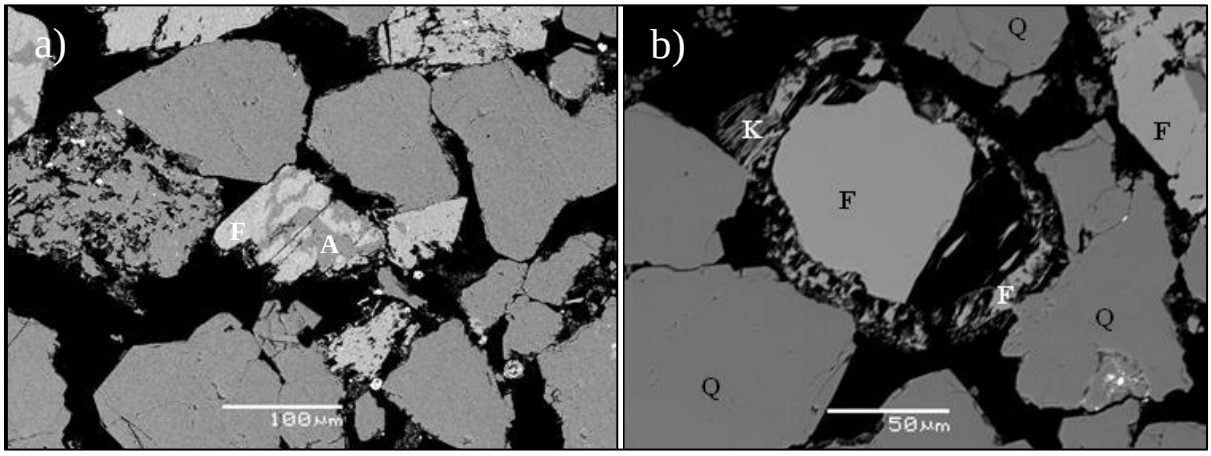

Figure 6. 26: a) SEM images of albitization of K-feldspar (F) at 1449.40 m depth. b) Secondary porosity with in dissolved feldspar grain at1356 m depth (A: Albite, K: Kaolinite and Q: Quartz).

6.4.5 Heavy Minerals

Heavy minerals have been observed both on gold coated stubs and carbon coated thin sections during SEM analysis. Pyrite is the dominant among the heavy minerals whereas sphalerite and zircon are present in small quantity. The authigenic framibiodal pyrite exists in all samples and it is a part of a pyritized sponge (Zimmerle, 1991). Other heavy minerals such as sphalerite, apatite and zircon have been also observed during SEM analysis (figure 6.27).

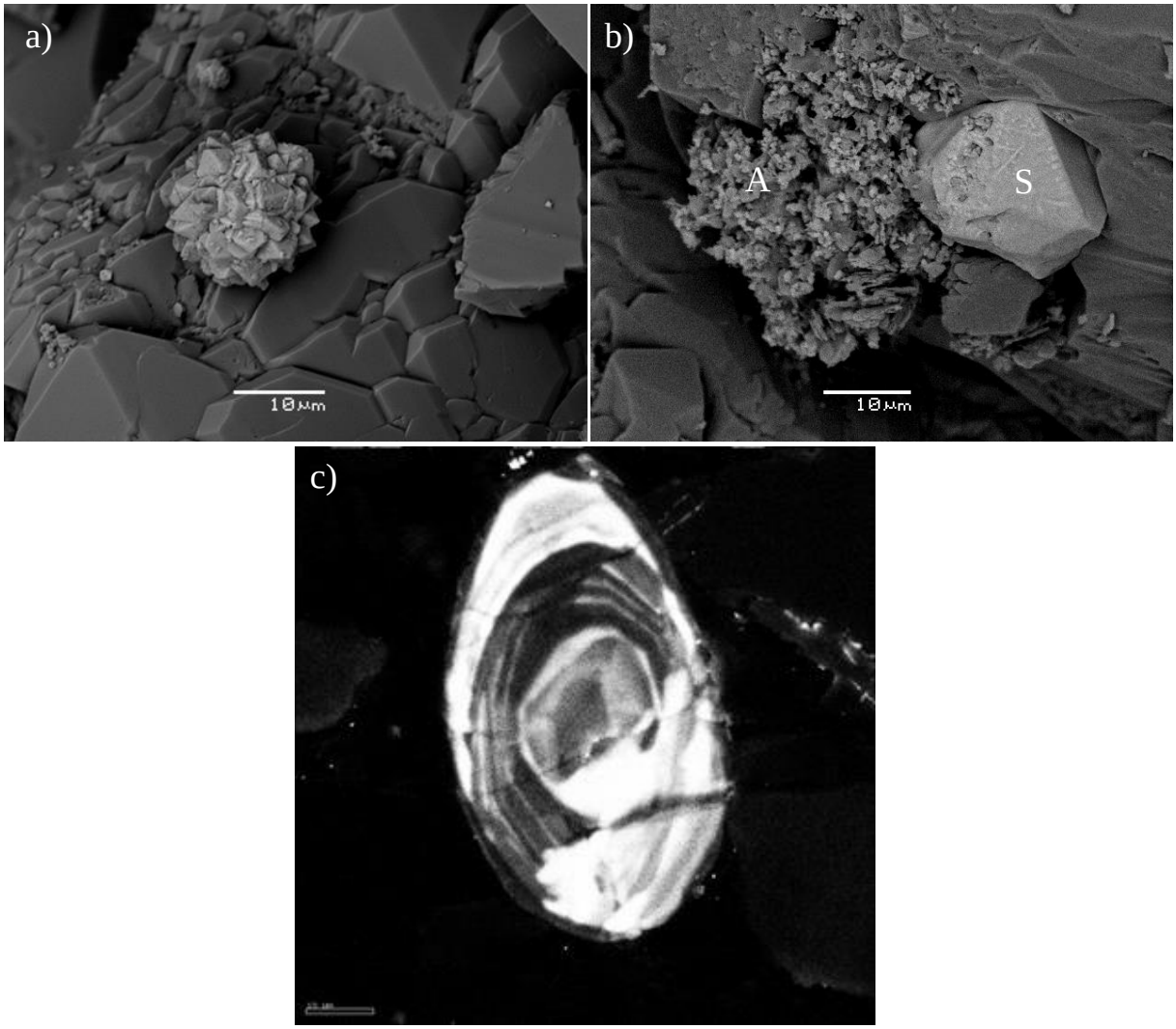

Figure 6. 27: SEM images of heavy minerals: a) Framibiodal pyrite with quartz overgrowth at 1425.76 m depth. b) Sphalerite (S) and Apatite (A) in low vacuumed electron microscopy at 1431.70 m depth. c) Zonation in zircon at 1439.80 m depth.

6.4.6 Ductile Components

Ductile components are deformed and reoriented due to mechanical compaction and are distributed within pore spaces. The presence of ductile components reduces porosity significantly (figure 6.28). For example, the sample from argillaceous sandstone at 1340.15 m depth has relatively higher amounts of ductile components with lower porosity value.

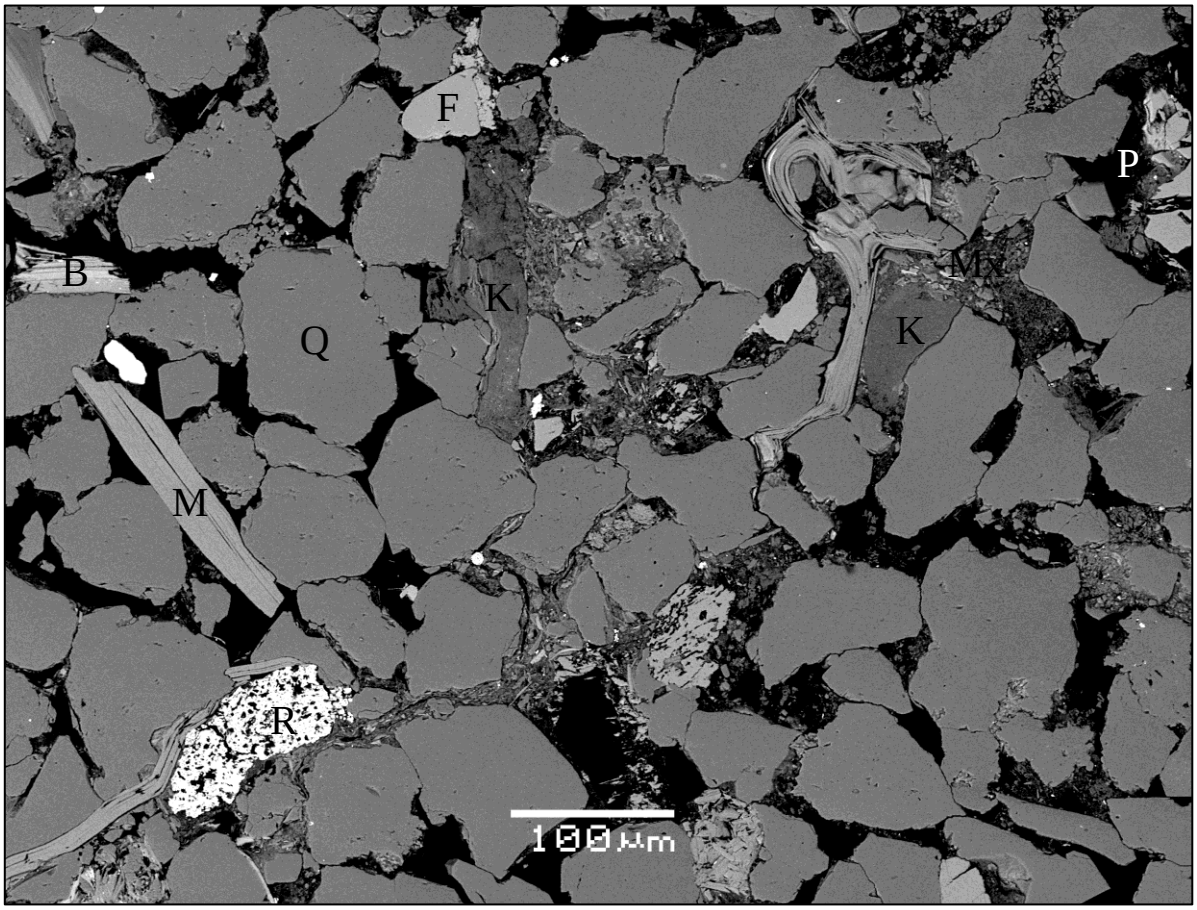

Figure 6. 28: Backscatter electron micrograph of thin section of argillaceous sandstone at the depth of 1340.15 m illustrating porosity and permeability reduction by ductile components. Additionally, reduction in IGV from deformation of ductile components due to compaction may also be estimated. Minerals are labelled Q are quartz, B is Biotite, M is Mica, K is kaolinite, Mx is Matrix, P is porosity, F is feldspar and R is rutile.

6.5 Point Counting and SEM Analysis

The point count analysis of thin sections is a very time consuming and tiresome job, while the scanning electron microscope (SEM) analysis is easy to perform in short time with more precise results. Porosity and the amount of minerals have been enumerated from scanning electron microscope to confirm point count results. The measurements of area in SEM analysis include percentage of porosity, clays, quartz, feldspar and heavy minerals (Figure 6.29). A favorable comparison of minerals and porosity values has been done between the SEM and point count results (Figure 6.30). The small differences in the quantification are due to area of observations because point count analysis covers the whole thin section whereas SEM covers only specific region of thin section. SEM quantifies mica and matrix as clay.

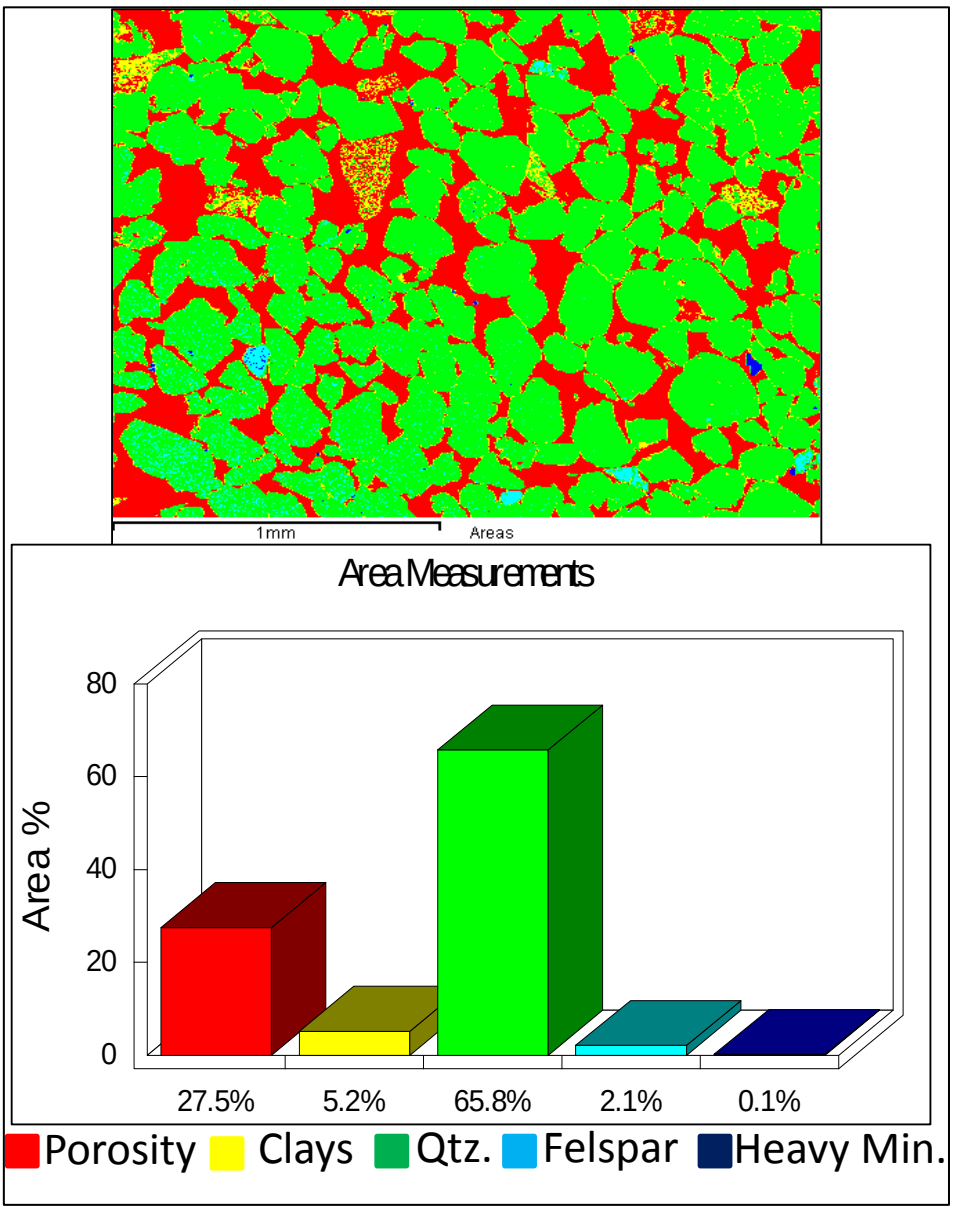

Figure 6. 29: Quantification analysis of porosity and minerals by SEM at 1444.36 m depth.

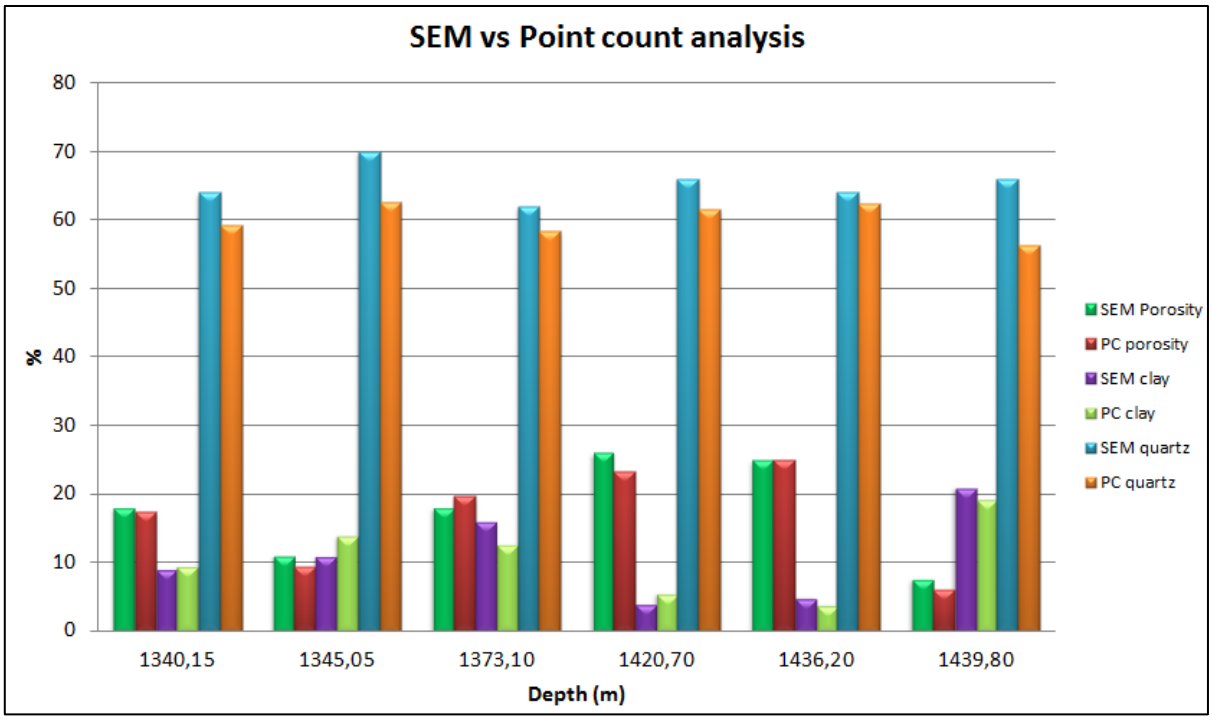

Figure 6. 30: Comparison of point count analysis and SEM analysis for the estimation of porosity, quartz, and clay at different depts.

6.6 X-Ray Diffraction (XRD) Analysis

The elemental analysis of Lower-Middle Jurassic sandstones has been performed by XRD technique for the minerals identification and semi-quantification (see Appendix B 11). The main objective of XRD analysis is to evaluate mineralogical variations across the Nordmela and Stø formations. The XRD results clearly indicate three primary predominant mineralogical components in all samples; quartz, kaolinite and feldspar (table 6.4 and figure 6.31). It should be noted that XRD results are not true representations of volume percentages because it does not estimate porosity present in the rock.

6.6.1 Stø Formation

The mineralogy of Stø Formation has been studied on 8 samples by bulk XRD analysis of the samples from well 7220/5-1. XRD results shows that quartz is the dominating mineral with an average content of 87.0 XRD%. Moreover, kaolinite is the second dominating mineral ranges in between 1 and 6 XRD% with an average content of 3.8 XRD%. The higher concentration of quartz and the fewer amounts of authigenic clays add values to the quality of Stø Formation for being a good reservoir. Other dominating minerals are K-feldspar and illite/mica with an average content of 3.5 XRD% and 2.4 XRD% respectively. The average concentration of albite (sodium plagioclase) is 1.59 XRD% while heavy minerals such as pyrite, ankerite and sphalerite exist as trace minerals (<1 XRD %). Carbonates and evaporitic minerals such as halite, gypsum and sylvite are also present in a trace amount and termed as secondary minerals. Secondary minerals are formed as a result of chemical reactions between drilling mud and drill cuttings and salts are formed due to evaporation of brine. All those minerals are considered to be trace minerals whose bulk chemistry does not resemble the bulk chemistry of rock and rock properties are not dependent on those minerals.

6.6.2 Nordmela Formation

The quantitative mineralogical analysis of Nordmela Formation has been performed on 7 samples. All samples are taken from the upper part of Nordmela Formation which mainly consists of sandstone as the dominant lithology. Quartz is the most prominent mineral with an average content of 89 XRD% whereas K-feldspar is the second dominating mineral with an average of 3.2 XRD%. The amount of albite and feldspar is higher in Nordmela Formation as compared to Stø Formation. Albite and kaolinite concentrations fall between 2.3 XRD% and 1.9 XRD% respectively. Heavy minerals, salt and carbonates also exist in the Nordmela Formation as trace minerals.

Table 6. 4: Numerical values of minerals in percentage obtained from bulk XRD analysis in the well 7220/5-1.

Fms	Depth (m)	Quartz	K-feldspar	Kaolinite	Albite	Illite/Mica	Heavy Minerals	Secondary Minerals
Stø	**1340,2**	84,89	4,35	4,44	1,745	3,265	0,188	1,132
	1345,1	87,66	1,62	5,37	1,443	2,31	0,589	0,969
	1349,4	90,95	0,79	3,6	1,546	1,372	0,077	1,664
	1356,1	89,7	3,11	2,74	1,532	2,06	0,2	0,682
	1363,1	93,27	2,67	1,506	1,093	0,524	0,306	0,626
	1369,8	83,46	4,48	4,44	1,74	3,59	0,806	1,519
	1373,1	84,03	5,33	3,97	1,801	2,55	0,931	1,349
	1379,5	82,83	5,38	4,26	1,835	3,27	0,89	1,445
Nordmela	**1420,7**	95,61	0,5	0,84	1,528	0,64	0,082	0,809
	1425,8	94,09	1,2	1,381	1,15	0,727	0,667	0,746
	1431,7	91,71	2,85	1,19	1,629	0,281	0,55	1,343
	1436,2	91,94	2,99	1,181	1,681	0,842	0,32	1,054
	1439,8	75,4	5,61	5,63	2,76	7,12	1,6	1,851
	1444,4	95,12	0,81	0,683	1,211	0,522	0,56	1,101
	1449,4	80,73	8,11	2,25	5,941	0,828	0,57	1,572

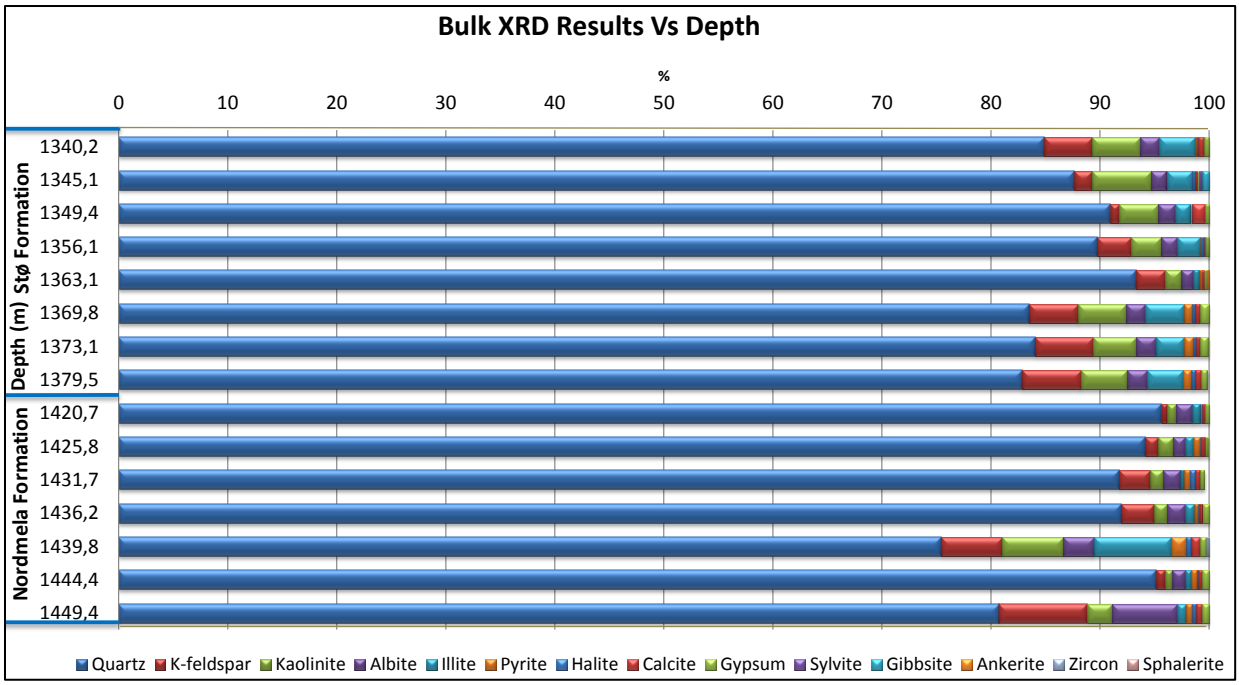

Figure 6. 31: Bar chart of identified minerals from bulk XRD analysis.

In general, the amount of kaolinite is higher than illite in both Nordmela and Stø formations. Kaolinite ranges in between 1.5 and 5.4 XRD% whereas illite content fluctuates between 0.5 and 3.6 XRD% in the Stø Formation (figure 6.32). Illite distribution in the Nordmela Formation varies from 0.3 to 7.2 XRD%.

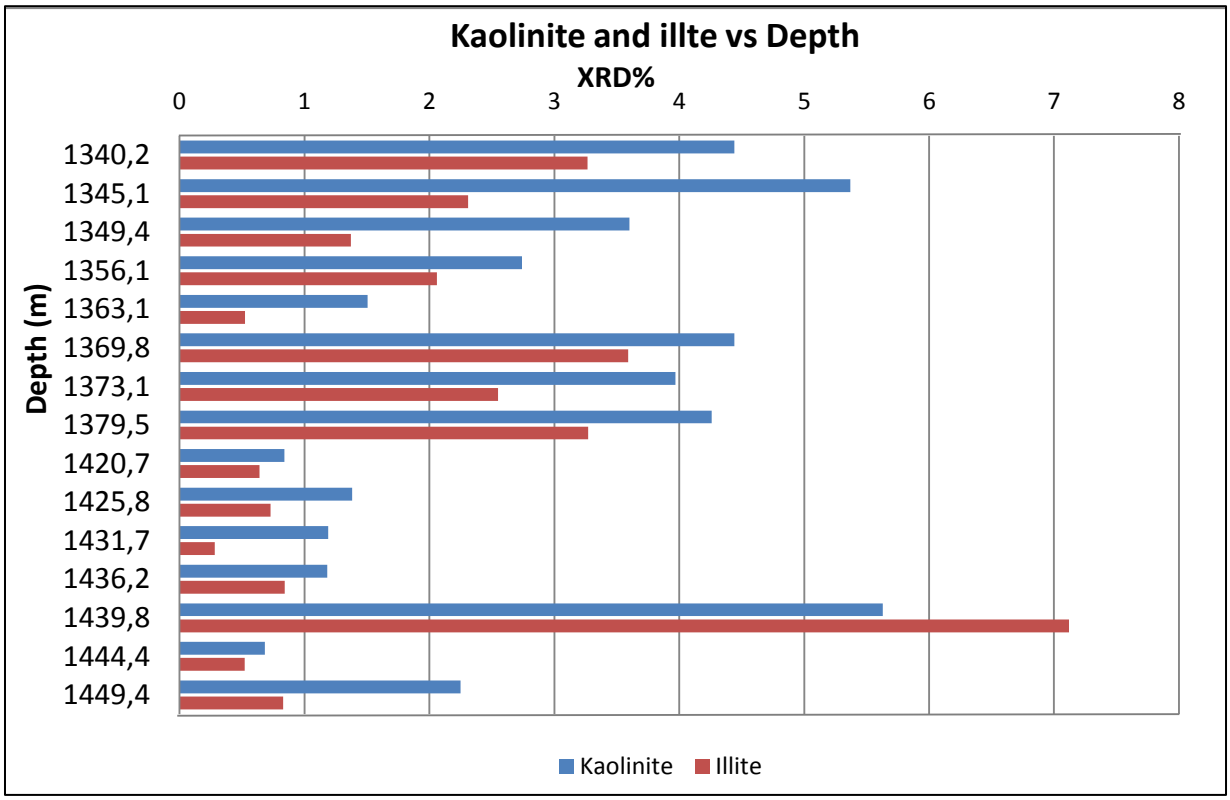

Figure 6. 32: Clay (kaolinite and illite) distribution within Stø and Nordmela formations.

6.7 Core Analysis

Core analysis has been carried out from 1458 m to 1337 m depth for the sedimentological characterization and depositional environments of Stø and Nordmela formations (See Appendix C). Sandstone and siltstone are the major lithologic constituents of each core. While minor constituents of the cores are shales and conglomerates. Facies distribution in Lower-Middle Jurassic sandstones is described as below:

6.7.1 Cross Laminated Sandstones

The cross laminated sandstones are the dominant among all facies and are present at 1434.4-1428 m and 1415.7-1380.2 m depth intervals. This facies consists of fine to medium grained, well sorted and light greyish sandstones (figure 34a). It is mainly characterized by cross lamination and coarsening upward sequences. This facies is common in fluvial deposits and represents coastal plain depositional environments.

6.7.2 Bioturbated Sandstone and Mudrock Facies

The bioturbated sandstones and mudrock facies lack stratification and are present at 1449-1446.9 m and 1348.3-1339 m depth intervals. This facies is characterized by fine-grained bioturbated sandstone containing mud-lined and pelleted burrows filled by fine-grained material (figure 33a). These types of sediments are common in both shoreface and tidally influenced deposits.

6.7.3 Bioturbated Alternating Siltstone/Sandstone

The bioturbated siltstone/sandstone facies are observed frequently in the upper part of Nordmela Formation and are present at 1458-1452.3 m, 1439.9-1434.4 m and 1380.2-1349.1m depth intervals. This facies consists of majorly thinly bedded argillaceous siltstone and sandstone with lenticular or convolute lamination. It is characterized by moderate bioturbation, soft sediments deformation structures and coarsening upward sequences (figure 33c).

6.7.4 Low Angle Laminated Siltstones

Low angle laminated siltstones are present within the Nordmela Formation at 1452.3-1449.3 m and 1444.3-1439.9m depth intervals. This facies is mainly characterized by filled burrows and chert concretions (figure 33b). Absence of mud drapes and wave ripples in this low angle laminated siltstone facies suggest that these are deposited in deeper part of basin rather than in tidal environment.

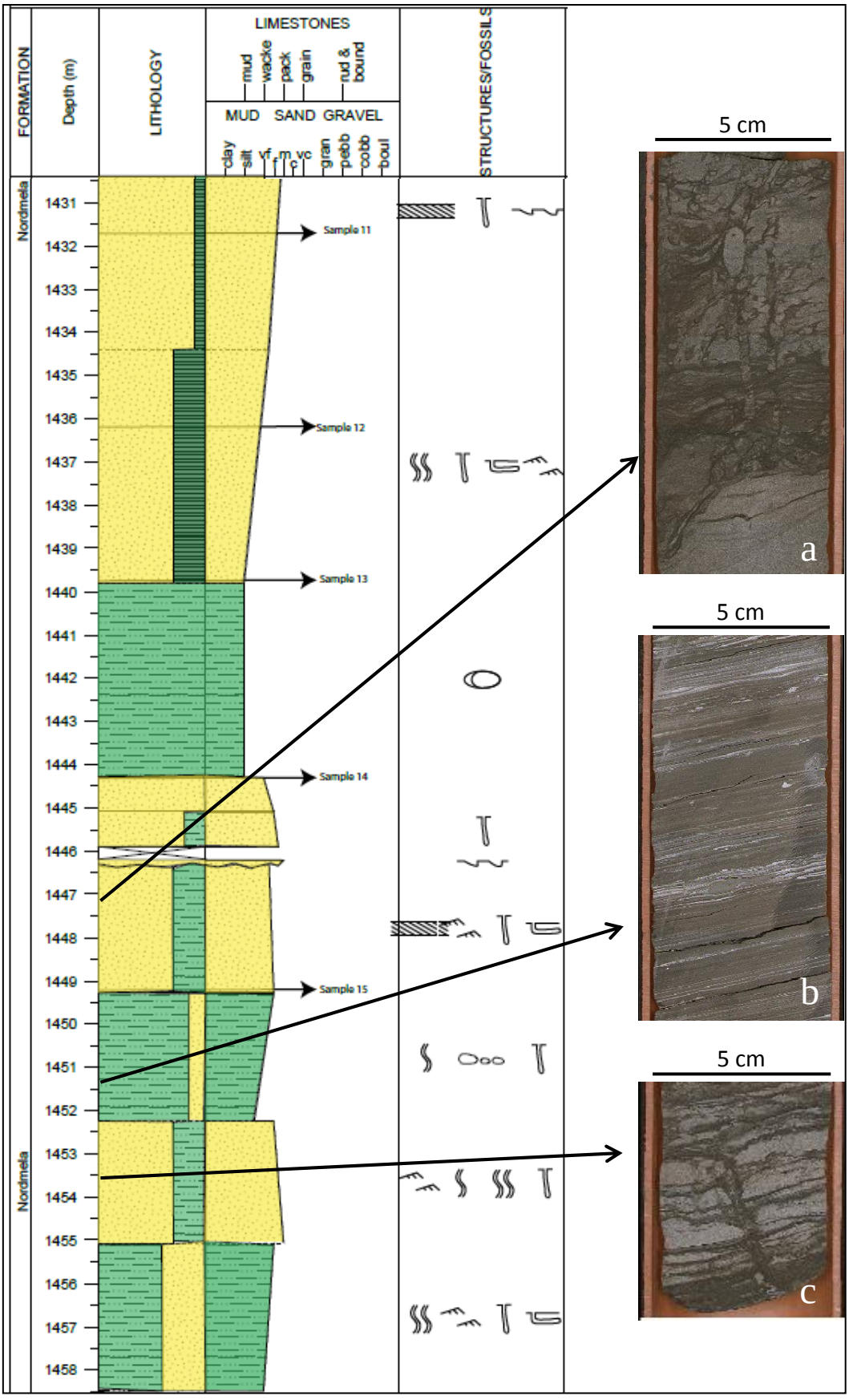

Figure 6. 33: Sedimentological core logging with core photos of Nordmela Formation. a) Bioturbated sandstone and mudrock facies. b) Low angle laminated siltstone. c) Moderately bioturbated alternating siltstone/sandstone.

6.7.5 Conglomerates

Conglomerates are present as a minor constituent in different cores with maximum 20 cm thickness at 1416-1415.8 m depth. Conglomerates are matrix supported and consist of sub-angular to rounded clasts (figure 34b).

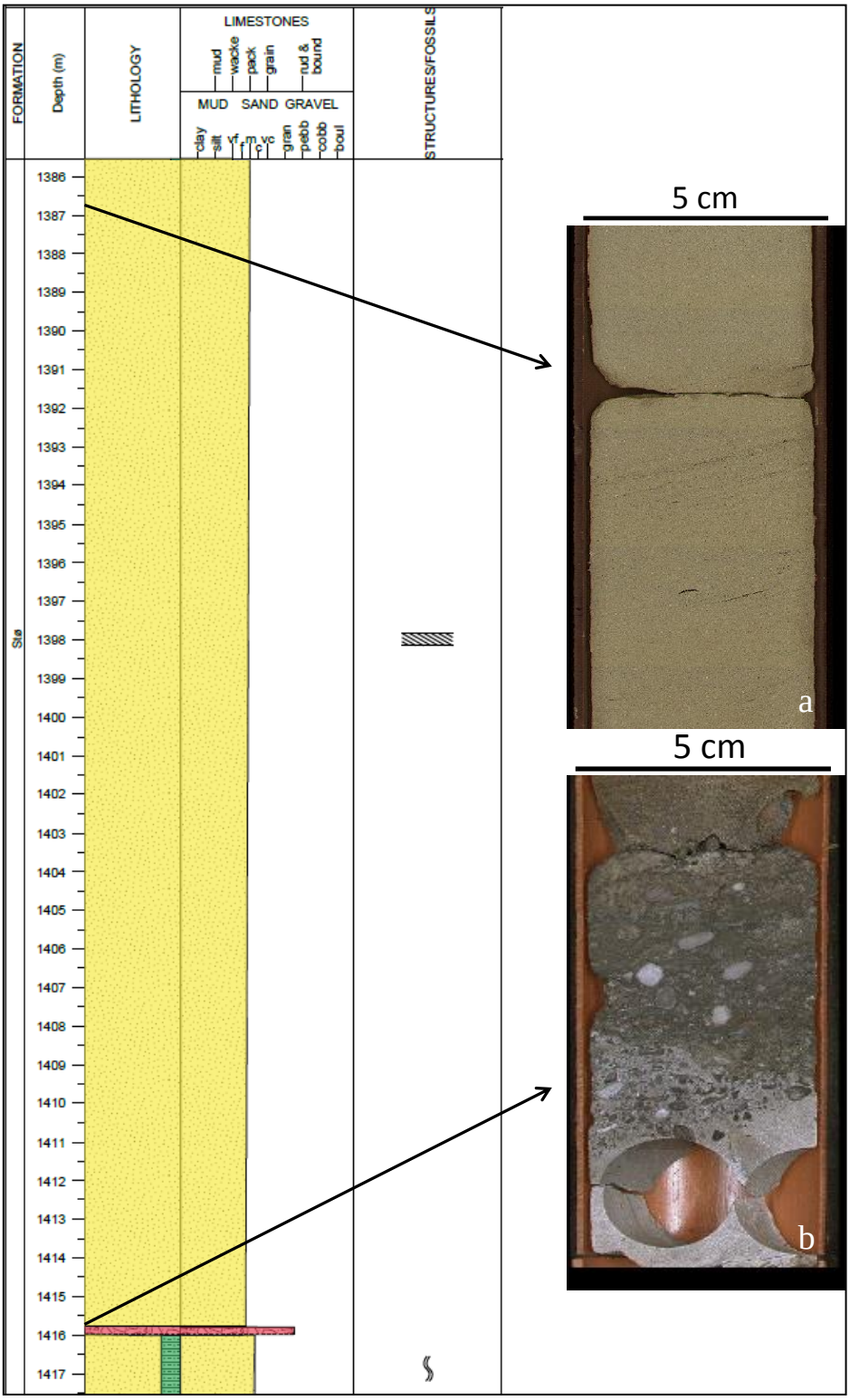

Figure 6. 34: Sedimentological core logging with core photos of Stø Formation. a) Cross laminated sandstone. b) Matrix supported conglomerates with rounded clasts.

CHAPTER 7

DISCUSSIONS

- MECHANICAL COMPACTION
- IGV (INTERGRANULAR VOLUME)
- AUTHIGENIC CLAYS AND POROSITY
- ALBITIZATION
- CHEMICAL COMPACTION
- QUARTZ CEMENTATION
- POROSITY PRESERVING MECHANISMS
- PETROPHYSICAL EVALUATION
- CORE ANALYSIS
- INTEGRATED STUDY
- RESERVOIR QUALITY

7.1 Mechanical Compaction

The reservoir quality is strongly dependent on diagenetic processes particularly mechanical compaction in sandstones buried to intermediate depth. The mechanical compaction of sediments by effective vertical stress and overburden results in reduction of bulk rock volume and porosity with depth. If an initial porosity is assumed to be 40% for the porous sandstones then about 10-15% of the total porosity is lost as a result of mechanical compaction.

Figure 7.1 illustrates that the major porosity loss (point A) which occurs in these sandstones is due to mechanical compaction. Prior to quartz cementation, porosity loss occurs mainly as a result of grain rotation, reorientation, slippage and deformation of ductile components. The sandstone reservoirs had undergone chemical compaction for a short period of time and then started to uplift. Chemical compaction and quartz cementation of sandstones continued also during uplift before it approached mechanical compaction zone (point B).

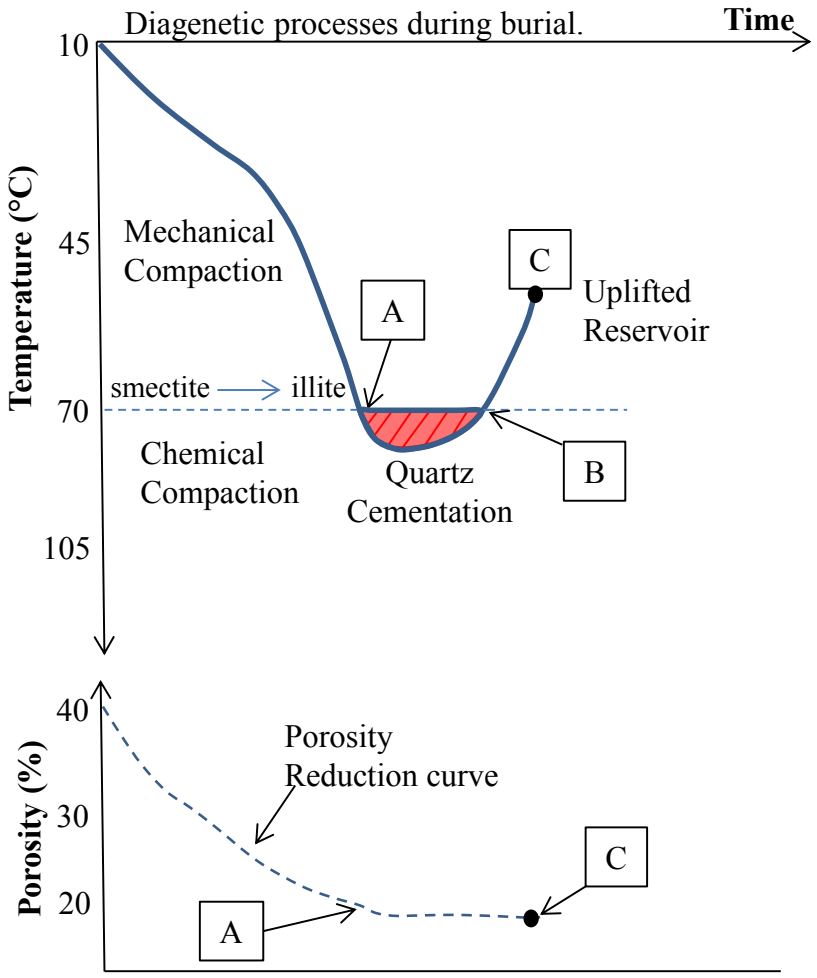

Figure 7. 1: Diagenetic processes as a function of temperature and time. Note that quartz cementation will continue also during uplift as long as the temperature exceeds 70-80 ^{o}C. Modified from (Bjørlykke and Jahren, 2010).

The rate of quartz cementation may have decreased and continued with slower rate during uplift (Bjørlykke and Jahren, 2010). The bore hole temperature (52 ^{o}C) in the well 7220/5-1 suggests that the quartz cementation ceased and reservoir is present in mechanical compaction zone (point C in figure 7.1).

7.2 Burial History Curve

The burial history curve is based on the thickness of each lithostratigraphic unit encountered in the well 7220/5-1 (figure 7.2). This curve illustrates that Lower-Middle Jurassic sandstones have experienced temperature in the range of chemical compaction and quartz cementation during Early Tertiary. It is also assumed that the geothermal gradient has increased due to heat flow from deeper rocks during uplift of the basin. While temperature gradient and geothermal history in the well 7220/5-1 suggests that the reservoir sandstones has experienced temperatures higher than 70 ^{o}C prior to uplift. The P-wave velocities in the sandstones are higher than expected and suggest that these sandstones have been buried to the chemical compaction zone and experienced quartz cementation for a short length of time (figure 5.10). Burial rate was higher during Early-Late Paleogene and reservoir sandstones experienced maximum depth of 2.2 km prior to uplift.

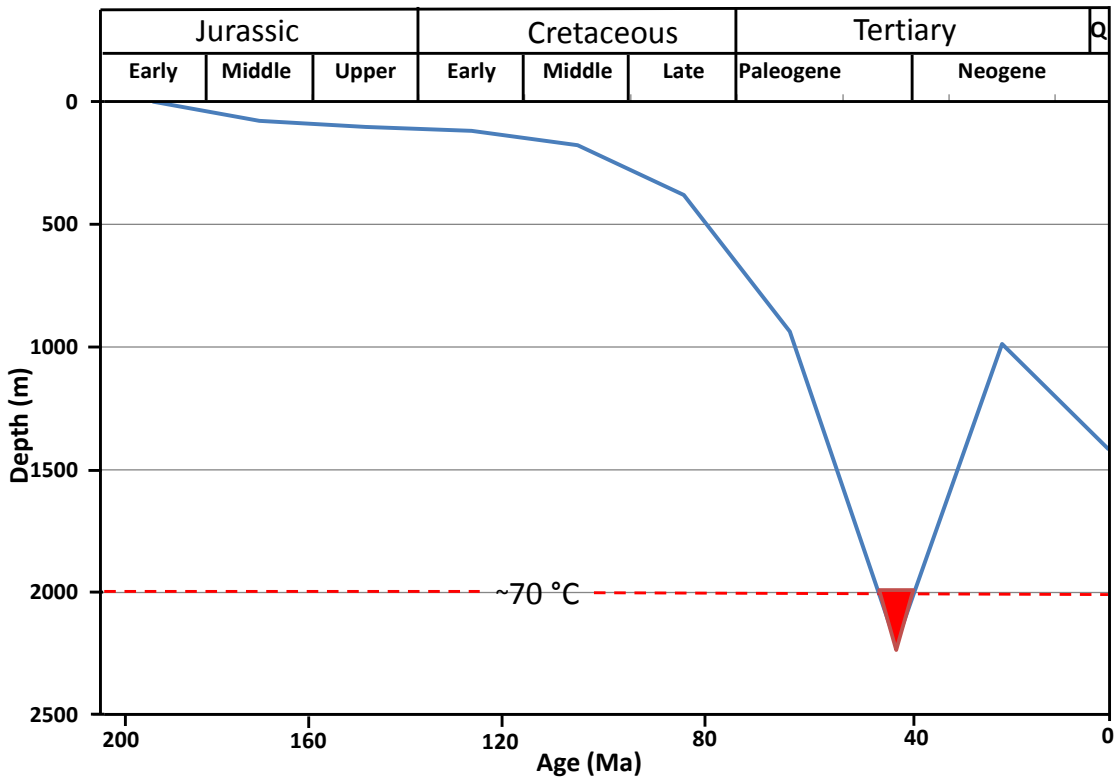

Figure 7.2: Estimated burial-history curve of the Lower-Middle Jurassic sandstones from the well 7220/5-1 at the Johan Castberg Field in the Barents Sea. The length of time, the sediments has been exposed to temperature higher than 70 ^{o}C has been illustrated by red color.

The amounts of uplift estimated in the wells 7220/5-1 and 7220/8-1 are 1272 m and 1120 m respectively. Well 7220/5-1 is located 3 km to the north of well 7220/8-1 and amount of uplift increases towards the north of Barents Sea (Ohm, 2008).

7.3 Intergranular Volume

Intergranular volume (IGV) is the sum of porosity, quartz cement, authigenic kaolinite and depositional matrix (figure 7.3). The IGV values measure the degree of compaction and ranges from 25.2% to 34.5% in these sandstones (table 6.1). The framework-supported sandstones with higher IGV values indicate a minimum degree of compaction and vice versa (see Appendix B2). IGV decreases with burial depth due to effective stress and overburden. According to Paxton et al. (2002) the relationship between IGV and the degree of compaction is best applied to framework-supported sandstones (and not to matrix-supported sandstones). Therefore, the IGV concept for the matrix-supported sandstone at 1439.80 m depth is less useful.

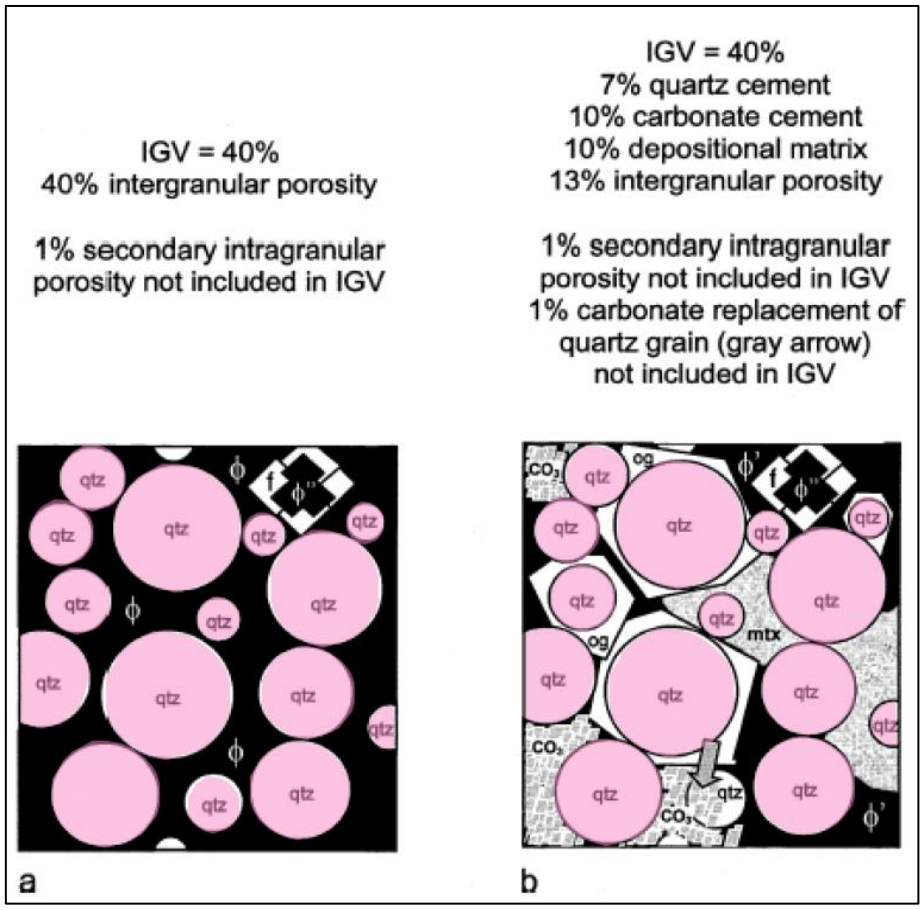

Figure 7. 3: a) IGV in clean sandstone. b) Same IGV with lower intergranular porosity. Note that intragranular components are not included (Paxton et al., 2002).

In Lower-Middle Jurassic sandstones, most of IGV values are occupied by the depositional matrix, organic matter, authigenic clay and intergranular porosity. Secondary porosity observed in K-feldspar has not been included in IGV. IGV is strongly affected by grain size, grain shape, sorting and mechanical compaction (figures 6.11-13). No apparent trend has been observed between depths and IGV values due to closely spaced samples.

The calculated IGV values have been used to quantify and monitor compaction of sandstones (table 6.1). The initial IGV values for unconsolidated sandstones are assumed to be 39-42%. The loss of IGV is higher in shallow depth diagenetic processes and may decline to 28-30% around 1.5 km burial depth. Figure 6.28 delineates a sandstone consists of closely packed deformed ductile grains and IGV value reduced to 28.5%. The further increase in burial depth may slightly decrease IGV and lower limit of IGV of well sorted sandstone is 26% (Paxton et al., 2002). The IGV values of the sandstones suggest that these reservoir sandstones have been buried to approximately 2-2.5 km prior to uplift.

7.3.1 Sorting

Most of the Lower-Middle Jurassic sandstones are moderate to well sorted and exhibit strong relationship between IGV and degree of sorting (figure 6.12). The well sorted sandstones have higher IGV values than the poor to moderate sorted sandstones. The reason is that poorly sorted sandstones contain sand particles of dissimilar sizes and fine-grained sand occupies the available pore spaces between coarse-grained particles (see Appendix B2). It is well noticed that sorting of sandstones together with grain size are important for the resulting IGV values within mechanical compaction zone. The sandstones of the Nordmela Formation are relatively better sorted and have higher IGV values than the Stø Formation.

7.3.2 Grain Size

The Lower-Middle Jurassic sandstones are fine to medium grained and show an inverse trend between IGV values and grain size (figure 6.11). Most of these sandstones are fine-grained and exhibits higher IGV values than the medium-grained sandstones. It is evident from the table 6.1 that the highest IGV values are preserved in fine sands, which subsequently shows that the effect of mechanical compaction is less in fine-grained sandstones. Coarse-grained sand is more compressible and will lose more IGV than fine-grained sand. The reason is that fine-grained sand has higher grain to grain contacts and therefore, the distribution of vertical effective stress on each contact will be less. Well sorted coarse-grained sand is more

compressible due to crushing than the well sorted fine-grained sand (Bjørlykke and Jahren, 2010).

7.3.3 Grain Shape

The grain shape also has a pronounced effect on the IGV values in these sandstones. The frequent grain shape of sandstones is sub-angular to sub-rounded (table 6.1). IGV values increases with the roundness of sand grains. Rounded grains have higher IGV values as compared to angular grains (figure 6.13). Angular grains have the tendency to compact more as compared to rounded grains. Smaller contact areas in angular grains promote crushing and compressibility (Fawad et al., 2011).

7.4 Textural Maturity

The Lower-Middle Jurassic sandstones are mineralogically and texturally mature. The degree of textural maturity has been determined from grain size, sorting and shape, and amount of clay in the sandstones (figure 6.14). It is evident that the well-sorted and well-rounded samples with lesser amount of clay demonstrate higher textural maturity. The Nordmela Formation exhibits well sorting, lower amount of clays and higher textural maturity than the Stø Formation.

7.5 Ductile Components

Mica, depositional matrix, lithic fragments and authigenic clays such as kaolinite and illite have significant effect on the porosity of these sandstones. Figure 6.9 illustrates an inverse relationship between ductile components and porosity. In fact, porosity reduction is a function of the amount and distribution of ductile components within these sandstone reservoirs buried to intermediate depths. The sample with maximum amount of ductile components has minimum porosity value at 1439.80 m depth (figure 6.28 and table 6.1).

7.6 Authigenic Clays

Three types of authigenic clays; kaolinite, illite and chlorite have been observed in the sandstones. Authigenic clays occurred as laminar, structural (grain) and dispersed in the sandstones (see Appendix B1). The amount of kaolinite is comparatively higher than illite. The reason is that these sandstones were not buried to greater depths and kaolinite is not transformed to illite. Kaolinite occurs as clusters, blocky and vermicular shapes (see Appendix B7 and figure 6.20). It is formed at shallow depths due to leaching of minerals like feldspar and mica. The amount of precipitated kaolinite depends on the average groundwater

flux (the rate of groundwater flow per unit area of rock). The groundwater flow removes the cations such as Na^+, K^+ and silica constantly from mica and feldspar and precipitates kaolinite (Bjørlykke and Jahren, 2010). This reaction can be written as:

$$2K(Na)AlSi_3O_8 + 2H^+ + 9H_2O = Al_2Si_2O_5(OH)_4 + 4H_4SiO_4 + 2K^+(2Na^+)$$

Illite is the second dominating mineral observed during SEM and XRD analysis in the sandstones. Illite is formed from smectite at shallow burial depths and at lower temperatures. During intermediate burial diagenesis, smectite starts to dissolve to form mixed layer minerals (I-S) in the presence of K-feldspar at approximately 65 ^oC.

$$\text{Smectite} + K^+ \longrightarrow \text{Illite} + \text{Silica (via mixed-layer minerals)}$$

(Bjørlykke et al., 1995)

According to Hoffman (1979) above reaction may also precipitates chlorite. Illite-Smectite mixed layers become more illitic with increase in temperature. Smectite generally disappears at 75 ^oC and converts to illitic layer (Dypvik, 1983). Illite is more abundant in Nordmela Formation than Stø Formation and approaches up to 7.2 XRD%. Smectite is very similar in structure with illite and is considered to be an ideal substrate for the illite to grow at lower temperatures.

The weathering products of acidic rocks such as granites lead to the formation of smectite. The surface of K-feldspar grain is leached/weathered and may be coated by smectite. This smectite is formed due to weathering in dry environments. The stability of smectite mineral is a function of silica concentration and K^+/H^+ ratio. Higher concentration of silica in the porewater is obtained from biogenic silica or evaporation (Bjørlykke and Jahren, 2010).

7.6.1 Influence on Reservoir Quality

Authigenic clays minerals have profound effect on the quality of reservoirs. Origin, texture, mineralogy and distribution of authigenic clays have been studied for better understanding of their influence on reservoir quality. Kaolinite is present as pore-filling material and reduces porosity significantly in the reservoir. For example, one sample at 1439.80 m depth has 10.6 % authigenic clays that reduce porosity to 6% in the sandstone. However, large amounts of kaolinite are not seen to hinder the flow path of hydrocarbons but are commonly found in specific sandstone intervals.

Illite altered from smectite and has been observed commonly as pore-filling and grain coating clay in these sandstones (see Appendices B4 and B5). The illitisation of these sandstones may improve the reservoir quality as illite has lower specific area than smectite (Bjørlykke and Jahren, 2010). Illitic layers have been found in small quantity and are not believed to have any recognizable influence on the reservoir quality.

7.7 Albitisation

The albitisation process starts with more or less the same temperature that is required for the illitisation of smectite and increases with depth (Aagaard et al., 1990). Albitisation has been observed as a partial replacement of K-feldspar and plagioclase grains in these sandstones (figure 6.26). In general, the albitisation process in these sandstones is incomplete and observed as irregular patches. The reaction takes place at 60-150 ^{o}C in a following order (Baccar et al., 1993).

$$\underset{\text{K-feldspar}}{KAlSi_3O_8} + Na^+ \longrightarrow \underset{\text{Albite}}{NaAlSi_3O_8} + K^+$$

7.8 Chemical Compaction

7.8.1 Quartz Cementation

Quartz cementation is a function of kinetics, pH of porewater, time and temperature (Bjorlykke and Egeberg, 1993). About 70-80 ^{o}C temperature is required for the onset of quartz cementation. Cathode Luminescence (CL) petrographic study shows small amount of quartz cementation at greater depths particularly in Nordmela Formation (See Appendix B8). The quartz overgrowth was difficult to observe in optical microscope so it may be slightly underestimated during point count analysis and therefore, IGV values are also underestimated to some extent in these sandstones.

The amount of quartz cementation varies from 0 to 1.6% (table 6.1) and it indicates that the sandstones reservoir have never been buried to temperatures higher than 80 ^{o}C. The small amount of quartz cementation is enough to cease mechanical compaction and start chemical compaction (Bjørlykke and Jahren, 2010). Most of the detrital quartz grains have sub-rounded shapes whereas quartz with authigenic growth has many different shapes with various widths.

The possible sources for quartz cementation in these sandstones are illitisation of smectite, amorphous silica/Opal CT and possible incipient formation of micro stylolites. Silica released

from illite-smectite reaction does not affect the porosity of rock because precipitated quartz and illite replaces the smectite without any significant change in volume of rock.

The micro-quartz cement has been observed as locally precipitated in these sandstones. It is assumed that this is originally sourced from silica, precipitated as a result of smectite to illite conversion (see Appendix B6). There could also be possibility of biological source for this occasional micro-quartz cement. Amorphous silica (biological origin) transported out as sand sized particle and recrystallized as micro-quartz cement.

Micro-quartz precipitates at lower temperatures (60-70^{o}C) due to supersaturation of quartz through the dissolution of Opal A and Opal CT. Micro-quartz formed from Opal CT may help to retard quartz cementation at higher temperatures and can preserve porosity at greater depths.

7.8.2 Influence on Reservoir Quality

Although, the quartz cementation is low in these sandstones it still has some influence on the porosity (figure 6.19 & 7.1). Quartz precipitation occurred on the grains and in the pore spaces. Quartz overgrowth is relatively higher in clean sandstones than slightly argillaceous sandstones. The micro-quartz cementation does not affect the reservoir quality due to its rare occurrence in the sandstones.

7.9 Porosity Preserving Mechanism

The possibility of maximum porosity loss is supposed to be at maximum burial depth and temperature experienced by sandstones prior to uplift. However, these sandstones are mechanical stable at the present depths. The small amount of quartz cementation and chemical compaction has increased the mechanical strength of sandstones and these are instinctively stronger than the vertical effective stress of overburden.

The porosity is preserved by grain coating to some extent at greater depths. Some of sandstones are found to be coated with illite. While micro-quartz occurred occasional and does not have any influence on the preservation of reservoir quality.

7.9.1 Illite Coating

Illite coating has been frequently observed on both quartz and K-feldspar grains during SEM analysis (see Appendix B5 and figure 6.18). Illite coatings are formed as a result of leaching out of elements from the weathered K-feldspar surface and illite-smectite reaction. Illite is present on the quartz grain surface and retards quartz cementation. So illite was precipitated

on the quartz surface before the onset of quartz cementation. The illite precipitated from smectite is assumed to be best for the porosity preservation in intermediate to deeply buried sandstone reservoirs. The honeycomb substrate inherits the morphology of smectite during progressive illitisation process (Pollastro, 1985). Illite precipitation from kaolinite at 120 ^{o}C - 140 ^{o}C temperatures is too late to retard quartz cementation.

7.9.2 Influence on Reservoir Quality

The illite coatings in these sandstones may have inhibited quartz cementation to some extent. Nevertheless, the effect of illite coating on porosity is difficult to estimate but it is probably minor due to low reservoir temperature. However, the potential for preserving porosity has been assumed that illite coating preserves more porosity as compared to micro-quartz coating in these sandstones. The amount of illite coating is hard to predict, but in few samples illite coating have greater importance locally in retarding quartz cementation.

7.10 Petrophysical Evaluation

Petrophysical evaluation indicates a 77 m thick column of hydrocarbons within in Stø Formation. Moreover, the reservoir holds very good neutron porosity values with an average of 28%. Good permeability of reservoir can be predicted by the effective porosity values together with small amount of authigenic clays.

Depositional environments and sequence stratigraphy of Stø Formation have been reconstructed on the basis of gamma ray log. Gamma ray log indicates three major depositional sequences in Stø Formation that are identified as aggradational, progradational and retrogradational parasequences (figure 5.1).

7.10.1 Aggradational Parasequence (1415-1379m):

The lower part of Stø Formation has boxcar GR log trend that represents aggradational parasequence of sediments deposited during constant sea level. The lower part has 36m thickness and consists of very clean and porous sandstone (figure 5.1).

7.10.2 Progradational Parasequence (1379-1356m):

The middle part of the Stø Formation has funnel-shaped GR log trend with 23m thickness. In general, this funnel-shaped succession represents deposition of cleaning upward sand due to gradual fall in the local mean sea level. The lowermost part of progradational parasequence set contains offshore shale facies whereas uppermost part contains coastal plain sand (figure

5.1). These shallowing/coarsening upward successions are mainly characterized by prograding delta, regressive barrier bars and prograding marine shelf delta (Selley and Sonnenberg, 2014).

7.10.3 Retrogradatinal Parasequence (1356-1337m):

The upper part of Stø Formation has a typical bell-shaped response of gamma ray log with a thickness of about 19m. This finning upward succession is indicative of transgressive sands with more tidal influence in the upper part. The lowermost part of this parasequence represents coastal plain sandy facies while uppermost part indicates offshore fine grained facies (figure 5.1).

7.11 Core Analysis

Sedimentary structures observed during core logging are used for the interpretation of depositional environments (see Appendix C). The lower part of Stø Formation consists of fine to medium grained cross laminated sandstone deposited by fluvial channel near the shoreline (figure 34a). Upper part of Stø Formation consists of moderately bioturbated silty sandstones and mud filled burrows (figure 33a). The deposition of silty sandstone occurred as a result of sea level rise. The middle and upper part of Stø Formation followed regressive and transgressive cycles respectively.

Nordmela Formation consists of diverse facies and is dominated by low angle laminated siltstone facies, conglomerates, bioturbated and cross laminated sandstone/siltstone, and mudrock facies (figure 33 & 34). The cross laminated sandstones with mud drapes indicate tidal channels or tidally influenced fluvial channel deposits whereas the mudrock facies represents tidal flat to flood-plain environments of deposition.

7.12 Relationship between Petrophysical, Petrographical and Core Analysis

Core logging, petrographic and petrophysical results support each other. Well logs and core photos illustrate that the upper parts of Stø and Nordmela formations consist of silty sandstones and sandstones respectively (figure 5.2). Core logging and point count results of all samples within Stø Formation have been correlated at their respective depths (see Appendix B 12). Furthermore, quantitative figures of point counting results without porosity have been calculated to correlate with XRD results (See Appendix B10).

Clean sandstone with GR values of 30 API at 1356.1 m depth shows higher amount of quartz (~90%) in XRD, clean and porous sandstone in thin section, and fine to medium grained sand in core sample (figure 7.4). Integrated study has been carried out for the argillaceous sandstone at 1439.80 m depth. Higher amounts of clay and depositional matrix have been observed in thin section microscopy and scanning electron microscope. The gamma ray value at this depth is 149 API suggests shales and core photo illustrates dark grey mudrock facies. Point counting and XRD also give higher amount of matrix and authigenic clays at 1439.80 m depth (See Appendix B9).

7.13 Reservoir Quality

The reservoir quality is mainly controlled by two diagenetic processes: compaction and quartz cementation (Lander and Walderhaug, 1999). Additionally, the reservoir properties are a function of primary mineralogical composition, amount and distribution of matrix and authigenic clays, grain shape, size and sorting of sandstones. These are further related to climate, depositional environment and provenance of these sandstones.

The Lower-Middle Jurassic sandstones in the south-western Barents Sea possess excellent porosity values at the depth of about 1.4 km. It is evident from thin section microscopy, XRD, and SEM analysis that the Lower-Middle Jurassic sandstones have lower amount of authigenic clays and quartz cementation and are mineralogically mature (table 6.1). In addition, the dissolution of alkali feldspar also increases intragranular porosity within sandstones.

Secondary porosity in the sandstones of Nordmela and Stø formations is resulted due to partial dissolution of grains and brittle fracturing during mechanical compaction. The partial dissolution of grains is commonly observed in the feldspar and plagioclase (figure 6.26), but are observed only in small amounts and do not contribute sufficiently to the total porosity.

The Lower-Middle Jurassic sandstones of Nordmela and Stø formation are classified as subarkosic sandstones on the basis of petrographic classification (figure 6.2). Sandstones are fine to medium grained, moderate to well sorted and mineralogical mature (figure 6.14). These sandstones hold excellent porosity values and exhibit very good reservoir quality.

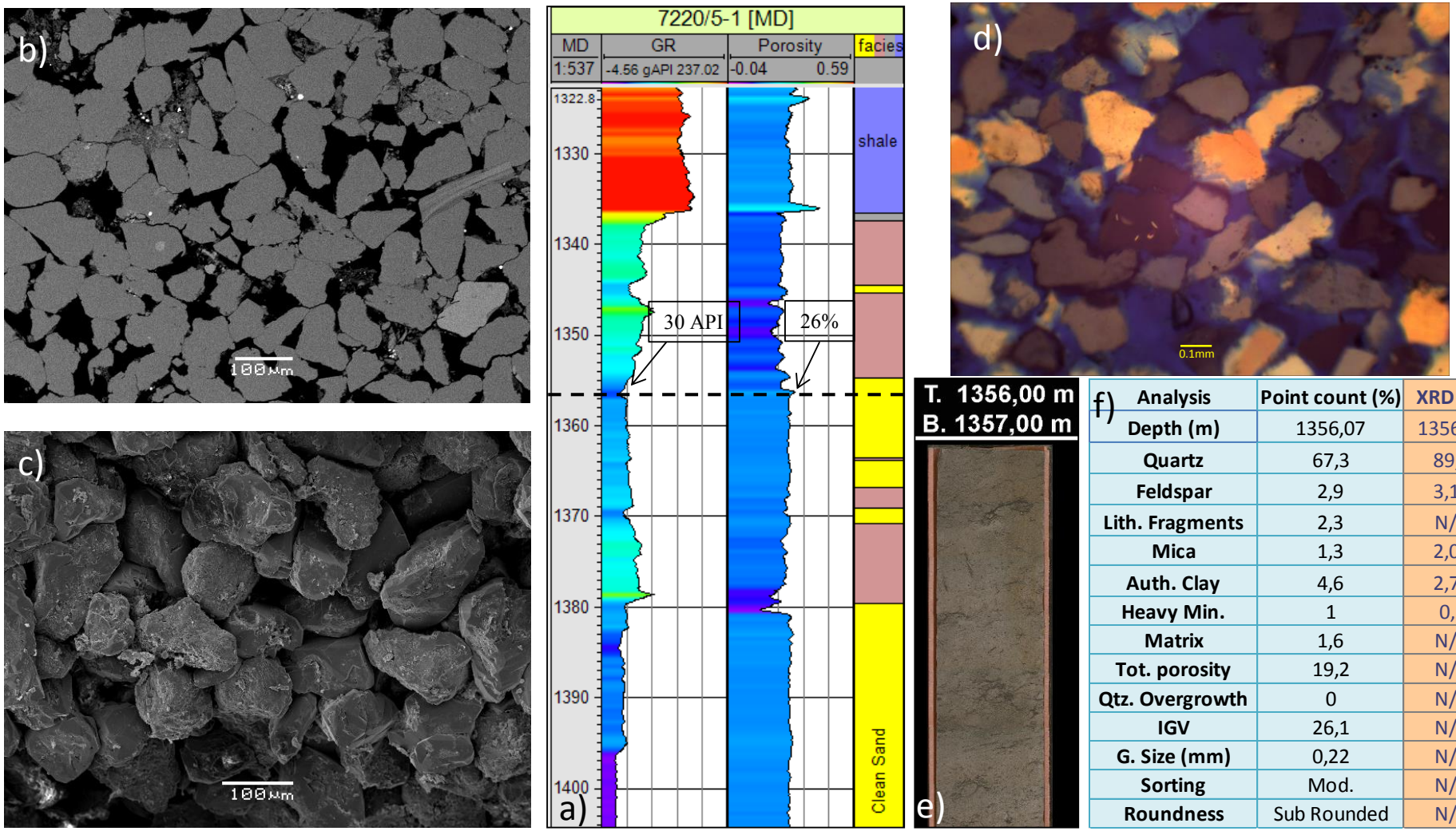

f)

Analysis	Point count (%)	XRD (%)
Depth (m)	1356,07	1356,07
Quartz	67,3	89,9
Feldspar	2,9	3,11
Lith. Fragments	2,3	N/A
Mica	1,3	2,06
Auth. Clay	4,6	2,74
Heavy Min.	1	0,2
Matrix	1,6	N/A
Tot. porosity	19,2	N/A
Qtz. Overgrowth	0	N/A
IGV	26,1	N/A
G. Size (mm)	0,22	N/A
Sorting	Mod.	N/A
Roundness	Sub Rounded	N/A

Figure 7. 4: Integrated study of Core, petrographical and petrophysical analysis at 1356.07 m depth. a) GR, porosity and facies log in the well 7220/5-1. b & c) SEM microphotographs of carbon coated thin section, gold coated stub. d) Thin section overview in optical microscope. e) Core photo of sandstone. f) Quantitative analysis of mineralogy composition by point counting and XRD techniques.

CHAPTER 8

CONCLUSION

- The sandstones of the Stø and Nordmela formations are classified as subarkosic and sublitharenites respectively. The provenance of the reservoir sandstones is suggested to be from cratonic setting and sediments are derived from granitic/acidic rocks.

- Sedimentary structures suggest fluvial to coastal plain and tidal flat to flood-plain depositional environments of the Stø and Nordmela formations respectively.

- IGV reflects the degree of mechanical compaction and exhibits strong relationship with grain shape, size and sorting of sandstones. The sandstone with lowest IGV (25.2%) indicates maximum degree of compaction. Well sorted, rounded and fine grained sandstones have higher IGV values.

- Porosity is largely destroyed by grain rotation, re-orientation, and slippage during mechanical compaction. While, the small amount of quartz cementation has minor effect on porosity loss.

- The Amount of authigenic clays and depositional matrix has significant effect on the porosity of the sandstones in the area. Sandstones with higher amount of clays and matrix reflect lower porosity values.

- The amount of quartz cementation in the Nordmela Formation is comparatively higher than the Stø Formation and the sources of quartz cementation are illitisation of smectite, Opal CT and possible incipient formation of micro stylolites.

- The amount of quartz cementation and the burial depth curve suggest that Lower-Middle Jurassic sandstones have been subjected to approximately 80 ^{o}C temperature prior to uplift.

- Illite coating is seldom observed in the study area. The reservoir sandstones have never experienced intense quartz cementation and therefore, the effect of illite coating on reservoir quality is hard to estimate.

CHAPTER 9

REFERENCES

AAGAARD, P., EGEBERG, P., SAIGAL, G., MORAD, S. & BJORLYKKE, K. 1990. Diagenetic Albitization of Detrital K-Keldspars in Jurassic, Lower Cretaceous and Tertiary Clastic Reservoir Rocks from Offshore Norway, II. Formation Water Chemistry and Kinetic Considerations. *Journal of sedimentary Research,* 60.

AASE, N. E., BJORKUM, P. A. & NADEAU, P. H. 1996. The effect of grain-coating microquartz on preservation of reservoir porosity. *AAPG bulletin,* 80**,** 1654-1673.

AHARONOV, E. & KATSMAN, R. 2009. Interaction between pressure solution and clays in stylolite development: insights from modeling. *American Journal of Science,* 309**,** 607-632.

BACCAR, M. B., FRITZ, B. & MADE, B. 1993. Diagenetic albitization of K-feldspar and plagioclase in sandstone reservoirs: thermodynamic and kinetic modeling. *Journal of Sedimentary Research,* 63.

BARRÈRE, C., EBBING, J., SKILBREI, J. & ZEYEN, H. Lithospheric Characterisation by Joint Interpretation of Potential Field and Thermal Modelling–Southwestern Barents Sea, Norway. EGM 2007 International Workshop, 2007.

BEN-AWUAH, J., ADDA, GW., MIJINYAWA, A., ANDRIAMIHAJA, S., & SIDDIQUI, N. 2013. 2D Basin Modelling and Petroleum System Analysis of the Triassic Play in the Hammerfest Basin of the Norwegian Barents Sea. *Maxwell Scientific Organization, Research Journal of Applied Sciences, Engineering and Technology,* 6(17)**,** 3137-3150.

BERGLUND, L., AUGUSTSON, J., FÆRSETH, R., GJELBERG, J. & RAMBERG-MOE, H. 1986. The evolution of the Hammerfest Basin. *Habitat of hydrocarbons on the Norwegian continental shelf***,** 319-338.

BJORLYKKE, K. & EGEBERG, P. 1993. Quartz cementation in sedimentary basins. *AAPG bulletin,* 77**,** 1538-1548.

BJØRLYKKE, K., AAGAARD, P., EGEBERG, P. K. & SIMMONS, S. P. 1995. Geochemical constraints from formation water analyses from the North Sea and the Gulf Coast Basins on quartz, feldspar and illite precipitation in reservoir rocks. *Geological Society, London, Special Publications,* 86**,** 33-50.

BJØRLYKKE, K. & JAHREN, J. 2010. Sandstones and sandstone reservoirs. *Petroleum Geoscience.* Springer.

BLOCH, S., LANDER, R. H. & BONNELL, L. 2002. Anomalously high porosity and permeability in deeply buried sandstone reservoirs: Origin and predictability. *AAPG bulletin,* 86**,** 301-328.

BONDAREV, V., CHERKESOVA, S., ENOKYAN, V. & ROMANOVICH, B. 1973. Geologic Structure of Novaya Zemlya, Vaygach, Pay-Khoy, Polar Urals, and Northern Pechora: Regional Arctic Geology of the USSR.

BREIVIK, A. J., FALEIDE, J. I. & GUDLAUGSSON, S. T. 1998. South-western Barents Sea margin: late Mesozoic sedimentary basins and crustal extension. *Tectonophysics,* 293**,** 21-44.

BUGGE, T., ELVEBAKK, G., FANAVOLL, S., MANGERUD, G., SMELROR, M., WEISS, H. M., GJELBERG, J., KRISTENSEN, S. E. & NILSEN, K. 2002. Shallow stratigraphic drilling applied in hydrocarbon exploration of the Nordkapp Basin, Barents Sea. *Marine and Petroleum Geology,* 19**,** 13-37.

BURLEY, S. & WORDEN, R. 2009. *Sandstone Diagenesis: Recent and Ancient (Reprint Series 4 of the IAS)*, John Wiley & Sons.

CHUHAN, F. A., BJØRLYKKE, K. & LOWREY, C. 2000. The role of provenance in illitization of deeply buried reservoir sandstones from Haltenbanken and north Viking Graben, offshore Norway. *Marine and Petroleum Geology,* 17**,** 673-689.

DALLAND, A., WORSLEY, D. & OFSTAD, K. 1988. *A Lithostratigraphic Scheme for the Mesozoic and Cenozoic and Succession Offshore Mid-and Northern Norway*, Oljedirektoratet.

DICKINSON, W. R. 1985. Interpreting provenance relations from detrital modes of sandstones. *Provenance of arenites.* Springer.

DICKINSON, W. R., HARBAUGH, D. W., SALLER, A. H., HELLER, P. L. & SNYDER, W. S. 1983. Detrital modes of upper Paleozoic sandstones derived from Antler Orogen in Nevada; implications for nature of Antler Orogeny. *American Journal of Science,* 283**,** 481-509.

DORÉ, A. 1995. Barents Sea geology, petroleum resources and commercial potential. *Arctic***,** 207-221.

DURAN, E. R., DI PRIMIO, R., ANKA, Z., STODDART, D. & HORSFIELD, B. 2013. Petroleum system analysis of the Hammerfest Basin (southwestern Barents Sea): Comparison of basin modelling and geochemical data. *Organic Geochemistry,* 63**,** 105-121.

DYPVIK, H. 1983. Clay mineral transformations in Tertiary and Mesozoic sediments from North Sea. *AAPG Bulletin,* 67**,** 160-165.

DYPVIK, H., TSIKALAS, F. & SMELROR, M. 2010. *The Mjølnir Impact Event and Its Consequences*, Springer.

EHRENBERG, S. 1993. Preservation of anomalously high porosity in deeply buried sandstones by grain-coating chlorite: examples from the Norwegian continental shelf. *AAPG Bulletin,* 77**,** 1260-1286.

FALEIDE, J., VÅGNES, E. & GUDLAUGSSON, S. Late Mesozoic–Cenozoic evolution of the southwestern Barents Sea. Geological Society, London, Petroleum Geology Conference series, 1993a. Geological Society of London, 933-950.

FALEIDE, J. I., BJØRLYKKE, K. & GABRIELSEN, R. H. 2010a. Geology of the Norwegian continental shelf. *Petroleum Geoscience.* Springer.

FALEIDE, J. I., BJØRLYKKE, K. & GABRIELSEN, R. H. 2010b. *Geology of the Norwegian continental shelf.* Springer.

FALEIDE, J. I., GUDLAUGSSON, S. T. & JACQUART, G. 1984. Evolution of the western Barents Sea. *Marine and Petroleum Geology,* 1**,** 123-150.

FALEIDE, J. I., VÅGNES, E. & GUDLAUGSSON, S. T. 1993b. Late Mesozoic-Cenozoic evolution of the south-western Barents Sea in a regional rift-shear tectonic setting. *Marine and Petroleum Geology,* 10**,** 186-214.

FANAVOLL, S., GABRIELSEN, P. & ELLINGSRUD, S. 2014. The impact of CSEM on exploration decisions and seismic: two case studies from the Barents Sea. *First Break,* 32**,** 105-110.

FAWAD, M., MONDOL, N. H., JAHREN, J. & BJØRLYKKE, K. 2011. Mechanical compaction and ultrasonic velocity of sands with different texture and mineralogical composition. *Geophysical Prospecting,* 59**,** 697-720.

FLEET, A. J. & BOLDY, S. Petroleum geology of northwest Europe: Proceedings of the 5th Conference. 1999. Geological Society of London.

FOLK, R. L. 1951. Stages of textural maturity in sedimentary rocks. *Journal of Sedimentary Research,* 21.

GABRIELSEN, R. 1984. Long-lived fault zones and their influence on the tectonic development of the southwestern Barents Sea. *Journal of the Geological Society,* 141**,** 651-662.

GABRIELSEN, R. H., FAERSETH, R. B. & JENSEN, L. N. 1990. *Structural Elements of the Norwegian Continental Shelf. Pt. 1. The Barents Sea Region*, Norwegian Petroleum Directorate.

GAO, Y. 2013. Reservoir Characterization of Snøhvit Field, Norwegian Barents Sea.

GERNIGON, L., BRÖNNER, M., ROBERTS, D., OLESEN, O., NASUTI, A. & YAMASAKI, T. 2014. Crustal and basin evolution of the southwestern Barents Sea: from Caledonian orogeny to continental breakup. *Tectonics,* 33**,** 347-373.

GLØRSTAD-CLARK, E., BIRKELAND, E., NYSTUEN, J., FALEIDE, J. & MIDTKANDAL, I. 2011. Triassic platform-margin deltas in the western Barents Sea. *Marine and Petroleum Geology,* 28**,** 1294-1314.

GLØRSTAD-CLARK, E., FALEIDE, J. I., LUNDSCHIEN, B. A. & NYSTUEN, J. P. 2010. Triassic seismic sequence stratigraphy and paleogeography of the western Barents Sea area. *Marine and Petroleum Geology,* 27**,** 1448-1475.

HALLAND, E., BJØRNESTAD, A., GJELDVIK, I., MAGNUS, C., MUJEZINOVIC, J., PHAM, V., RIIS, F., ... & TAPPEL, I. 2014. CO2 storage Atlas Norwegian Continental Shelf. *Norwegian Petroleum Directorate*.

HARWOOD, J., APLIN, A. C., FIALIPS, C. I., ILIFFE, J. E., KOZDON, R., USHIKUBO, T. & VALLEY, J. W. 2013. Quartz Cementation History of Sandstones Revealed By High-Resolution Sims Oxygen Isotope Analysis. *Journal of Sedimentary Research,* 83**,** 522-530.

HE, M., MOLDOWAN, J. M., NEMCHENKO-ROVENSKAYA, A. & PETERS, K. E. 2012. Oil families and their inferred source rocks in the Barents Sea and northern Timan-Pechora Basin, Russia. *AAPG bulletin,* 96**,** 1121-1146.

HENRIKSEN, E., BJØRNSETH, H., HALS, T., HEIDE, T., KIRYUKHINA, T., KLØVJAN, O., LARSSEN, G., RYSETH, A., RØNNING, K. & SOLLID, K. 2011a. Uplift and erosion of the greater Barents Sea: impact on prospectivity and petroleum systems. *Geological Society, London, Memoirs,* 35**,** 271-281.

HENRIKSEN, E., RYSETH, A., LARSSEN, G., HEIDE, T., RØNNING, K., SOLLID, K. & STOUPAKOVA, A. 2011b. Tectonostratigraphy of the greater Barents Sea: implications for petroleum systems. *Geological Society, London, Memoirs,* 35**,** 163-195.

HESLOP, K. & HESLOP, A. 2003. Interpretation of Shaly Sands. *Archive Template,* 4**,** 2003.

HOFFMAN, J. 1979. Clay mineral assemblages as low grade metamorphic geothermometers: application to the thrust faulted disturbed belt of Montana, USA.

HUSSAIN, A. 2012. Diagenesis and reservoir quality of Upper Jurassic sandstones in the South Viking Graben: A mineralogical, petrographical and petrophysical approach.

JOHANSEN, S., OSTISTY, B., BIRKELAND, Ø., FEDOROVSKY, Y., MARTIROSJAN, V., CHRISTENSEN, O. B., CHEREDEEV, S., IGNATENKO, E. & MARGULIS, L. 1992. Hydrocarbon potential in the Barents

Sea region: play distribution and potential. *Arctic Geology and Petroleum Potential, Norwegian Petroleum Society (NPF), Special Publication,* 2**,** 273-320.

LANDER, R. H. & WALDERHAUG, O. 1999. Predicting porosity through simulating sandstone compaction and quartz cementation. *AAPG bulletin,* 83**,** 433-449.

LARSSEN, G. B., G. ELVEBAKK, L. B. HENRIKSEN, S. E. KRISTENSEN, I. NILSSON, T. J. SAMUELSBERG, T. A. SVÅNÅ, L. STEMMERIK, & D. WORSLEY 2005. Upper Palaeozoic lithostratigraphy of the southern part of the Norwegian Barents Sea. *Nor. Geol. Unders***,** 444, 3-5.

LAWVER, L. A., GRANTZ, A. & GAHAGAN, L. M. 2002. Plate kinematic evolution of the present Arctic region since the Ordovician. *SPECIAL PAPERS-GEOLOGICAL SOCIETY OF AMERICA***,** 333-358.

LINJORDET, A. & GRUNG OLSEN, R. 1978. The jurassic Snøhvit gas field, hammerfest basin, offshore northern Norway. *Giant oil and gas fields of the decade,* 1988**,** 349-370.

MAAST, T. E. 2008. Reservoir quality of deeply buried, Upper Jurassic sandstones of the South Viking Graben: A sedimentological, petrophysical and modeling approach.

MAAST, T. E. 2013. *Reservoir quality of deeply buried sandstones–a study of burial diagenesis from the North Sea.* University of Oslo Norway.

MAGOON, L. B. & DOW, W. G. 1994. The petroleum system. *The petroleum system—From source to trap: AAPG Memoir,* 60**,** 3-24.

MARCUSSEN, Ø., MAAST, T. E., MONDOL, N. H., JAHREN, J. & BJØRLYKKE, K. 2010. Changes in physical properties of a reservoir sandstone as a function of burial depth–The Etive Formation, northern North Sea. *Marine and Petroleum Geology,* 27**,** 1725-1735.

MCCARTHY, K., ROJAS, K., NIEMANN, M., PALMOWSKI, D., PETERS, K. & STANKIEWICZ, A. 2011. Basic petroleum geochemistry for source rock evaluation. *Oilfield Review,* 23**,** 32-43.

MENACHERRY, S. 2008. *"Source to Sink" Sedimentology and Petrology of a Dryland Fluvial System, and Implications for Reservoir Quality, Lake Eyre Basin, Central Australia.* The University of Adelaide Australia.

MEUNIER, A. & VELDE, B. 2004. The Geology of Illite. *Illite.* Springer.

MONDOL, N. H. (2009). "Porosity and permeability development in mechanically compacted siltkaolinite mixtures". SEG Houston International Exposition and Annual Meeting.

MORAD, S., AL-RAMADAN, K., KETZER, J. M. & DE ROS, L. 2010. The impact of diagenesis on the heterogeneity of sandstone reservoirs: A review of the role of depositional facies and sequence stratigraphy. *AAPG bulletin,* 94**,** 1267-1309.

MORK, A., KNARUD, R. & WORSLEY, D. 1982. Depositional and diagenetic environments of the Triassic and Lower Jurassic succession of Svalbard.

MORK, M., VIGRON, J., SMELROR, M., FJERDINGSTAD, V. & BOE, R. 2003. Mesozoic mudstone compositions and the role of kaolinite weathering-a view from shallow cores in the Norwegian Sea (More to Troms). *Norsk Geologisk Tidsskrift,* 83**,** 61-78.

MØRK, A., DALLMANN, W., DYPVIK, H., JOHANNESSEN, E., LARSSEN, G., NAGY, J., NØTTVEDT, A., OLAUSSEN, S., PCHELINA, T. & WORSLEY, D. 1999. Mesozoic lithostratigraphy. *Lithostratigraphic lexicon of Svalbard. Upper Palaeozoic to Quaternary bedrock. Review and recommendations for nomenclature use***,** 127-214.

OHM, S. E., KARLSEN, D. A. & AUSTIN, T. 2008. Geochemically driven exploration models in uplifted areas: Examples from the Norwegian Barents Sea. *AAPG bulletin,* 92**,** 1191-1223.

OLAUSSEN, S., DALLAND, A., GLOPPEN, T. & JOHANNESSEN, E. 1984. Depositional environment and diagenesis of Jurassic reservoir sandstones in the eastern part of Troms I area. *Petroleum Geology of the North European Margin.* Springer.

PAXTON, S., SZABO, J., AJDUKIEWICZ, J. & KLIMENTIDIS, R. 2002. Construction of an intergranular volume compaction curve for evaluating and predicting compaction and porosity loss in rigid-grain sandstone reservoirs. *AAPG bulletin,* 86**,** 2047-2067.

PETTIJOHN, F. J. 1987. *Sand and sandstone*, Springer Science & Business Media.

PITTMAN, E. D. 1972. Diagenesis of quartz in sandstones as revealed by scanning electron microscopy. *Journal of Sedimentary Research,* 42.

PITTMAN, E. D. 1979. Porosity diagenesis and productive capability of sandstone reservoirs.

POLLASTRO, R. M. 1985. Mineralogical and morphological evidence for the formation of illite at the expense of illite/smectite. *Clays and Clay Minerals,* 33**,** 265-274.

RAMBERG, I. B. The making of a land: geology of Norway. 2008. Geological Society of London.

RAMM, M., FORSBERG, A. W. & JAHREN, J. S. 1997. Porosity--Depth Trends in Deeply Buried Upper Jurassic Reservoirs in the Norwegian Central Graben: An Example of Porosity Preservation Beneath the Normal Economic Basement by Grain-Coating Microquartz.

RICHES, P., TRAUB-SOBOTT, I., ZIMMERLE, W. & ZINKERNAGEL, U. 1986. Diagenetic peculiarities of potential Lower Jurassic reservoir sandstones, Troms 1 area, off northern Norway, and their tectonic significance. *Clay Miner,* 21**,** 565-584.

RIIS, F., LUNDSCHIEN, B. A., HØY, T., MØRK, A. & MØRK, M. B. E. 2008. Evolution of the Triassic shelf in the northern Barents Sea region. *Polar Research,* 27**,** 318-338.

ROBIN, P.-Y. F. 1978. Pressure solution at grain-to-grain contacts. *Geochimica et Cosmochimica Acta,* 42**,** 1383-1389.

SATTAR, N. 2008. Mapping of Lower Cretaceous (Knurr Sandstone) turbidite lobes using Seismic Stratigraphy and prospectivity along the southern Loppa High Margin, Hammerfest Basin, Barents Sea, Norway.

SCHÖN, J. H. 2011. *Physical properties of rocks: A workbook*, Elsevier.

SELLEY, R. C. & SONNENBERG, S. A. 2014. *Elements of petroleum geology*, Academic Press.

SMELROR, M., MØRK, A., MØRK, M. B. E., WEISS, H. M. & LØSETH, H. 2001. Middle Jurassic-Lower Cretaceous transgressive-regressive sequences and facies distribution off northern Nordland and Troms, Norway. *Norwegian Petroleum Society Special Publications,* 10**,** 211-232.

SZABO, J. & PAXTON, S. 1991. Intergranular volume (IGV) decline curves for evaluating and predicting compaction and porosity loss in sandstones. *AAPG Bulletin (American Association of Petroleum Geologists);(United States),* 75.

TAYLOR, T. R., GILES, M. R., HATHON, L. A., DIGGS, T. N., BRAUNSDORF, N. R., BIRBIGLIA, G. V., KITTRIDGE, M. G., MACAULAY, C. I. & ESPEJO, I. S. 2010. Sandstone diagenesis and reservoir quality prediction: Models, myths, and reality. *AAPG bulletin,* 94**,** 1093-1132.

VAN HULTEN, F. Rifting systems and its significance for hydrocarbon exploration in the Netherlands. Hulten, FFN van & Lutgert, JE (comp.). Rifting systems and its significance for hydrocarbon exploration in the Netherlands, workshop EBN-TNO, June, 2008.

WALDERHAUG, O. 1994. Temperatures of quartz cementation in Jurassic sandstones from the Norwegian continental shelf--evidence from fluid inclusions. *Journal of Sedimentary Research,* 64.

WALDERHAUG, O. 1996. Kinetic modeling of quartz cementation and porosity loss in deeply buried sandstone reservoirs. *AAPG bulletin,* 80**,** 731-745.

WALDERHAUG, O. & BJØRKUM, P. A. 2003. The effect of stylolite spacing on quartz cementation in the Lower Jurassic Stø Formation, southern Barents Sea. *Journal of Sedimentary Research,* 73**,** 146-156.

WALDERHAUG, O., BJØRKUM, P. A., NADEAU, P. H. & LANGNES, O. 2001. Quantitative modelling of basin subsidence caused by temperature-driven silica dissolution and reprecipitation. *Petroleum Geoscience,* 7**,** 107-113.

WANGEN, M. 1998. Modeling porosity evolution and cementation of sandstones. *Marine and Petroleum Geology,* 15**,** 453-465.

WELTJE, G. J. & VON EYNATTEN, H. 2004. Quantitative provenance analysis of sediments: review and outlook. *Sedimentary Geology,* 171**,** 1-11.

WORDEN, R. H. & MORAD, S. 2000. Quartz cementation in sandstones.

WORDEN, R. H., OXTOBY, N. H. & SMALLEY, P. C. 1998. Can oil emplacement prevent quartz cementation in sandstones? *Petroleum Geoscience,* 4**,** 129-137.

WORSLEY, D. 2008. The post-Caledonian development of Svalbard and the western Barents Sea. *Polar Research,* 27**,** 298-317.

WORSLEY, D., JOHANSEN, R. & KRISTENSEN, S. 1988. The Mesozoic and Cenozoic succession of Tromsøflaket. *A lithostratigraphic scheme for the Mesozoic and Cenozoic succession offshore mid-and northern Norway. Norwegian Petroleum Directorate Bulletin,* 4**,** 42-65.

ZIEGLER, P. 1978. North-western Europe: tectonics and basin development. *Geologie en Mijnbouw,* 57**,** 589-626.

ZIMMERLE, W. 1991. *Stratigraphic distribution, lithological paragenesis, depositional environments and diagenesis of fossil siliceous sponges in Europe*, Springer.

ØVREBØ, O. & TALLERAAS, E. 1977. The Structural geology of the Troms Area (Barents-Sea). *GeoJournal,* 1**,** 47-54.

Inoformation about well data are available at www.statoil.com (last update 05/03/2015).

Location of the study area and well data is available at www.npd.com (last update 17/02/2015).

Lihtostratigraphy of the area is available at www.nhm.uio.no (last update 16/03/2015).

Description of heavy minerals available at (http://www.cretaceous.de/Cretaceous.html) (last used 11/03/2015).

CHAPTER 10

APPENDICES

- APPENDIX A (LOGGING SHEET)
- APPENDIX B (PETROGRAPHY)
- APPENDIX C (SEDIMENTOLOGICAL LOG)

Appendix A

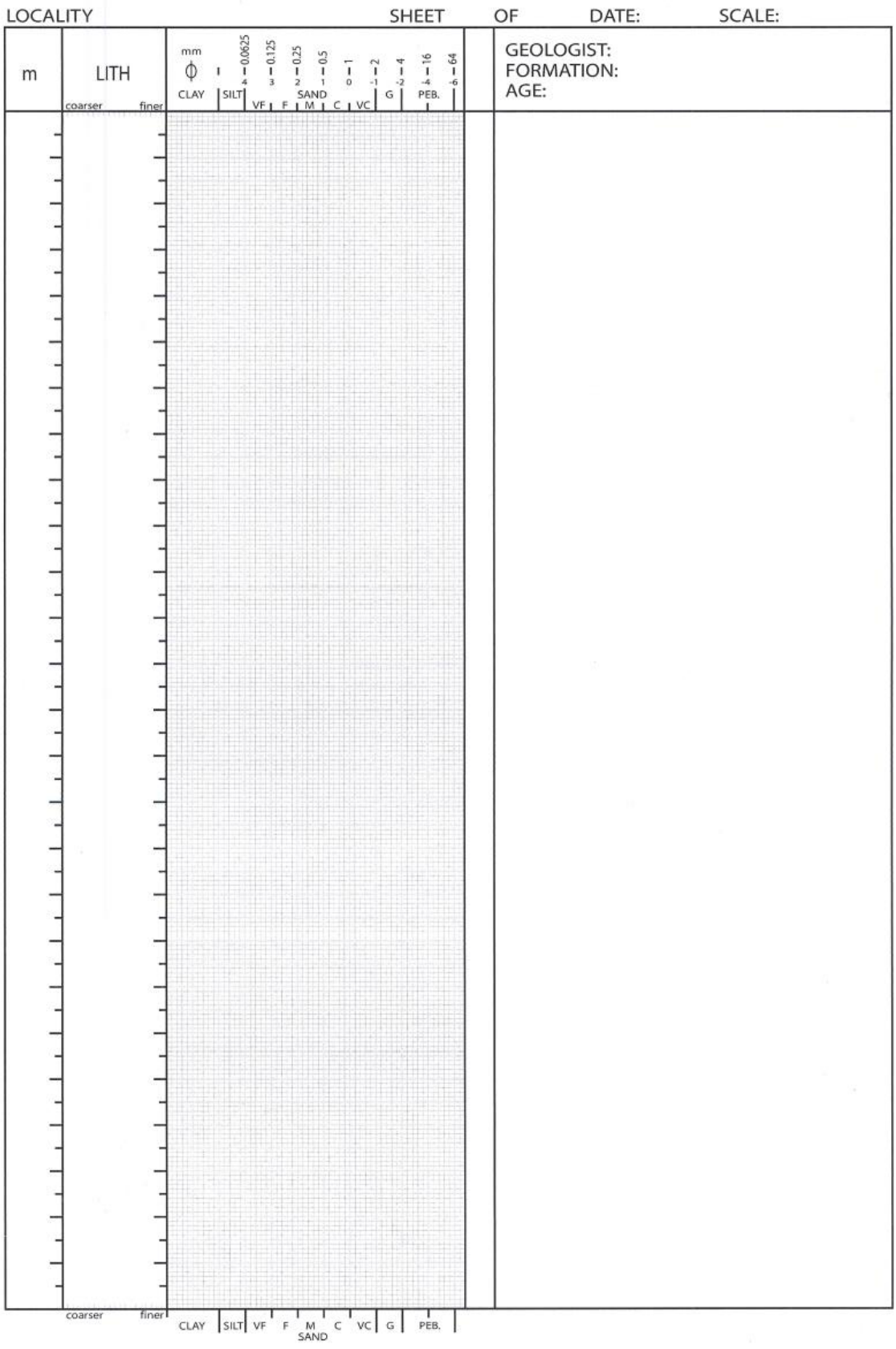

Appendix A 1: logging sheet used for core logging.

Appendix B

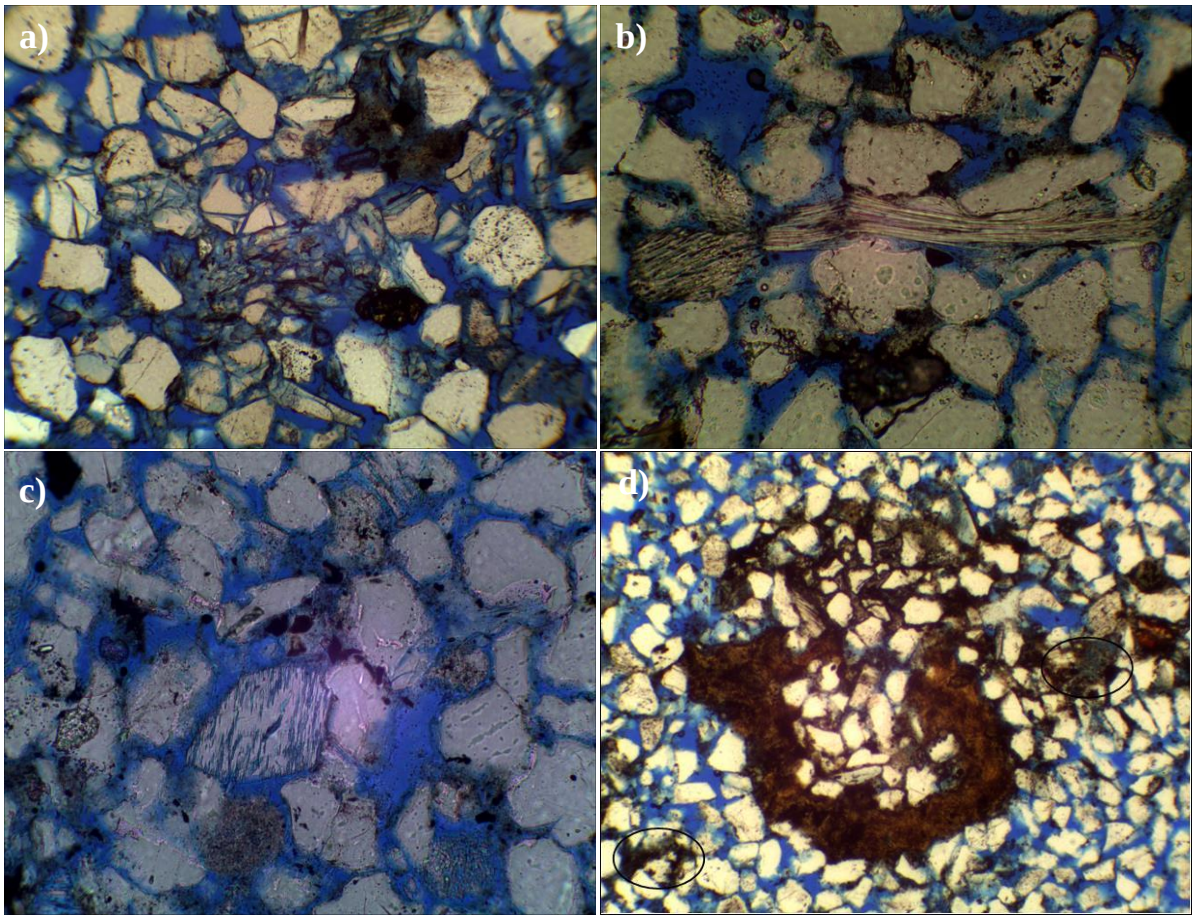

Appendix B 1: a) Highly fractured quartz grains due to vicinity of fault at 1349.36 m depth. b) Laminar mica sheet is deformed due to mechanical compaction at 1373.10 m depth. c) A clean sandstone with half dissolved feldspar grain and kaolinite at 1379.36 m depth. d) Brown organic matter with dispersed clay (circled) at 1373.10 m depth.

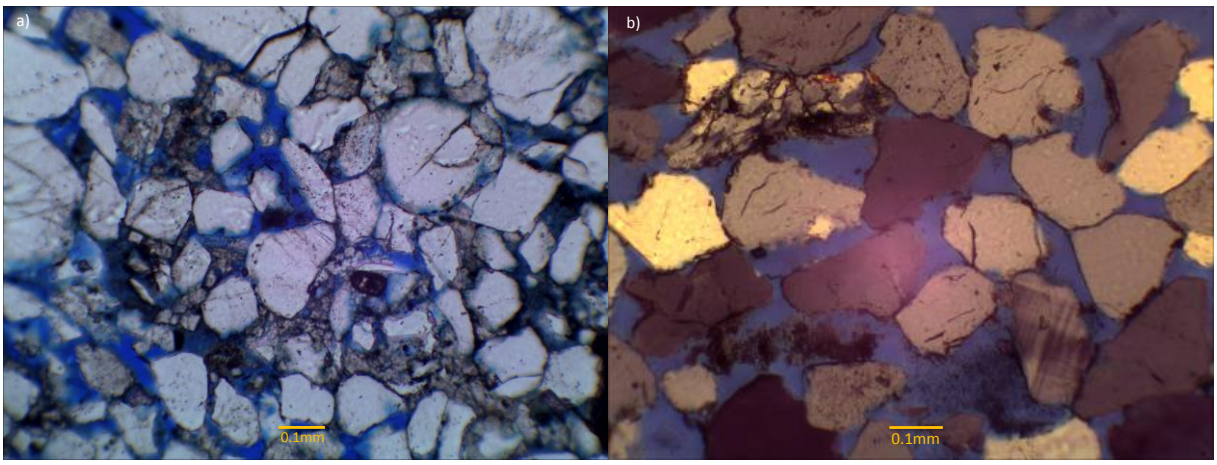

Appendix B 2: Well sorted clean sandstone (b) (1431.70 m depth) is comparatively less compacted than moderately sorted argillaceous sandstone (a) (1349.36 m depth).

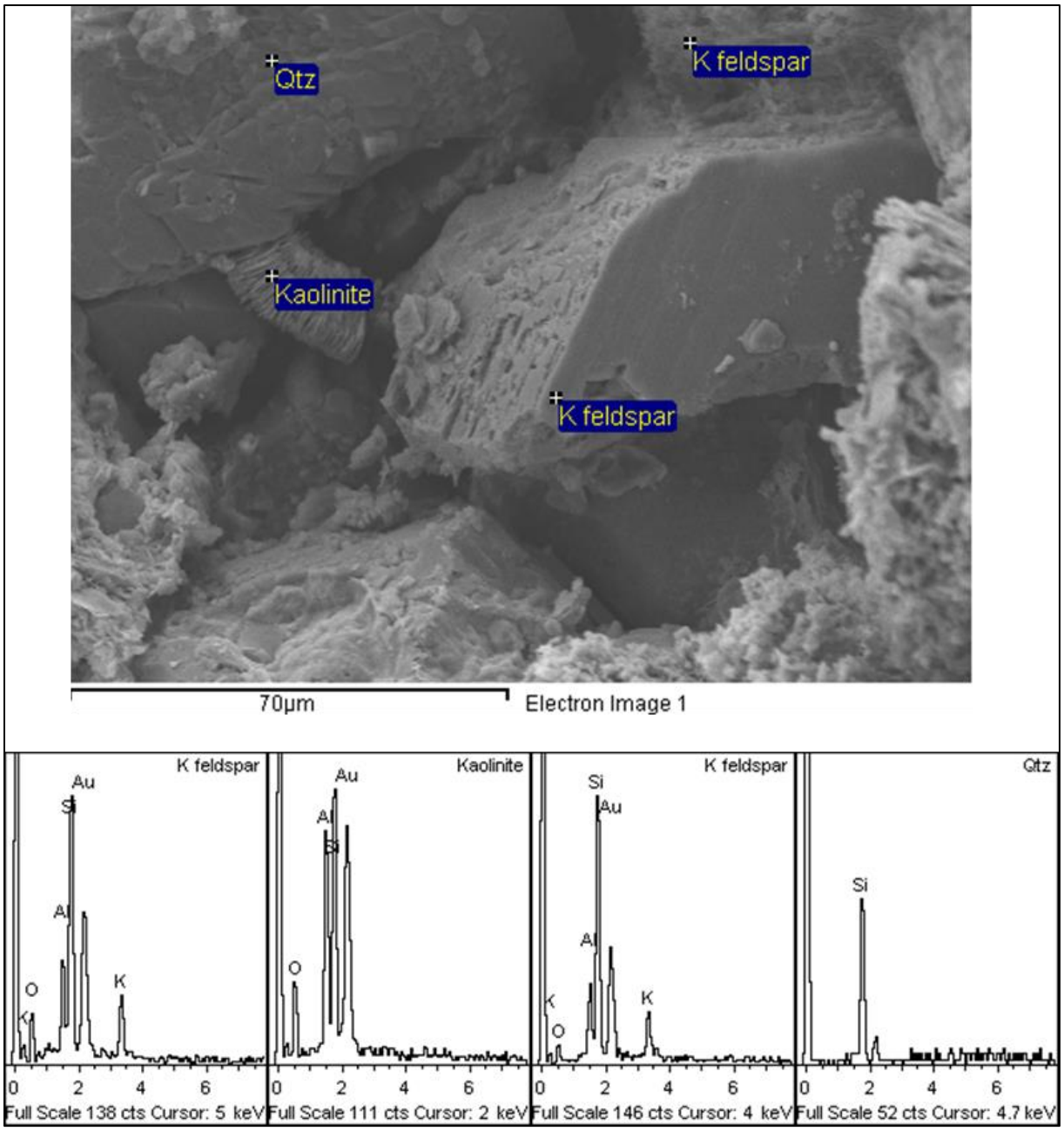

Appendix B 3: Authigenic kaolinite within primary pore spaces at 1379.5 m depth.

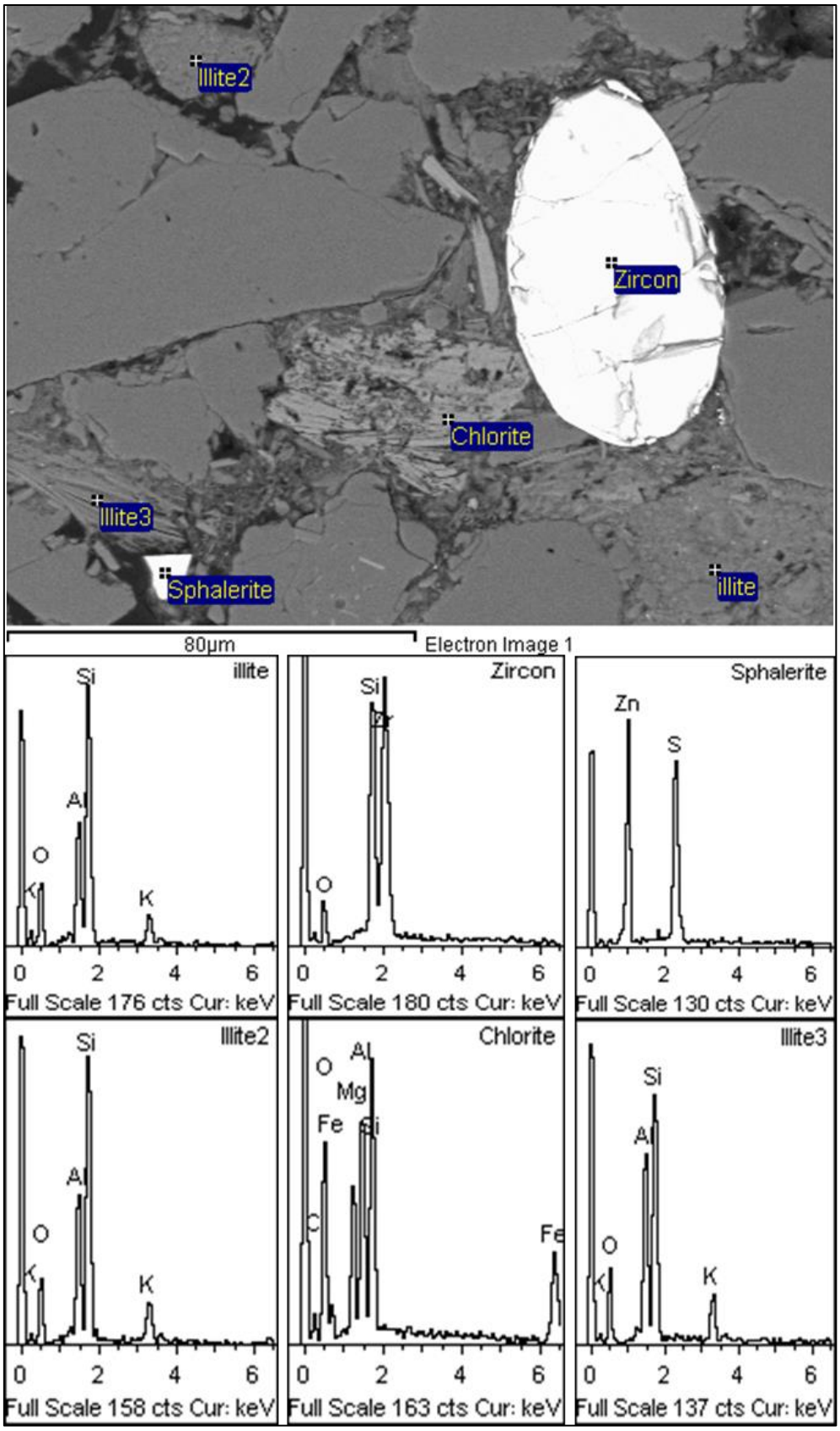

Appendix B 4: Authigenic clays chlorite and illite occupying all the porosity together with heavy minerals at 1439.80 depths.

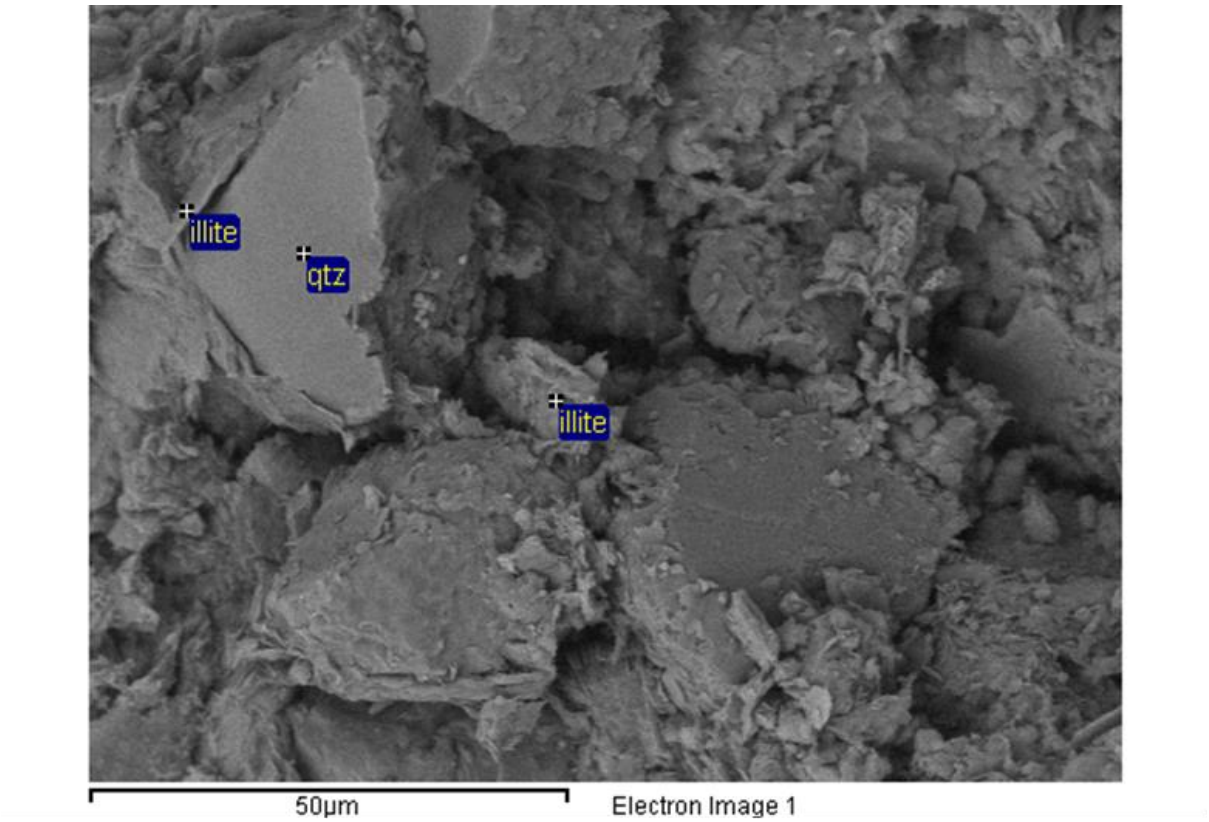

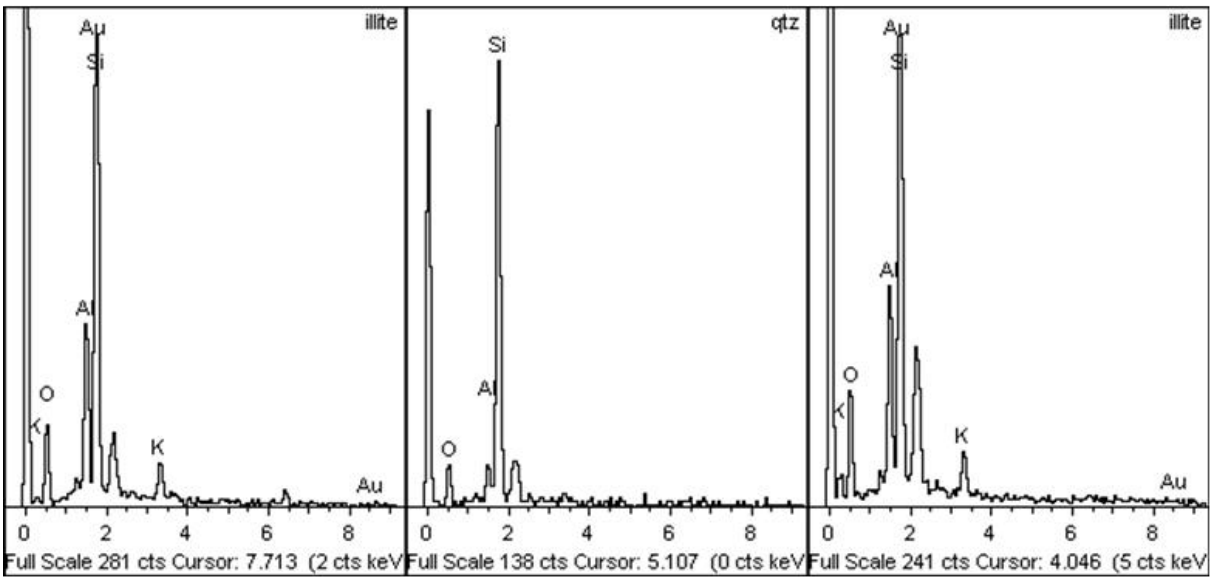

Appendix B 5: Illite coating on the quartz grain at 1439.80 m depth.

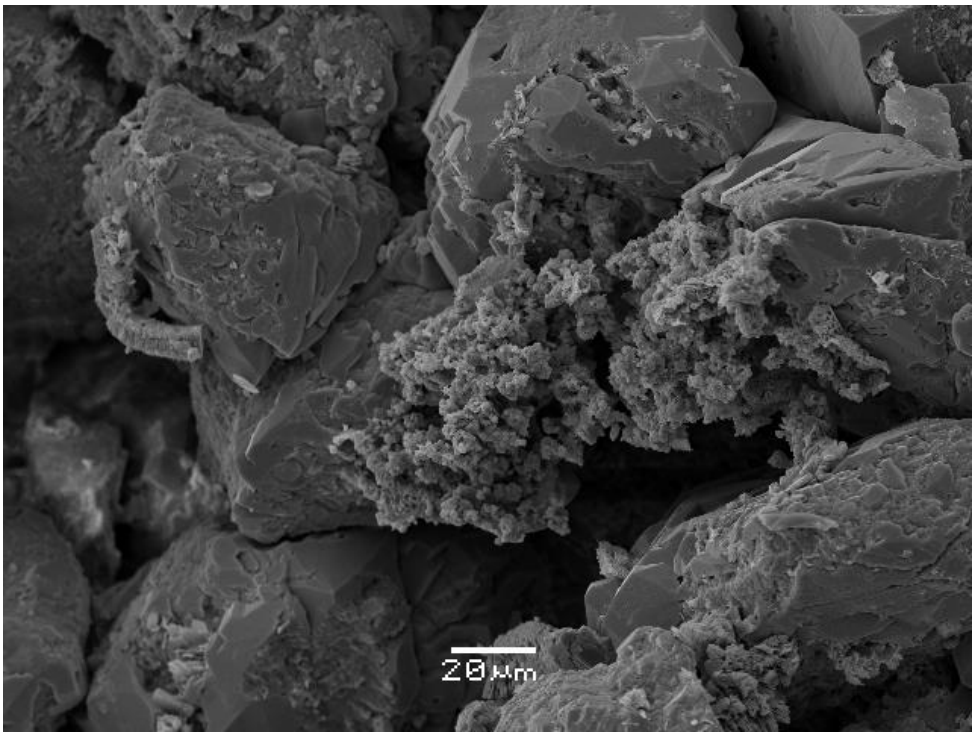

Appendix B 6: Micro-quartz cluster present at the depth of 1356.07m.

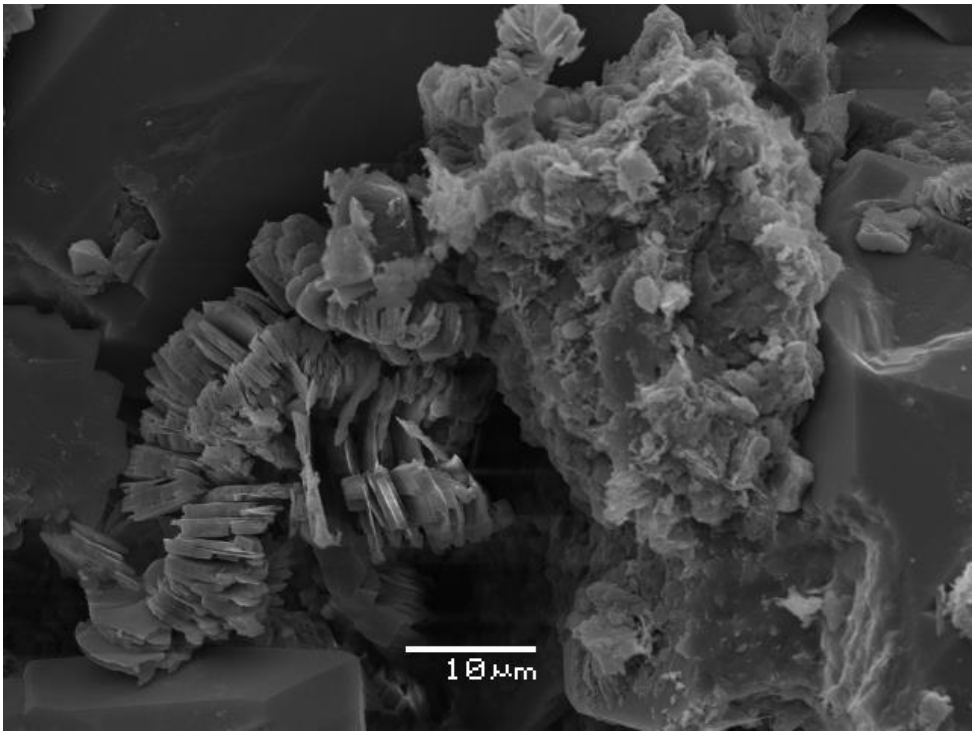

Appendix B 7: Kaolinite and illite at 1340.15 m depth.

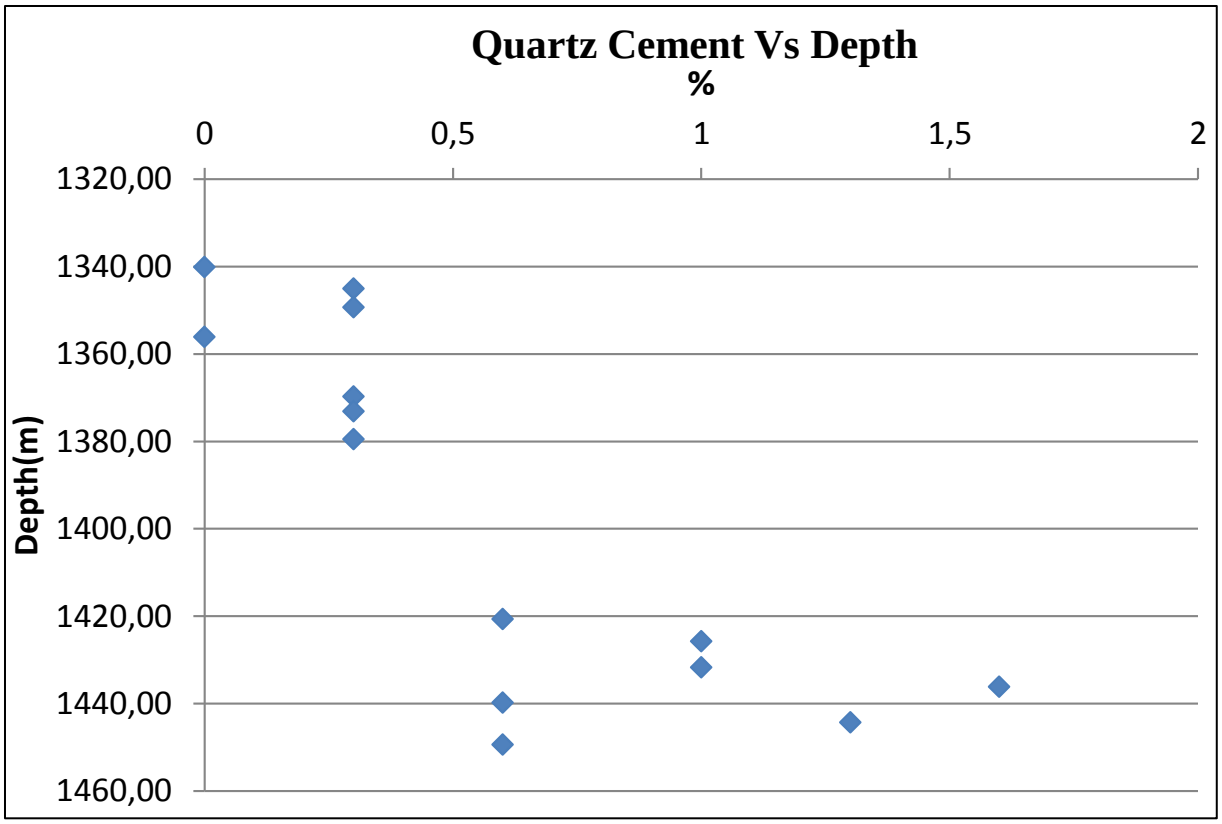

Appendix B 8: The amount of quartz cementation against depth.

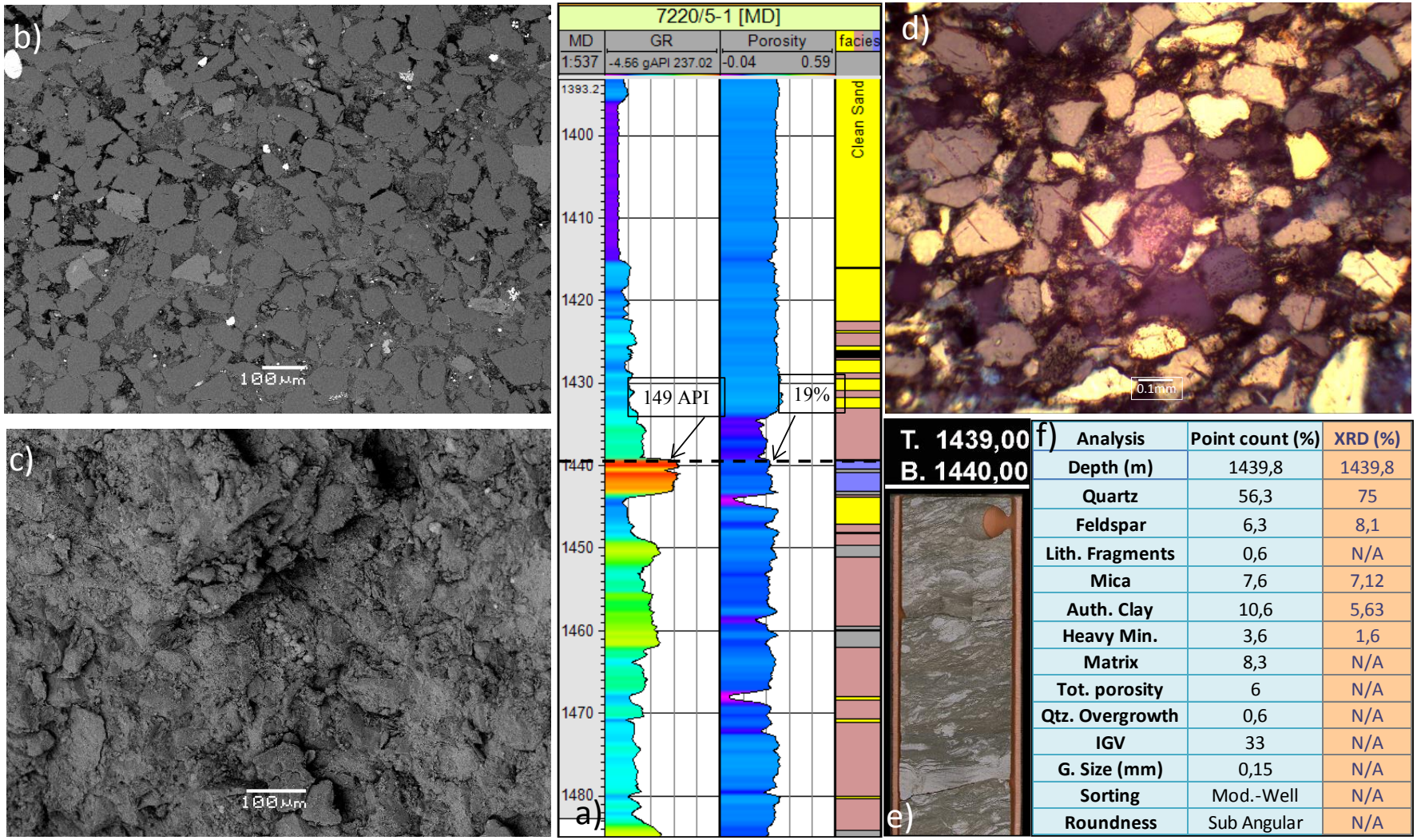

f)

Analysis	Point count (%)	XRD (%)
Depth (m)	1439,8	1439,8
Quartz	56,3	75
Feldspar	6,3	8,1
Lith. Fragments	0,6	N/A
Mica	7,6	7,12
Auth. Clay	10,6	5,63
Heavy Min.	3,6	1,6
Matrix	8,3	N/A
Tot. porosity	6	N/A
Qtz. Overgrowth	0,6	N/A
IGV	33	N/A
G. Size (mm)	0,15	N/A
Sorting	Mod.-Well	N/A
Roundness	Sub Angular	N/A

Appendix B 9: Integrated study of Core, petrographical and petrophysical analysis at 1439.80 m depth. a) GR, porosity and facies log in the well 7220/5-1. b & c) SEM microphotographs of carbon coated thin section, gold coated stub. d) Thin section overview in optical microscope. e) Core photo of sandstone. f) Quantitative analysis of mineralogy composition by point counting and XRD techniques.

	Point Count Results (%)					XRD Results (%)				
Depth (m)	Quartz	Feldspar	Kaolinite	Mica/illite	Heavy minerals	Quartz	K-feldspar	Kaolinite	Illite/Mica	Heavy Minerals
1340,15	85,01	7,69	9,91	2,09	3,00	84,89	4,35	4,44	3,265	0,188
1345,05	76,87	5,81	10,73	4,80	2,12	87,66	1,62	5,37	2,31	0,589
1349,36	85,19	3,36	8,45	2,66	0,69	90,95	0,79	3,6	1,372	0,077
1356,07	87,90	3,58	5,68	1,60	1,23	89,7	3,11	2,74	2,06	0,2
1369,77	87,03	5,16	5,16	2,28	0,72	83,46	4,48	4,44	3,59	0,806
1373,1	82,81	5,23	7,85	2,86	1,62	84,03	5,33	3,97	2,55	0,931
1379,5	80,25	6,00	8,43	3,81	1,85	82,83	5,38	4,26	3,27	0,89
1420,7	89,09	3,42	3,94	1,71	2,63	95,61	0,5	0,84	0,64	0,082
1425,76	90,35	2,06	4,25	1,67	2,96	94,09	1,2	1,381	0,727	0,667
1431,72	93,25	2,12	3,44	0,79	1,72	91,71	2,85	1,19	0,281	0,55
1436,2	89,77	3,96	4,50	1,77	2,18	91,94	2,99	1,181	0,842	0,32
1439,8	70,53	6,75	11,36	8,15	3,86	75,4	5,61	5,63	7,12	1,6
1444,36	93,57	2,14	3,48	0,80	1,74	95,12	0,81	0,683	0,522	0,56
1449,435	80,33	8,47	8,61	0,82	2,60	80,73	8,11	2,25	0,828	0,57

Appendix B 10: Point counting and XRD results have been compared for the correlation and confirmation purpose. Note that porosity is not included for the point count results.

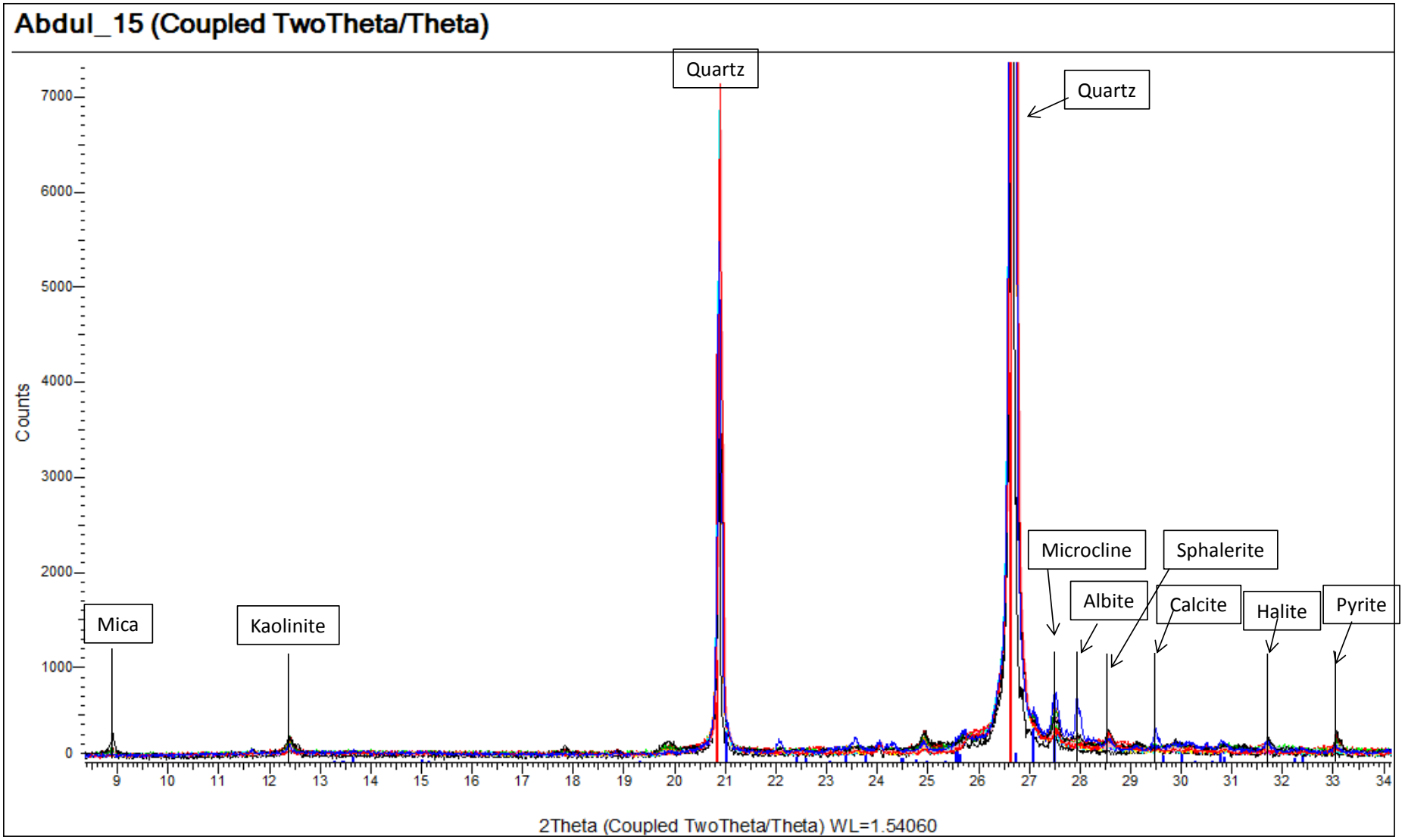

Appendix B11: Mineral identification of all 15 samples by X-Ray Diffraction technique using DIFFRAC EVA software.

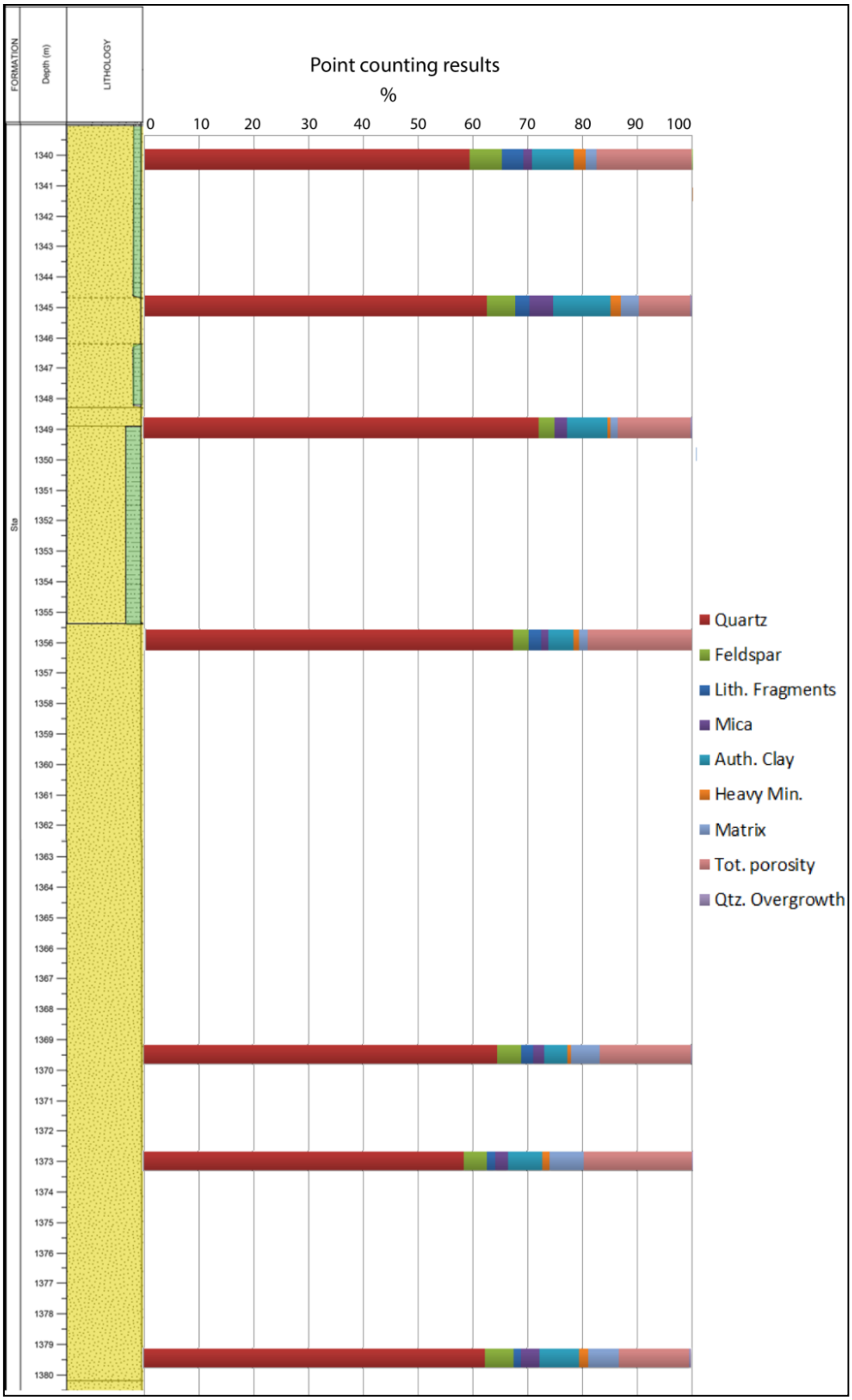

Appendix B 12: Point counting results plotted against the lithological column at respective depths of samples within reservoir sandstones.

Appendix C

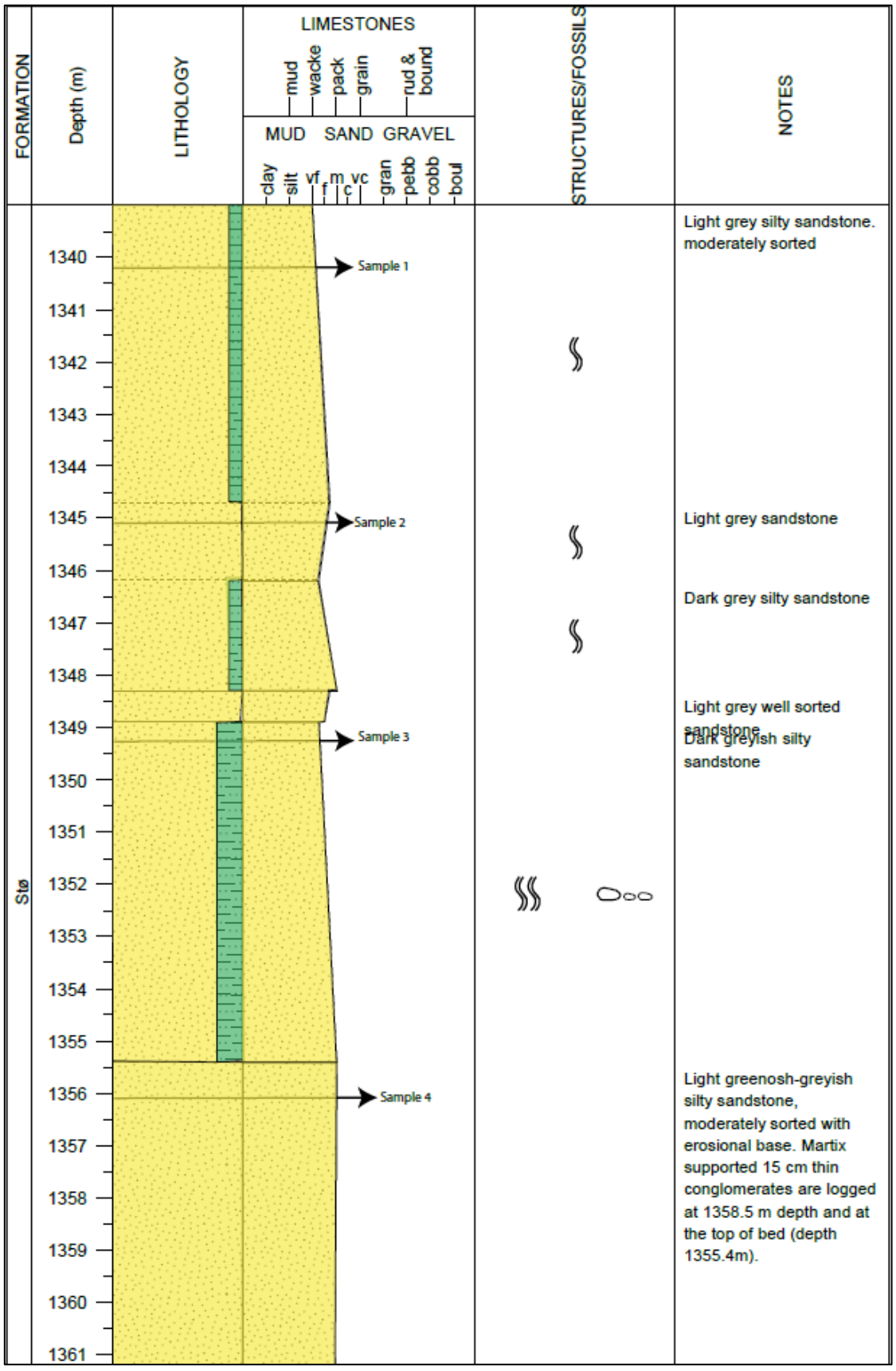

Appendix C 1: Core logging of depth interval 1458-1337 m.

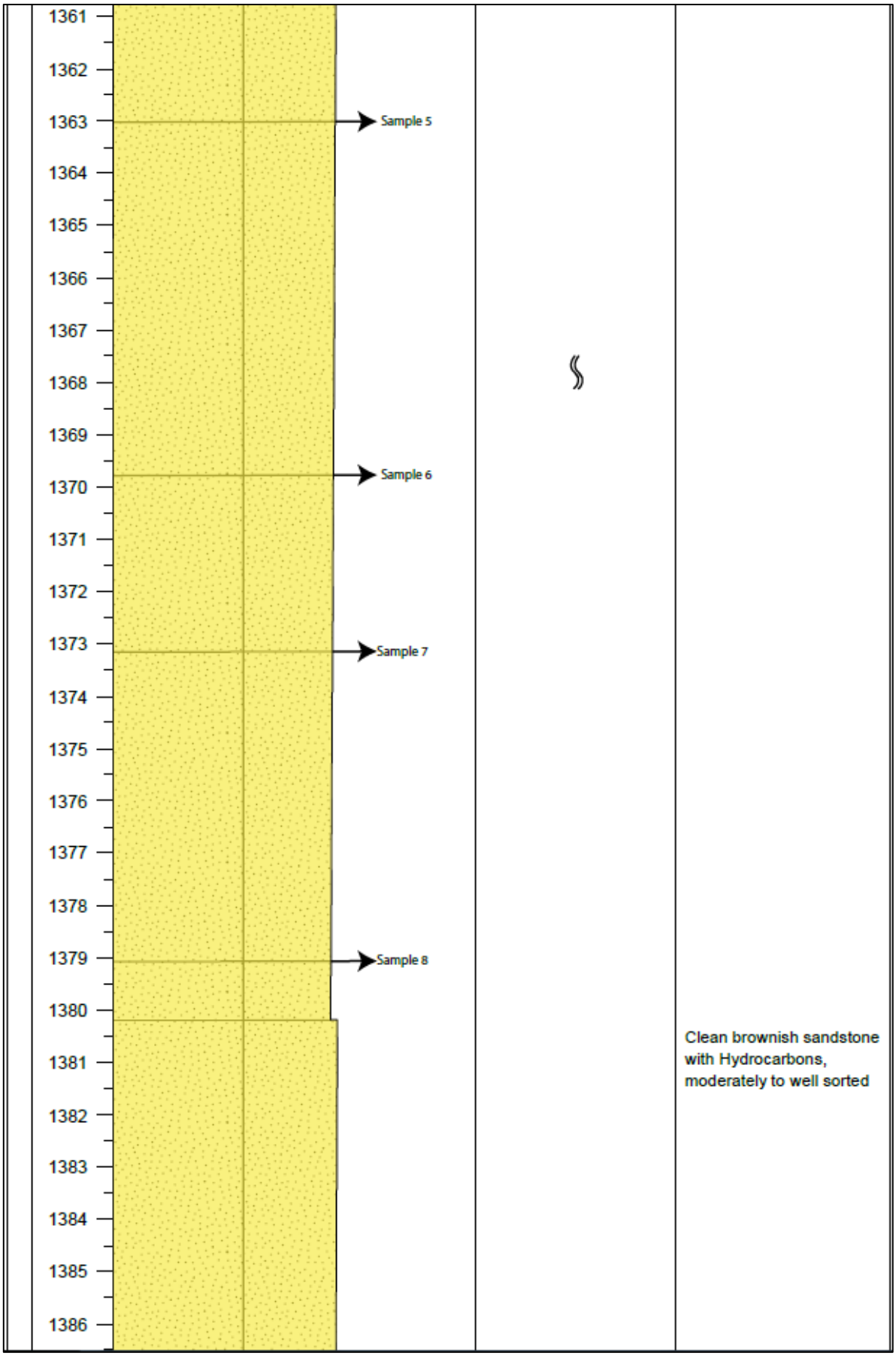
1361
1362
1363
1364
1365
1366
1367
1368
1369
1370
1371
1372
1373
1374
1375
1376
1377
1378
1379
1380
1381
1382
1383
1384
1385
1386
Sample 5
Sample 6
Sample 7
Sample 8
Clean brownish sandstone with Hydrocarbons, moderately to well sorted

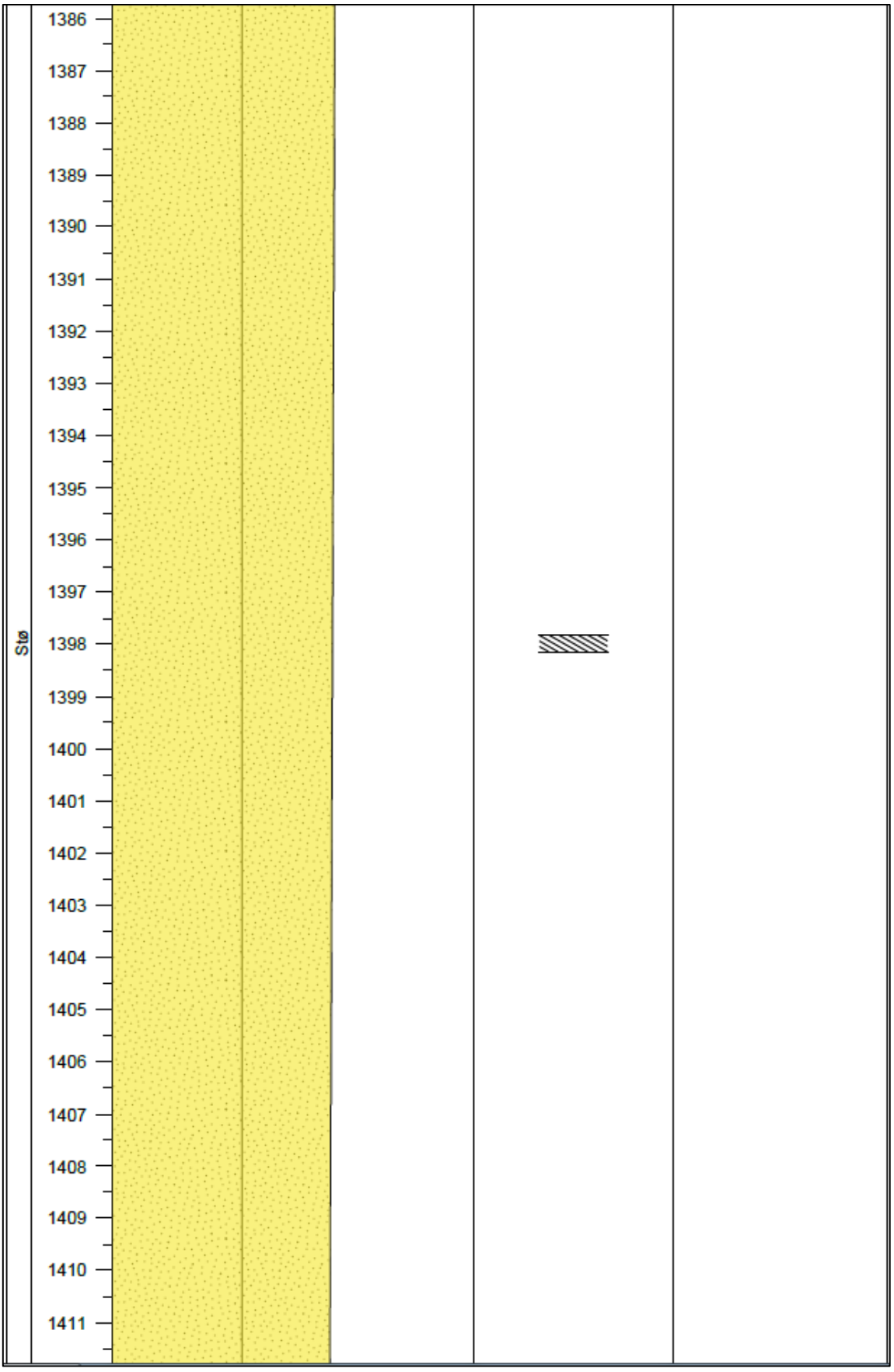
Stø
1386
1387
1388
1389
1390
1391
1392
1393
1394
1395
1396
1397
1398
1399
1400
1401
1402
1403
1404
1405
1406
1407
1408
1409
1410
1411

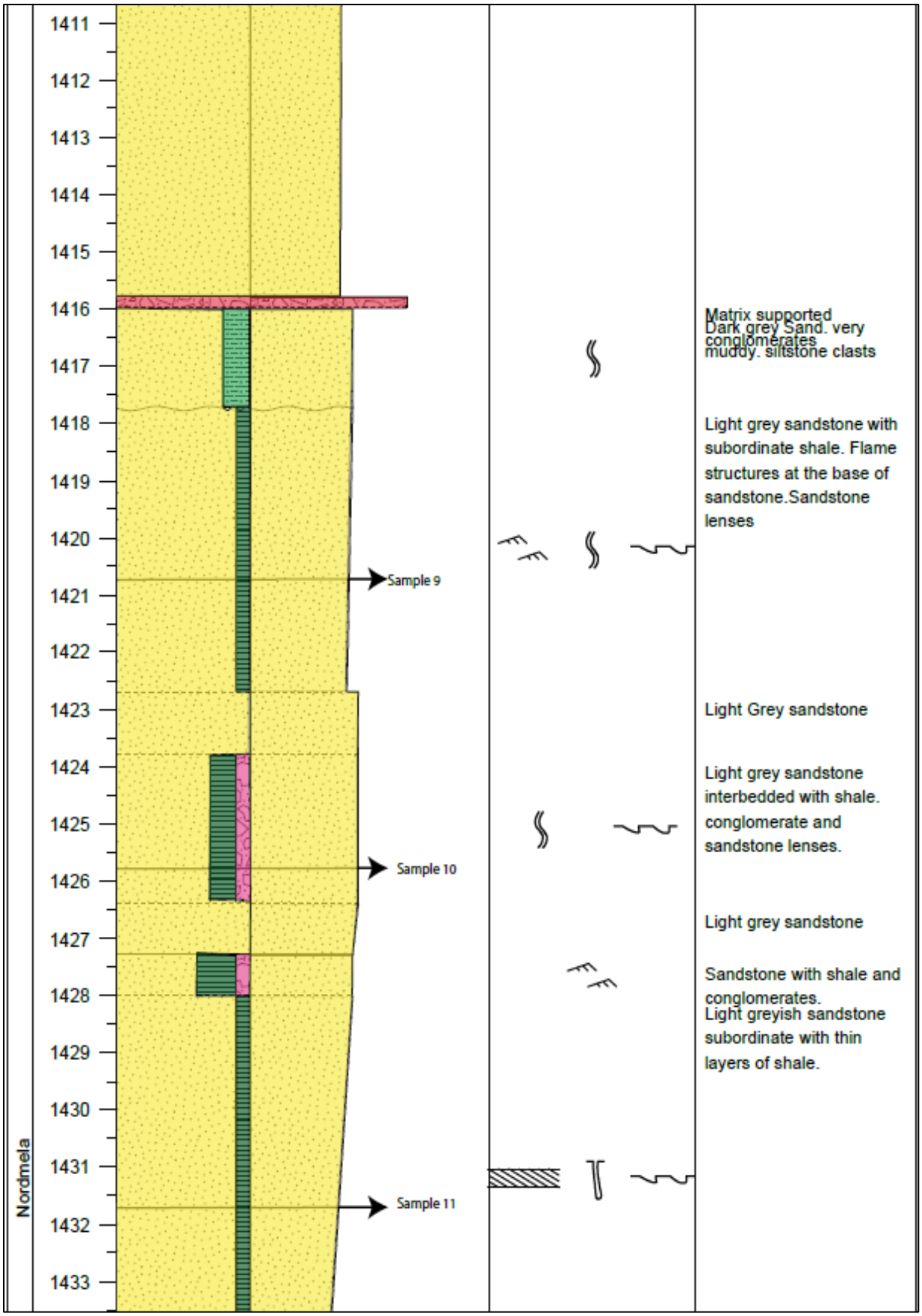
1411
1412
1413
1414
1415
1416
1417
1418
1419
1420
1421
1422
1423
1424
1425
1426
1427
1428
1429
1430
1431
1432
1433
Nordmela
Sample 9
Sample 10
Sample 11
Matrix supported conglomerates
Dark grey Sand. very muddy. siltstone clasts
Light grey sandstone with subordinate shale. Flame structures at the base of sandstone.Sandstone lenses
Light Grey sandstone
Light grey sandstone interbedded with shale. conglomerate and sandstone lenses.
Light grey sandstone
Sandstone with shale and conglomerates.
Light greyish sandstone subordinate with thin layers of shale.

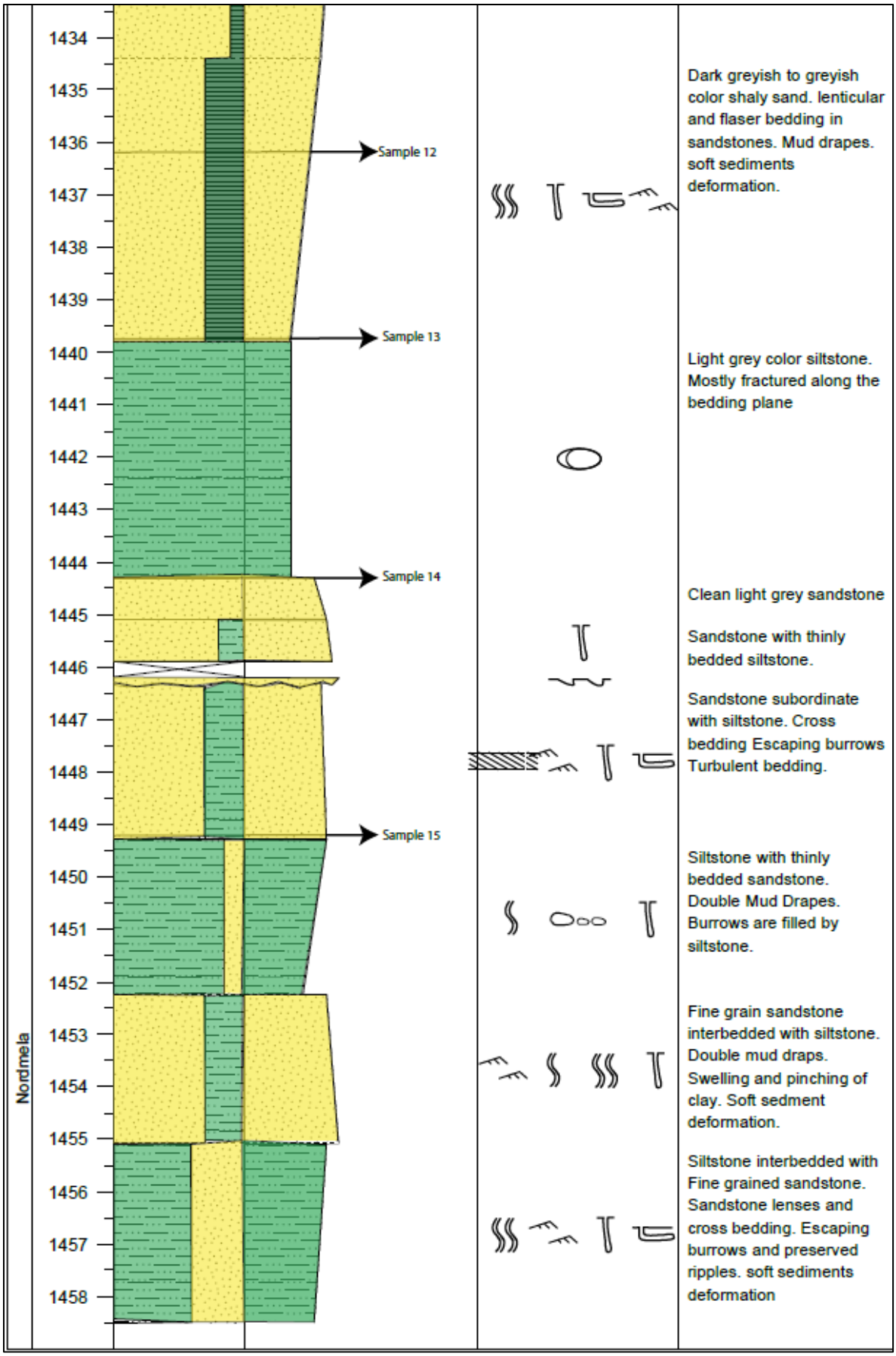
Nordmela
1434
1435
1436
1437
1438
1439
1440
1441
1442
1443
1444
1445
1446
1447
1448
1449
1450
1451
1452
1453
1454
1455
1456
1457
1458
Sample 12
Sample 13
Sample 14
Sample 15
Dark greyish to greyish color shaly sand. lenticular and flaser bedding in sandstones. Mud drapes. soft sediments deformation.
Light grey color siltstone. Mostly fractured along the bedding plane
Clean light grey sandstone
Sandstone with thinly bedded siltstone.
Sandstone subordinate with siltstone. Cross bedding Escaping burrows Turbulent bedding.
Siltstone with thinly bedded sandstone. Double Mud Drapes. Burrows are filled by siltstone.
Fine grain sandstone interbedded with siltstone. Double mud draps. Swelling and pinching of clay. Soft sedment deformation.
Siltstone interbedded with Fine grained sandstone. Sandstone lenses and cross bedding. Escaping burrows and preserved ripples. soft sediments deformation